Relaxation of electronic excitation in nitrogen/oxygen and fuel/air mixtures: fast gas heating in plasma-assisted ignition and flame stabilization

N.A. Popov, S.M. Starikovskaia

Relaxation of electronic excitation in nitrogen-oxygen and fuel-air mixtures: fast gas heating in plasma-assisted ignition and flame stabilization

N.A. Popov (Skobeltsyn Institute of Nuclear Physics, Moscow State University, Russia), S.M.Starikovskaia (Laboratoire de Physique des Plasmas, (CNRS, École Polytechnique, Sorbonne Universitiés, Univ. Paris-Sud), Institut Polytechnique de Paris, F-91128, Palaiseau, France)

Highlights:

- Available experiments on fast gas heating (FHG) are reviewed
- Fraction of energy spent on FGH η_R is suggested as a universal parameter
- Parameter η_R is analysed for 3 different ranges of reduced electric field
- Kinetic models of FGH for non-combustible mixtures are discussed
- FHG in hydrogen- and hydrocarbon-containing mixtures is analysed

Keywords:

Plasma assisted combustion
Plasma flow control
Plasma flame stabilization
Kinetics in gas discharge
Electronic excitation and relaxation
Fast gas heating

Abstract

Fast gas heating (FGH) is an abrupt increase in gas temperature in non-equilibrium transitive low-temperature plasma due to relaxation of electronically excited states of atoms and molecules. In the active flow control, fast gas heating is responsible for thermal frequency perturbations in the range of unstable frequencies of flow instabilities. In plasma-assisted combustion, abrupt temperature increase due to FGH, together with generation of radicals in plasma, induces acceleration of combustion chemistry providing shortening of the induction delay time and intensification of combustion. Over the last decade, significant progress has been made towards the understanding of kinetics of the fast gas heating. New observations of fast gas heating in air and nitrogen-air mixtures have been reported. The result of experiments, reporting heating to thousands of kelvins during tens of nanoseconds at atmospheric pressure in non-combustible mixtures, have provided new opportunities in the development of kinetic models. Electron-impact dissociation, quenching of electronically excited states of atoms and molecules, ion-molecular reactions, recombination of charged particles are reviewed analysing their role in the fast gas heating. The fraction of energy spent on fast gas heating η_R has been suggested as a universal parameter to generalize the results of empirical research on energy relaxation. This paper considers the dependence of η_R on reduced electric field, specific delivered energy, oxygen fraction in the mixture and other parameters. The analysis is grouped over three different ranges of the reduced electric field: $E/N \leq 120$ - 130 Td, $E/N = 150$ - 400 Td and $E/N > 400$ Td. Non-numerous experimental and theoretical studies of the fast gas heating in hydrogen- and hydrocarbon-containing mixtures are discussed and compared to the results in non-flammable mixtures. This article is to provide a comprehensive overview of the progress of kinetics of fast gas heating and to indicate the lack of experimental data and consequently, the gap in the knowledge of energy relaxation in discharges in combustible mixtures.

Acronyms and abbreviations

1D	1-dimensional
2D	2-dimensional
3D	3-dimensional
B_e	rotational constant
CARS	coherent anti-Stokes Raman spectroscopy
CMOS	complementary metal oxide semiconductor
CRDS	cavity ring down spectroscopy
d	interelectrode distance
DBD	dielectric barrier discharge
DC	direct current
E	electric field
E_{rot}	rotational energy
E-FISH	electric field induced second harmonic generation
ER	equivalence ratio
FGH	fast gas heating
FIW	fast ionization wave
FWHM	full width half magnitude
G	G-value, number of atoms per 100 eV of deposited energy
GRI-Mech	Gas Research Institute mechanism
HCCI	homogeneous charge compression ignition
ICCD	intensified charge coupled device
j	current density
k	Boltzmann constant
K	rate constant of chemical reaction
LIF	laser induced fluorescence
M	Mach number
N	gas number density
N_e	electron density
OES	optical emission spectroscopy
P	pressure
PAC	plasma assisted combustion
PAI	plasma assisted ignition
R	radius of plasma channel
SDBD	surface dielectric barrier discharge
SPS	second positive system
SRS	spontaneous Raman scattering
T, T_g	gas temperature
T_{rot}	rotational temperature
t_{RT}	RT-relaxation time
T_e	electron temperature
U	voltage
UV	ultraviolet
v', v''	vibrational levels
VT	vibrational-translational
VV	vibrational-vibrational
W	energy
Z	characteristic impedance of the coaxial cable
η_R	energy efficiency of fast gas heating
τ, τ_{imp}	pulse duration
η_{diss}	fraction of the discharge energy spent to dissociation
ε_R	kinetic energy of the products of pre-dissociation

Table of Contents

1. Introduction

In recent years, multidisciplinary research in plasma physics, combustion and flow control has resulted in the development of several new fields, namely plasma assisted ignition of combustible mixtures, plasma assisted flow control, and an emerging field - stabilization of ultra-lean mixture combustion by combining chemical and gas-dynamic impact of low-temperature plasma. Combustion of hydrocarbon fuels is the world's major source of energy. At present, about 80% of energy worldwide (transport, electric power generation, heating, and so on) is provided by combustion; it is very much worth studying and optimizing this process. A decrease in ignition delay time in the short residence time systems, such as supersonic combustion ramjet (scramjet) engines, the development of detonation engines and homogeneous charge compression ignition (HCCI) engines, efficient ignition of biofuels, new lean burn engines to meet modern emission standards and other challenges require new non-standard solutions. Recently, a concept of plasma-assisted combustion has been suggested and developed [1], [2], [3], [4], [5], [6]. The term "plasma-assisted ignition/combustion" (PAI/PAC) is used for combustion, initiated or sustained by low-temperature non-equilibrium plasma of gas discharges.

Another example of the potential use of low-temperature plasma for airspace applications is plasma flow control [7], [8], [9], [10], [11]. Plasma flow control includes drag reduction, lift enhancement, shock wave control, aerodynamic noise reduction, boundary layer re-attachment. Various discharges are used for plasma flow control, but the most efficient action is typically related to fast thermal energy release at specific points of flow in the discharge area [8], [9], [10], [12].

Benefits of plasma-assisted combustion and plasma flow control are merged together [13] in the field of plasma ignition of lean combustible mixtures and plasma stabilization of lean flames.

Specific attention to lean combustion is related to strict limitations for thermal NO_x emission: as far as lean mixtures burn at lower temperature than stoichiometric mixtures, NO_x emissions are lower [14].

At high pressures, ignition of combustible mixtures starts in separated discharge channels localized in space. Ignition in the whole volume of combustion chamber is driven by propagation of combustion waves. In lean mixtures, combustion waves are so slow (for example, in mixtures of methane, propane, butane with air at ER < 0.7, and T_0 = 300 K, flame propagation velocity does not exceed 30 cm/s [15]) that even in milliseconds combustion can be localized near the ignition point only. One of the concepts discussed in [16], [17], [18], [19] is that the speed of combustion wave can be increased when a system of transitory weak shock waves interacts with the main combustion wave front. So, ignition of lean mixtures can be efficient if gas heating in ignition zones occurs at characteristic times shorter than a typical gas-dynamic time.

One of the solutions for efficient combustion of lean mixtures is using a lean premixed swirl burner. Although rotating gas flow stabilizes the flame by induced recirculation of hot combustion products near the nozzle [20], the flame instabilities still can be high in these burners. Recently, high efficiency of plasma control in increasing flame stability and lowering the blow-off limit were demonstrated [21], [22], [23], [24], [25]. The authors used repetitively-pulsed nanosecond discharges which effectively generate active species and gas-dynamic perturbations due to heat release in the discharge. According to [23], [24], pulsed nanosecond discharges allow stabilization of lean premixed flames in laboratory burners with plasma power typically less than 1% of the power released by the flame.

A few plasma “sub-classes” are distinguished in plasma physics. The terms "high-temperature plasma" and "low-temperature plasma", "equilibrium plasma" and "non-equilibrium plasma" are widely used. The term "high-temperature plasma" applies to the cases when the temperature exceeds 10^6 - 10^8 K and the ionization degree is close to the unity or higher. Classical examples are plasma of stellar interior of fusion plasma. In this sense, any plasma used for combustion or other "common" industrial applications, is low-temperature plasma. Low-temperature plasma is divided into equilibrium and non-equilibrium plasma. Low-temperature non-equilibrium plasma (typically corresponding to the electron temperature about thousands of K and the ionization degree on the level of $N_e/N < 10^{-3}$) was introduced into technological processes in the 70th of the XXth century [26], [27], [28]. "Non-equilibrium" means that there is no (contrary to the case of equilibrium plasma) common temperature for all the sub-systems; due to the effect of the electric field and to the hindered energy exchange between different sub-systems, such as translational, vibrational, and electronic degrees of freedom, the relation $T_g << T_e$, where T_g is gas temperature, and T_e is electron temperature, is true for non-equilibrium plasma. Mean electron energy for low-temperaure plasma, a few eV (1 eV = 11,610 K), is comparable to the energy of chemical bonds in the molecules, while gas temperature can vary between ambient and electron temperature, depending

upon the conditions. Physical details of low-temperature gas discharge plasma can be found in [26], [27], [28].

Different types of discharges were tested for PAI/PAC including pulsed nanosecond discharges, gliding arcs, microwave discharge, corona discharges, dielectric barrier discharges (DBDs) and plasma torches; the review can be found in [1], [5], [6]. Discharges used for active flow control are reviewed in [9], [10].

A possibility to control plasma parameters, in particular mean electron energy, provides the opportunity to change the energy branching in plasma mainly from the excitation of low-energy vibrational levels to the excitation of high- energy electronic states and ionization. At high electric fields, the main dissociation pathway is *via* the excitation of the electronic states of molecules by electron impact [26].

In fuel-air mixtures, the combination of the efficient excitation with fast quenching of electronically excited molecules and atoms provides: (i) dissociation of oxygen and fuel molecules, partial gas mixture reforming; (ii) an increase of gas temperature (so-called "fast gas heating", [29]) triggering development of a chain reaction of combustion or localized heat release in air initiating formation of vortices in the boundary layer for plasma flow control.

Reviews [2], [30] describe the peculiarities of the energy branching in non-equilibrium plasma and kinetics of plasma-assisted ignition; the current review focuses on the details of the fast gas heating mechanism in nitrogen-oxygen and fuel-air plasma. In this paper, the term "fast gas heating" (FGH) is used for heating occurring in the time much shorter than the time of VT-relaxation, VV- and VV'-exchange. At high pressures, the discharge usually develops as a system of thin plasma channels; in this case, FGH can be faster than a typical gas-dynamic heating.

Review [5] notices that, in spite of several significant advances in understanding of non-thermal and thermal effects, kinetic pathways of atomic oxygen production, experimental proof of lower lean blowout and flammability limits, flame regime transition of the classical ignition S-curve, there are still many missing reaction pathways in plasma assisted combustion. We believe that FGH reactions are among these missing pathways. They are uncommon either to discharge physics or to combustion but they are very important for PAI/PAC, providing, together with extra-density of radicals, an increase in gas temperature, and thus intensification of combustion reactions at sub-microsecond time scale.

Discharge/combustion chemistry and hydrodynamics are closely linked in the problem of plasma assisted combustion. Papers [31], [32] study so-called thermal-chemical instability in combustible mixtures. Heat release due to combustion chemistry leads, at times longer than gas-dynamic times, to expansion of a plasma channel. Mean electron energy in the discharge is determined by reduced electric field E/N; where E is the electric field and N is the number density of

gas [27]. Decrease of a gas density results in increase of *E/N*, efficiency of ionization and development of ionization-heating instability accompanying by contraction of plasma channel [31], [32].

We review the early papers on fast gas heating and discuss the renewal of interest in fast gas heating during the last 20 years. We provide modern ideas on the efficiency of fast gas heating as a function of reduced electric field in the discharge. An analysis of experimental approaches and measurement techniques allows estimating the accuracy of the available measurements. Since most of the data is available for non-combustible mixtures and since most practical combustion mixtures contain air, we provide a detailed review of measurements/calculations in air and a comparative analysis of hydrogen-air and hydrocarbon-air mixtures. Data on FGH in pure nitrogen and nitrogen with small additions of oxygen provide supplementary ideas on the kinetics of fast gas heating due to quenching of electronically excited nitrogen molecules, and potentially important for the development of FGH models for combustible mixtures. These data are given in Appendix.

2. Early papers on fast gas heating

Rates of generating the species is a strong (typically multi-exponential) function of *E/N*. If the duration of the discharge pulse exceeds a typical gas-dynamic time, gas heating results in a decrease in the gas number density and so, in an increase in the reduced electric field *E/N*. As a result, the ionization rate increases, the specific power increases and gas heating increases again leading finally to discharge constriction. This scenario is called ionization-heating instability [27]; in this case, the discharge contraction can significantly affect the ignition of combustible mixtures. This instability is observed in direct current (DC) discharges [27], [29], microwave discharges [33], [34], [35] and some other plasma types. Gas heating can also cause different discharge modes: it was shown in [36] that transition from Trichel pulses to pulseless glow mode of negative DC corona discharge in atmospheric pressure air is controlled by fast gas heating.

Early experimental papers [33], [37] reviewed in details in [29] reported heat release at times shorter than VT-relaxation time in MW discharge in nitrogen at reduced electric fields *E/N* = 80-200 Td (1 Td = 0.33 V cm^{-1} $Torr^{-1}$ = 10^{-17} V cm^2 at 20° C). About 10-15% of the total discharge energy released this fast way. Early papers [29], [33], [37], [38], [39], [40] concluded that fast gas heating can be explained by fast thermalization of a part of energy stored in electronically excited states of molecular nitrogen.

In [38], on the basis of observations of gas expansion, the dynamics of gas temperature in a pulsed, τ_{imp} = 1 μs, DC discharge in molecular nitrogen was measured (*P* = 100 Torr, delivered energy ≈ 0.5 J/cm^3·atm). The authors distinguish two stages of gas heating: fast, with the energy release about 10% of the energy stored in the discharge - within 30 μs, and slow, corresponding to the energy release of 40% within 0.5 ms. Theoretical study [41] explained the slow stage using a model of VV-exchange in the system of anharmonic oscillators. However, any attempts to explain

the fast stage have failed. It was underlined [41] that the observed effect can be a consequence of heat release due to the quenching of electronically excited nitrogen molecules. Similar results were obtained in a wide range of delivered energies in [39], [40] etc.

Later studies [33], [37], [42] reported time-resolved temperature measurements in a pulsed microwave discharge. The majority of measurements was made in nitrogen and air at pressures P = 10 - 40 Torr and reduced electric fields E/N = 80 - 250 Td. Details of the experimental techniques are given in the section 4. The results confirmed an increase in gas temperature (as observed earlier) faster than VT-relaxation. It was also shown [33] that the rate of fast gas heating increases with gas pressure and significantly increases with electric field reduction.

A suggested theoretical explanation of fast gas heating involved the fact that a substantial amount of energy, up to electron volts, is released in collisional deactivation of electronically excited nitrogen molecules – and so the greater is electric field reduction, the higher is fast gas heating. The first proposed kinetic mechanism was based on pooling reaction of $N_2(A^3\Sigma_u^+)$ molecules [37], [42]:

$$N_2(A^3\Sigma_u^+) + N_2(A^3\Sigma_u^+) \rightarrow N_2(B^3\Pi_g, v) + N_2(X^1\Sigma_g^+, v').$$

However, the model based on pooling reaction did not explain the experimental data on the heating rate in the mixtures with different percentage of molecular oxygen [33], [42]. According to the model, fast gas heating should decrease in $N_2 : O_2$ mixtures as a consequence of $N_2(A^3\Sigma_u^+)$ depletion through quenching by O_2 molecules, while the experimentally measured heating rate increased with oxygen fraction [42]. In [43], it was suggested that quenching of electronically and vibrationally excited molecular nitrogen at the levels higher than $N_2(A^3\Sigma_u^+, v$=3,4) (the excitation energy is 6.6 eV) in collisions with ground state N_2 molecules results in energy release for gas heating. For example, quenching of $N_2(a^1\Pi_g)$-state with the excitation energy of 8.6 eV provides about 2 eV for FGH. This suggestion was in contradiction with the available experimental data [44], [45] showing that quenching of electronically excited nitrogen by ground state $N_2(X^1\Sigma_g^+)$ molecules results in minimum possible energy release for gas heating.

Thus, several models of fast gas heating ([33], [37], [43]) were suggested before 2000. They allowed describing a part of the experimental data in the narrow range of electric fields. Over the past 20 years, the development of a comprehensive model of fast gas heating in a wide range of the fields, E/N = 50 - 1000 Td, has become an important task.

3. Renewal of interest in fast gas heating during the last 20 years. Fast gas heating in air as a function of reduced electric field

The renewal of interest to fast gas heating was provoked by the study of plasma flow control [7], [8], [9], [46], [47], [48] and plasma assisted ignition and combustion [1], [2], [4], [5], [30], [49], [50], [51], [52] by pulsed nanosecond discharges. A peculiarity of nanosecond plasma is that

the electric fields in the discharge are high, on the order of 100 Td and higher [53], [54], [55], [56], [57].

Surface dielectric barrier discharge (SDBD) plasma actuators powered by nanosecond duration pulses demonstrate flow reattachment at high flow velocities up to M = 0.85 [58]. The main difference of the actuators powered by nanosecond pulses, comparing to the alternative current (AC) DBD actuators, is synchronized, on a sub-nanosecond time scale, start of parallel plasma channels (streamers) from the edge of the high-voltage electrode. Each streamer generates weak compression waves caused by fast heat release in the discharge on the time scale shorter than the acoustic time scale. In airflow configuration of the electrodes, two waves are observed - a spherical wave near the high-voltage electrode and a cylindrical wave along the plasma channel. The resultant of individual waves from each streamer generates two compression waves: a cylindrical wave along the high-voltage electrode and a plane wave from the dielectric surface [8], [59], [60], [61]. As a result, the nanosecond SDBD discharge, repeating with a certain frequency in the flow around the airfoil, excites shear layer instabilities and generates coherent flow structures (spanwise vortices) providing flow reattachment [47], [58], [62].

Two important effects related to fast heat release should be noted in applications of nanosecond plasma for combustion: first, temperature increase induces acceleration of chemical reactions providing shortening of the induction delay time and intensification of combustion process [2], [4], [5]; second, in particular case of pulse-periodic nanosecond discharges, fast heat release in each pulse causes gas-dynamic perturbations. Interaction of these perturbations with already existing heat region causes expansion of the region over a large volume (a cubic centimeter at atmospheric pressure) within a time shorter than the typical ignition delay time [63]. These effects, together with fast and efficient production of radicals, provide significant, of a few orders of magnitude, reduction in the ignition delay time or sustain combustion of lean mixtures.

With the exception of hydrogen and simplest hydrocarbons, the fraction of fuel molecules in stoichiometric and lean fuel-air mixtures is relatively small. Fast gas heating in these mixtures is based mainly on the kinetics of fast gas heating in nitrogen-oxygen mixtures. This is a reason why we will first analyze the mechanism of gas heating in air and in nitrogen with O_2 admixtures, and then will review the FGH features in stoichiometric hydrogen-air and methane-air mixtures.

To systematize knowledge gained from work on different plasmas, it was vitally important to select some universal parameters to describe fast gas heating. The experiments were made in different discharges at different reduced electric fields, at different initial pressures and specific delivered energy. The parameter suggested in [29], [64] is the fraction of a total energy delivered to plasma spent on fast gas heating η_R. We will call this parameter the energy efficiency of fast gas heating. The value of η_R is a function of reduced electric field in the discharge and practically does

not depend upon the electron density and gas pressure. The available experimental data and theoretical curves are given in Figure 1 as a function of the FGH efficiency η_R upon reduced electric field *E/N*.

The data were obtained in air at different pressures, from 3 Torr [65] to 800 Torr [66]. The symbols represent the experimental results [65], [66], [67], [68], [69], [70], [71]. The results of calculating the energy efficiency of fast gas heating $\eta_R(E/N)$ according to the model [29], [64] are given by the curve (I); the maximum theoretically possible value $\eta_R^{max}(E/N)$ = 100% - $\eta_{diss}(E/N)$ is given by the curve (II). Here, η_{diss} is the fraction of the discharge energy spent to dissociation of nitrogen and oxygen molecules, calculated using *Bolsig+* code [72] assuming that quenching of $N_2(A^3\Sigma_u^+, B^3\Pi_g, C^3\Pi_u, a'^1\Sigma_u^-)$ electronically excited states by molecular oxygen results in O_2 dissociation.

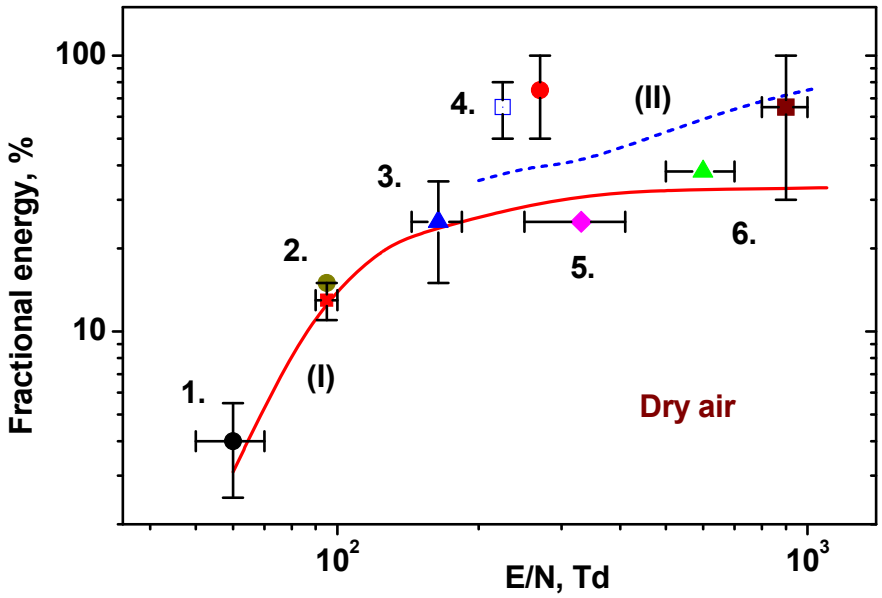

Figure 1. Fraction of energy spent on fast gas heating η_R (or the energy efficiency of FGH) as a function of *E/N*. Symbols represent the experimental data: 1 - [67], 2 - [68], 3 - [70], 4 - [71], 5 - [65], 6 - [66]; lines are the results of calculations (see text for details).

4. Experimental approaches: measurements related to fast gas heating

Only a few tens of papers on experimental studies simultaneously quantify the rate of energy thermalization in the known electric field and the magnitude of temperature rise with nanosecond resolution; our review of the experimental technique and accuracy of measurements will be based mainly on these publications. Early experimental studies of fast has heating at the second half of the 20th century [37], [39], [40], [67] were motivated by the use of gas discharges as active media for lasers; stability of volumetric discharges was influenced by the change in gas temperature. The results of fast energy release are available mainly for two gas discharges at moderate pressure: stationary DC self-sustained discharge powered by a voltage pulse with a 100-ns high voltage peak and sub-microsecond plateau after the peak, the discharge ignited in molecular nitrogen at *P* = 76

Torr [39], [40]; and pulsed microwave (MW) discharge in nitrogen and air with 10% of NH_3 at total pressure of 8 - 30 Torr [37].

Volumetric DC discharge in nitrogen, 2.5×4×40 cm^3, was initiated with the help of UV pre-ionization from multiple spark discharges situated 2.4 cm apart from the grid cathode. The authors report, without detailed explanations, a stationary value of reduced electric field to be around (7-8)·10^{18} V·cm^2. Laser interferometry (using He-Ne laser in [39] and ruby laser in [40]) provided, with a resolution of one microsecond, the map of gas density changes. The authors observed a region of enhanced heat release in the discharge at the time scale shorter than typical acoustic time [39], [40] and supposed, on the basis of theoretical consideration, that (i) rapid energy release is explained by relaxation of energy from electronic levels directly to heat; (ii) the fraction of energy spent to fast gas heating is a function of reduced electric field, *E/N*.

The advantage of a self-sustained microwave discharge localized in space is that the value of electric field *E* can be obtained with known amplitude of the electric field, discharge frequency and gas density: $E = \frac{E_{mw} \cdot \nu_e}{\sqrt{2(\nu_e^2 + \omega^2)}}$, where ν_e is the electron-neutral collision frequency, E_{mw} and ω are the amplitude and the frequency of the MW field respectively.

Intracavity laser absorption was used to measure the distribution of population of the NH_2 molecule rotational levels in pulsed (60 μs) self-sustained microwave discharge, freely localized in space [37]; the accuracy of rotational temperature measurements was reported to be 10%. Spatial resolution of measurements was limited by the laser beam diameter, 3 mm, and temporal resolution was determined by the laser generation duration, 1.5 μs. Rotational temperature was additionally measured by optical emission spectroscopy of the second positive system (SPS) of molecular nitrogen; two techniques have shown good consistency. The authors reported that during the pulsed MW discharge, the rate of gas heating is up to 10-15 K/μs. The final rotation temperature was about 500 K.

Early experiments on fast gas heating do not provide experimental information about specific delivered energy, furthermore, no data on FGH are available for the reduced electric field exceeding 100 Td. These data have been obtained recently for pulsed nanosecond discharges [65], [66], [69], [71], [73], [74], [75], [76], [77], [78]. It should be noted that measurements using laser interferometry, available only in the earliest papers [39], [40], appear again in the latest publications [79], [80] combining schlieren and interferometry techniques with time resolution of 70 ps and spatial resolution of 3-4 μm.

The experimental techniques to study fast energy release in nanosecond discharges include time-resolved voltage and current measurements for all papers analyzed below and different supplementary measurements, namely capacitive probes to measure electric field [65], [76], [78]; optical emission spectroscopy to measure rotational distribution related to gas temperature [65], [66], [69], [70], [73], [76], [77], [78], schlieren or shadow imaging [66], [71], [74] related to energy

release and allowing, in some cases, judgment about delivered energy or energy density; E- (SRS) to measure gas temperature and vibrational distribution of N_2 and O_2 molecules in early afterglow at atmospheric pressure [69], [75]; picosecond CARS spectroscopy [74] at moderate pressure to measure time- and space-resolved gas temperature.

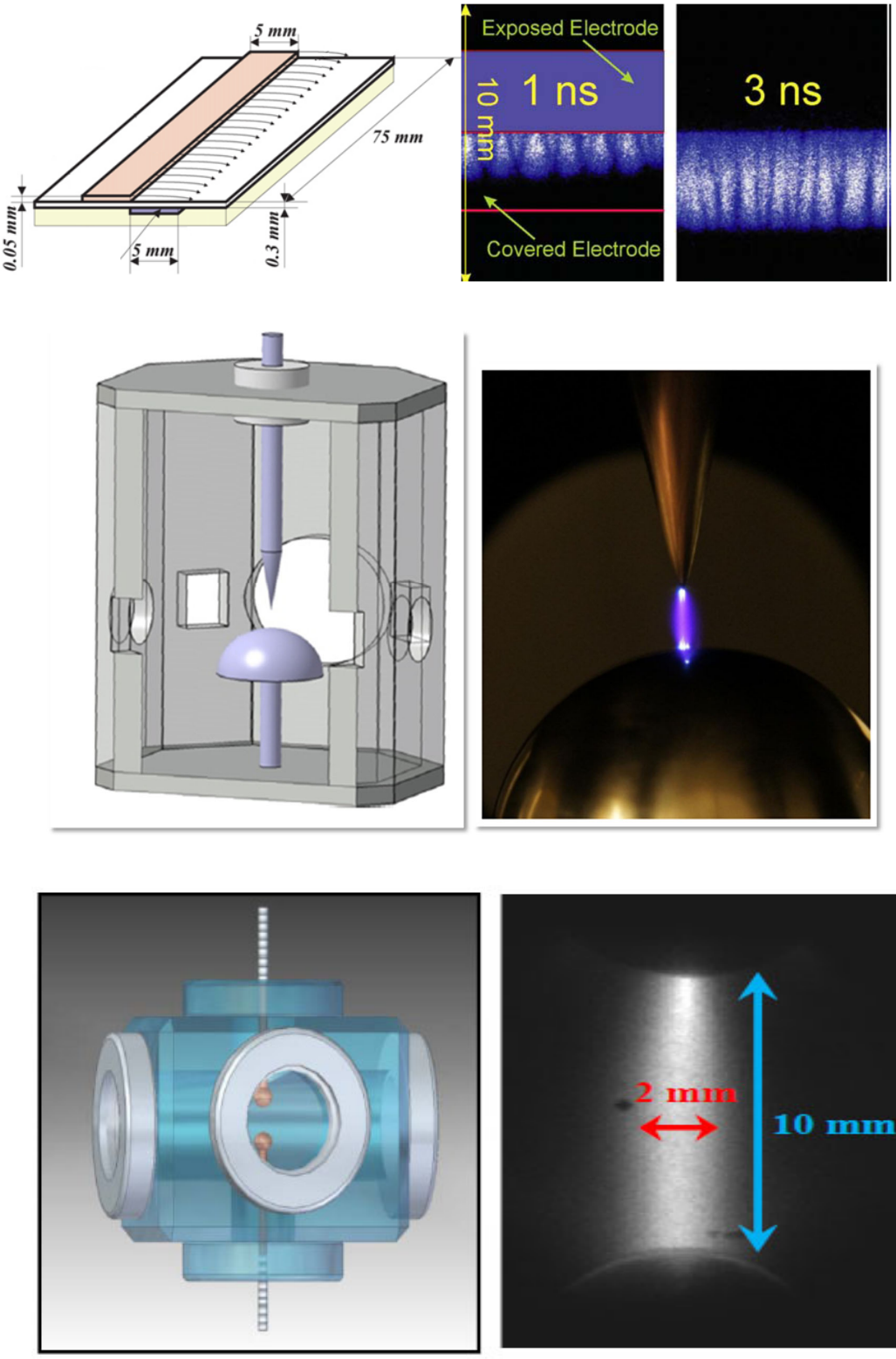

Figure 2. Typical geometries of the discharge cells used to study fast gas heating (line-by-line: [8], [81], [74]).

A few geometries of nanosecond discharges were used to quantify FGH experimentally: surface dielectric barrier discharges similar to airflow configuration at pressure between 300 Torr and 1 atm [66], [77], pin-to-pin atmospheric pressure discharges at room or elevated (up to 1000 K) initial temperature [69], [70], [71], [73], [75], and uniform volumetric discharges at moderate pressure and initial temperature T =300 K [65], [66], [76], [78] including the volumetric nanosecond glow discharge not confined in the discharge tube [74]. The examples of experimental setups are shown in Figure 2.

Obtaining experimental waveforms of voltage on the electrodes and electrical current is similar for all the considered nanosecond discharges. Commercially available or custom-made broadband voltage and current probes based on the principle of capacitive/resistive voltage/current division or on the measurement of magnetic flux through the coil are typically used. It is important to take into account the time of the electromagnetic signal propagation through the cables (the speed of electromagnetic wave for coaxial cables with polyethylene filling is about 20 cm/ns) and to provide synchronization within a part of nanosecond between the waveforms.

Energy deposited in the discharge is obtained by multiplying voltage and current waveforms, and integrating the result over time:

$$W = \int_0^\tau U(t) \cdot I_{cond}(t) dt$$

$U(t)$ is a voltage over the discharge gap and $I_{cond}(t)$ is a conductivity current. Special precautions are usually taken to extract, before the integration, the current of charging the discharge cell capacitance before the development of conductivity and the displacement current I_{disp}. Displacement current can be found knowing reactor capacitance C and time derivative of voltage dU/dt [69], [70], [71], [73], [75]:

$$I_{disp} = C \cdot dU/dt;$$
$$I_{cond} = I_{tot} - I_{disp}.$$

Another approach to find the energy deposited in plasma was used in [65], [66], [76], [77], [78] where the discharge cell was inserted into a break of a long coaxial cable. The length of the cable between the high voltage pulse and the discharge cell, several tens of meters, allowed separate measurements of the incident pulse and the pulse reflected from the discharge cell because of electrical mismatching. The cable after the discharge cell, up to 200 m in length [65], [76] provided an adjustable delay between the discharge and the probe pulse due to the mismatching and different values of the terminal load, for the measurements of plasma parameters in early afterglow. Calibrated custom-made back current shunts were installed in the cable before and after the discharge cell, at a distance about 15 m from the cell. The following electric current pulses were measured: incident I_{inc}, reflected from the discharge cell I_{ref} and transmitted through the discharge cell I_{tr}. Attenuation in the cable and charging of the electrode were taken into account by calibration at

well-defined conditions, at too low or too high pressure for the discharge development. The absence of the discharge was checked by the absence of the emission and the absence of ionization wave. Finally, the energy deposited in the discharge was found as the difference between the energy stored in incident pulse, and the sum of energies in reflected and transmitted pulses:

$$W = \int I_{inc}^2(t) \cdot Z dt - \int I_{ref}^2(t) \cdot Z dt + \int I_{tr}^2(t) \cdot Z dt$$

Here Z is a characteristic impedance of the cable. In case of discharge with open electrodes, the accuracy of measurements of total energy delivered to the discharge can be as low as a few percent (3-5%). In case of capacitive load, such as the discharge in surface DBD configuration, the current for charging the electrode can be comparable to or higher than the current flowing when generating plasma, causing possible systematical errors. We estimate maximum possible error of energy measurements for the capacitive load as 15-20%.

Time-resolved emission from the discharge is used to analyze the discharge uniformity and to estimate the plasma volume in case of non-confined discharge. In case of nanosecond discharges, the main input to the emission in the near UV and visible range is due to transitions of the second positive system (SPS) of molecular nitrogen. For air, the quenching time of SPS radiation is determined by collisions of $N_2(C^3\Pi_u)$ state with molecular oxygen, the rate constant being equal [82] to $k_q = 2.7 \times 10^{-10}$ cm^{3}s^{-1}. The efficient lifetime of $N_2(C^3\Pi_u)$ is 0.7 ns at atmospheric pressure, thus ICCD imaging adequately reflects the discharge spatial structure, and time resolution is limited by the camera gate.

Typically, to experimentally obtain specific delivered energy, total delivered energy is divided by the discharge volume assuming that spatial energy distribution is uniform in plasma. More sophisticated approach can be used when analyzing experimental results with numerical modeling: electric field in the discharge is calculated in 1D radial approximation at a given initial distribution of electrons and waveform of the conductivity current derived from the experiments. The resulting E-field is used to calculate total energy delivered to plasma, and experimentally measured deposited energy is used to validate the data. Finally, we can derive specific delivered energy from the calculations for any distance from the discharge axis.

Time- and space-resolved emission of the second positive system of molecular nitrogen was used in [66], [77] to estimate the specific deposited energy in a spatially non-uniform case of a surface DBD discharge. Although the idea on the proportionality between energy input and the intensity of $N_2(C^3\Pi_u)$ emission is controversial, this was a reasonable approximation in case of a complex 3D structure of the SDBD discharge. Measurement accuracy of plasma volume and the discharge spatial uniformity influence calculation accuracy of specific delivered energy, and each case should be analyzed separately. As confirmation of the controversy situation, we provide (see

Figure 3) the results of calculating radial distributions of electron density and emission of the second positive system for plasma channel in atmospheric pressure air. Different FWHM values, 0.16 mm for the electron density and 0.25 mm for emission, are clearly seen.

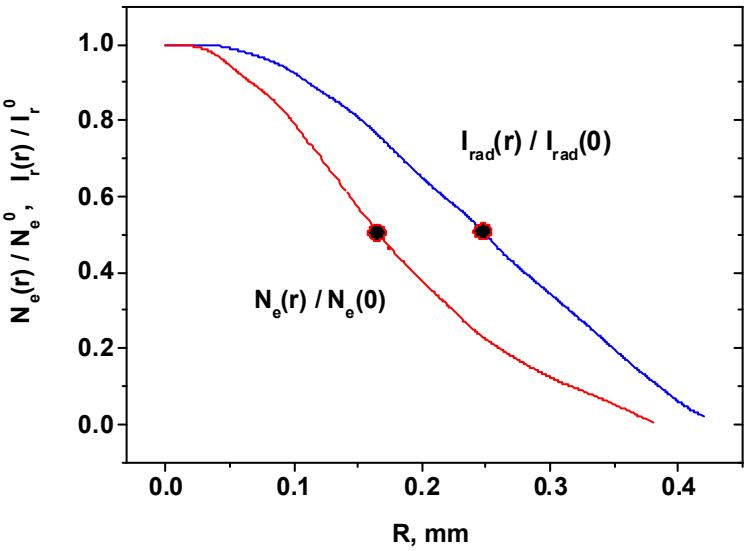

Figure 3. Radial distribution of electron density and emission of the second positive system of molecular nitrogen in air built based on the calculations [83]; R_0 = 0.16 mm, R_1 = 0.25 mm.

Direct electric field measurement is a complicated issue. In non-confined open electrode discharges [70], [74], the electric field is often estimated as the ratio of the applied voltage and the gap distance. The electric field in pin-to-pin atmospheric pressure discharge was estimated to be 250 Td or less during the discharge [70]; the electric field in nanosecond glow discharge [74] was estimated to be equal to 120 Td, and 90 Td upon the correction to the voltage drop on the cathode layer. Taking into account that a few data are available about the cathode voltage drop in nanosecond discharges, we estimate the accuracy of electric field provided this way as 15-30%. The reduced electric field in the surface DBD discharge [66], [77] was estimated from the ratio of the emission profiles of the first negative system (391.7 nm) of nitrogen ions and the second positive system (337.1 nm) of nitrogen molecules. The key idea of the technique is that if excitation occurs by direct electron impact and the radiation comes from the same spatial region for both molecular bands, then the ratio of the emission intensity for the bands, corrected for the quenching, is uniquely related to the absolute electric field value at a given point. The details are given in [84], [85], [86]. A few recent papers [87], [88], [89] discuss restrictions and the accuracy of *E*-field measurements by optical emission spectroscopy.

The restrictions can be significant for surface discharges: at least part of emission of electronically excited ions comes from a spatial region near a dielectric layer, while emission of excited molecules is integrated over all the streamer thickness [54], [90]. Spatial distribution of emission of the two considered transitions was analyzed in [54] experimentally and numerically. The main conclusion is that the results of measurements and calculations are in reasonable agreement for

negative polarity discharges; for positive polarity discharges, the measured ratio of emission of two transitions corresponds to higher values of emission of the nitrogen ion than that resulting from the modeling, indicating possible high electric fields. The values given in [66], [77] for the reduced electric fields (1000-1200 Td) are the highest provided in the review; we estimate their accuracy as at least 30 - 50% based on the analysis in [54] for a similar discharge.

The difficulties with the electric field measurement can be minimized if the discharge is confined in the long tube. In this case, the discharge develops as a fast ionization wave (FIW), where the ionization front develops with high velocities, up to a few cm per nanosecond. After passing the discharge front, the field is mainly longitudinal and can be measured by calibrated capacitive detector moving along the discharge gap in the slit of the metallic screen. In [65], [76], [78] the capacitive divider made measurements each 1 mm along the discharge gap; the accuracy limit of measuring the electric field behind the FIW front, in the region of the main energy input, can be estimated as 5-10%.

Over the last decade, considerable progress has been made in electric field measurements by picosecond laser techniques of E-field measurements. We can mention four-wave mixing [55] and the Electric Field Induced Second Harmonic (E-FISH) generation technique [56], [57]. Time resolution is limited by the laser pulse duration and the registration technique (e.g. oscilloscope bandwidth) and is typically sub-nanosecond. Spatial resolution can easily be sub-millimeter. These techniques are new, and although they are very promising, at the moment, (i) there is still questions about validation of the experimental approaches used [91]; (ii) no study combining the E-field measurement by laser techniques, specific delivered energy and gas temperature is known.

Measurements of gas temperature in nanosecond discharge are often based on analyzing the emission of rotational lines of the second positive system of molecular nitrogen [65], [66], [69], [70], [73], [75], [76], [77], [78]; the details of the technique for measuring rotational distribution in plasma are discussed in [92]. Typically, rotational distribution is a Boltzmann distribution, $\exp(-E_{rot}/(kT_{rot}))$, with rotational energy E_{rot}, Boltzmann's constant k and rotational temperature T_{rot}. The relation between rotational temperature of the excited specimen and the gas temperature value depends upon the rate of relaxation. There are two limiting cases depending upon the ratio of the experimentally observed lifetime of the emitting state t_{col} (including quenching in collisions) and characteristic time of rotational-translational relaxation t_{RT}. If $t_{col} >> t_{RT}$, the emitting atom/molecule is in the thermodynamic equilibrium with surrounding gas and measured rotational temperature T_{rot}^{exp} is equal to gas temperature. In another limiting case where $t_{col} << t_{RT}$, the molecule emits light without any perturbation of rotational distribution initially formed in the discharge.

In the last case, we should consider the history of excitation of the upper $N_2(C^3\Pi_u)$ level. At high *E/N* values typical for the nanosecond discharges, the main population of $N_2(C^3\Pi_u)$ is due to

direct electron impact, and rotational distribution of the excited state is similar to rotational distribution of the ground state according to the Franck-Condon principle. The ground state rotational temperature is equal to the translational one, and gas temperature can be calculated as

$$T_{rot}^{X} = \frac{B_e^X}{B_e^C} \cdot T_{rot}^{C}$$

where T_{rot}^{X} is ground state rotational temperature, and T_{rot}^{C} is the rotational temperature of $N_2(C^3\Pi_u)$ state, and $B_e^X/B_e^C = 1.998/1.825 = 1.095$ is the ratio [93] between rotational constants of $N_2(X^1\Sigma_g^+)$ and $N_2(C^3\Pi_u)$ states, respectively.

The disadvantage of emission optical spectroscopy technique is that spatial distribution of emission intensity should be taken into account. If plasma is axisymmetric, an Abel inversion is applied to get the optical emission intensity distribution over the radius [69], [70], [73], [75]. If rotational temperature is different in different regions, the resulting emission contains the information about some averaged efficient rotational temperature and this should also be analyzed [66], [77], [78]. Optical emission spectroscopy provides quite high accuracy of measurements of a few K in ideal uniform case with a single-temperature Boltzmann distribution over rotational lines. In conditions of non-uniform gas discharge plasma, the accuracy can vary from tens of K to a few hundreds of K, depending upon the experimental situation and the approach to the treatment.

Only a few papers studying the fast gas heating report alternative techniques of temperature measurements [66], [69], [71], [74], [75]. Shock wave propagation through the afterglow of a nanosecond pulsed gas discharge with different delays relative to the beginning of the discharge was studied in [66]. Heat release in the afterglow was calculated from the acceleration of the shock wave. The maximum observed increase in the shock wave velocity of 10-14% was obtained at delays of 100-200 μs after the discharge. Reduced electric field and deposited energy were measured in [66] as in fast ionization wave using custom-made calibrated current and voltage probes.

To determine the initial gas temperature and the fraction of energy transferred for ultrafast gas heating in the spatially non-uniform pin-to-pin open electrodes nanosecond discharge [71], contrast profiles resulting from experimental and numerical Schlieren images were compared. The suggested method is called “numerical Schlieren” and, according to [71], it is much more sensitive to gas temperature and fraction of energy transferred for heating than direct comparison of measured and predicted shock-wave and heated channel radii. The authors calculate the fraction of heating energy η_R and initial temperature T_0 through the following procedure: (1) fit the heated channel radius to get η_R, (2) fit the shock-wave radius to get initial temperature T_0 using η_R obtained in step (1), (3) check the contrast profiles to verify η_R and T_0 calculated in steps (1) and (2). They report the accuracy of gas temperature measurements by using the suggested technique to be equal to 6-25%, and the accuracy of η_R value determined simultaneously, to 4-33%.

Laser methods provide the highest possible spatial resolution. For example, laser technique was used for time- and space-resolved measurements of gas temperature in [74], where picosecond

CARS spectroscopy and phased-locked Schlieren imaging were used to measure time-resolved temperature and visualize compression waves in a nanosecond pulsed discharge between a pair of spherical electrodes in nitrogen and air at P = 100 Torr. A histogram of 80 spectra obtained under identical conditions yielded mean value of T = 302 K with a standard deviation of 1.5%. The authors reported a significant temperature rise up to ΔT = 200 K at 100 ns in air and at 1 μs in nitrogen, as well as the second temperature peak ΔT = 350 K at 100-500 μs in air.

In pin-to-plane atmospheric pressure nanosecond discharge in air initiated by high voltage pulses of 25 kV and 25 ns [69], [75], gas temperature during pulsed discharge was measured by OES of rotational bands in the 0-0 vibrational transition of the molecular nitrogen second positive system, while gas temperature in the afterglow and vibrational distribution function (VDF) of $N_2(X^1\Sigma_g^+)$ and $O_2(X^3\Sigma_g^-)$ molecules were obtained by spontaneous Raman scattering (SRS). The SRS measurement resolution was equal to 180 micrometers. SRS was induced by the second harmonic (532 nm) of a Nd:YAG laser; pulse duration was about 100 ns. Two thousand shot-averaged N_2 or O_2 experimental Raman spectra were acquired to get the desirable signal-to-noise ratio. The measurements were made at 1.5, 3.25 and 5 mm from the pin electrode, the interelectrode space being equal to 6.5 mm. The authors reported the accuracy of OES measurements as ± 50 K [69]; the accuracy of gas temperature SRS measurements are reported to be less than 5% [75]. The temperature rose up to 1400 K during first 300 ns of the post-discharge; strong vibrational excitation of N_2 and weak excitation of O_2 vibrational levels were detected; the second peak of translational temperature caused by V-T relaxation was observed between 50 and 100 microseconds. To measure densities of N_2 and O_2 in the ground state in time and space, the authors integrated the experimental SRS spectrum of each species knowing the Raman differential cross sections, the temperature, collection efficiency, laser power deposited and the probe volume length. The main error sources in these measurements were (i) the accuracy of temperature measurements of 5%; (ii) uncertainties in spectroscopic constants used for the calculation of the differential Raman cross section which are, according to [75], “more difficult to estimate”. Finally, from the measurements of N_2 and O_2 vibrational distributions and gas temperature, the authors calculated relative distribution (in time and space) of the energy deposited in the specific molecular modes. The energy deposited in fast gas heating calculated 150 ns after the increasing front of the electrical current, was reported to be 19% of the total energy deposited. At that time instant, the authors observed a high dissociation ratio of O_2 molecules, up to 33% on the axis of the discharge channel [75]. It should be noted that one of the main processes leading to fast gas heating is the dissociation of molecular oxygen in collisions with electronically excited N_2 molecules. This means that fast gas heating and high dissociation degree of O_2 in air are interrelated and appear together. This fact was proven experimentally for the atmospheric pressure pin-to-pin discharge in air preheated to 1000 K [70], where the temperature increase by 900 K during 20 ns is accompanied by 50% of dissociation of molecular oxygen, and for moderate pressure capillary nanosecond discharge in 24 - 30 mbar

synthetic air at initial room temperature [78], and where the temperature increase to 2000-2500 K during 1-2 microseconds after the discharge with duration of 30 ns, is accompanied by complete dissociation of oxygen [76].

5. Fast gas heating in air: experimental study and chemical kinetics

This section contains detailed analysis of data on fast gas heating shown in Figure 1. The analysis is grouped over three different ranges of the reduced electric field: $E/N \leq 120$ - 130 Td (subsection **5.1**), $E/N = 150$ - 400 Td (subsection **5.2**) and $E/N > 400$ Td (subsection **5.3**). For ease of analysis of a relative role of various processes in the mechanism of FGH, the calculated contribution of different reactions to fast gas heating are presented in Figure 4.

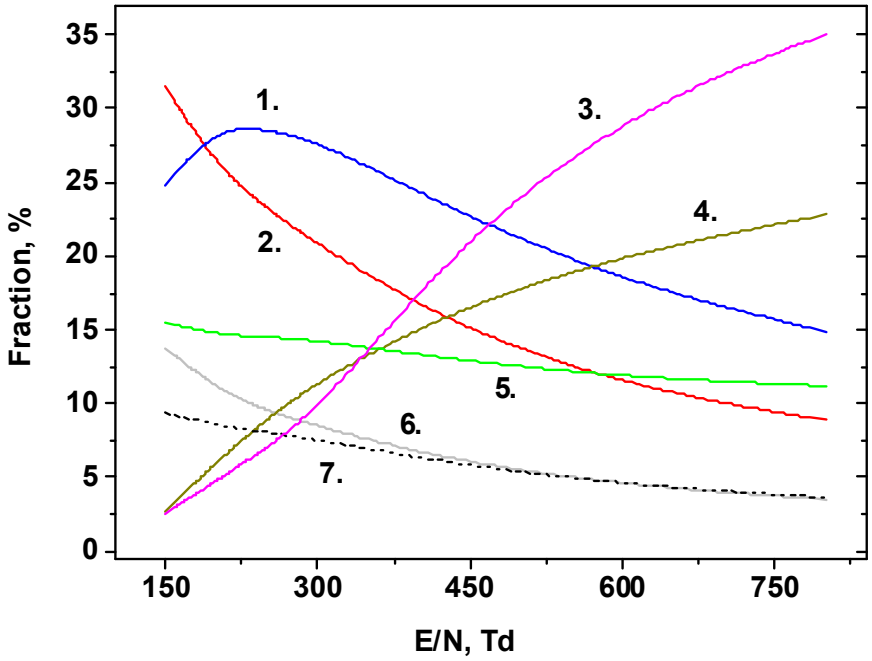

Fig. 4. Calculated dependence of contribution of each of the processes (1 - 7) to the overall balance of the fast gas heating on E/N [64]. Calculations are performed for air heating at P = 760 Torr, T_0 = 300 K.

Curves (*1-7*) correspond to the following processes: *(1)* is for quenching of the $N_2(C^3\Pi_u)$ states by oxygen; *(2)* is for quenching of the $N_2(B^3\Pi_g)$ states by oxygen; *(3)* is for reactions involving charged particles; *(4)* is for dissociation of N_2 molecules by electron impact followed by quenching of $N(^2D)$ atoms; *(5)* is for quenching of excited $O(^1D)$ atoms by nitrogen; *(6)* is for dissociation of O_2 molecules by electron impact; and *(7)* is for quenching of the excited molecules $N_2(A^3\Sigma_u^+)$ and $N_2(a'^1\Sigma_u^-)$ by oxygen. This processes will be discussed in details in the Section 6.

5.1. Studies of fast air heating in the field range of $E/N \leq 150$ Td

The papers [42], [94] considered the heating of $N_2 : O_2$ mixtures by a pulsed microsecond discharge in a tube with a radius of $R = 0.5$ cm at pressures $P = 0.4$ - 1 Torr. The average discharge

current density was j = 0.5 - 10 A/cm^2 at a pulse duration $\tau \leq 100$ μs. Gas temperature was measured with a time resolution of 1 μs by relative intensities of the rotational transition structure lines (v'=0 → v''=2) of the second positive system of molecular nitrogen.

Calculations [29] , performed for the conditions of the experiments [42], show that at t >10 μs both E/N and electron density vary insignificantly, amounting to E/N = 95 ± 2 Td and N_e = (2-3)·10^{12} cm^{-3}, respectively. At these times, an approximately constant rate of gas heating should be expected.

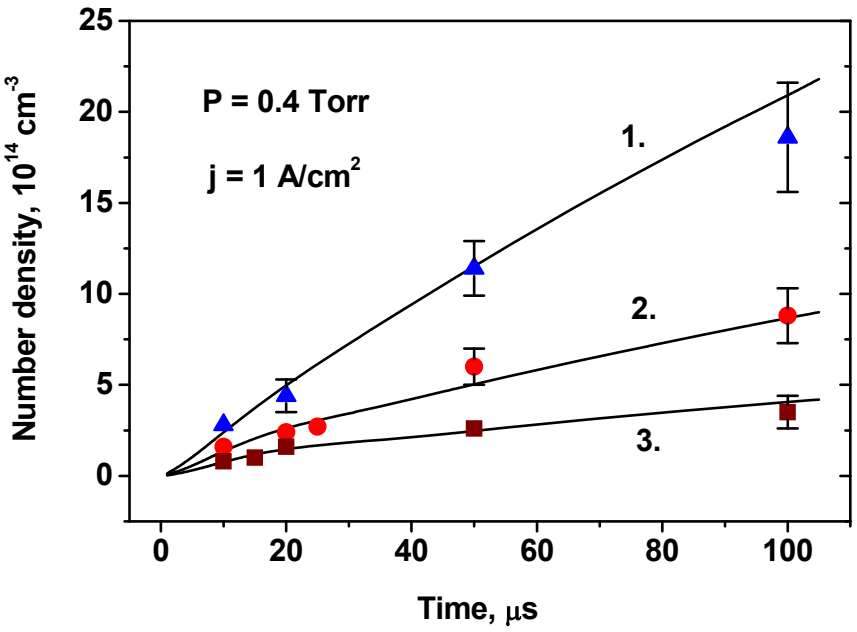

Figure 5. The dynamics of O(^{3}P) density at the discharge axis in N_2 : O_2 mixture at P = 0.4 Torr, j = 1 A/cm^2 and different fractions of oxygen in the mixture: 1 - 20%, 2 - 8.5%, 3 - 4%. The symbols represent experimental data [42] (in arb. units), the curves represent calculation results [29].

In [42], along with gas heating, kinetic curves of oxygen atoms in arbitrary units were measured. The corresponding values of $[O(^3P)]_{rel}$ were calculated based on the measurements of relative emission intensity for line O($3p^3P \rightarrow 3s^3S$) of oxygen atom and bands $N_2(C^3\Pi_u \rightarrow B^3\Pi_g)$ of the 2$^+$ system of nitrogen. Temporal evolution of O-atom density at P = 0.4 Torr and j = 1 A/cm^2 is shown in Figure 5 for different values of oxygen fraction in the mixture. To compare the experiments with the results of calculations (curves 1-3 in Figure 5), the corresponding relative values are multiplied by 6·10^{14} cm^{-3}. Dissociation degree of molecular oxygen at the end of the discharge pulse is approximately $[O(^3P)]/[O_2] \approx 1$ and weakly depends on oxygen fraction.

Figure 6 shows experimental data [94] (symbols) and the results of calculations [29] (solid curves) of air heating dynamics near the discharge axis at P = 0.5 Torr. Curves 1 - 3 correspond to the average values of current density j = 4 A/cm^2, 2 A/cm^2, and 1 A/cm^2 (I = 3.14 A, 1.57 A, and 0.785 A). The results of calculations [29] are in good agreement with experimental data. The

dashed line represents the calculation for $j = 4$ A/cm^2 without taking into account gas cooling due to the thermal conductivity; the difference with solid line 1 at $T \geq 800$ K is clearly seen.

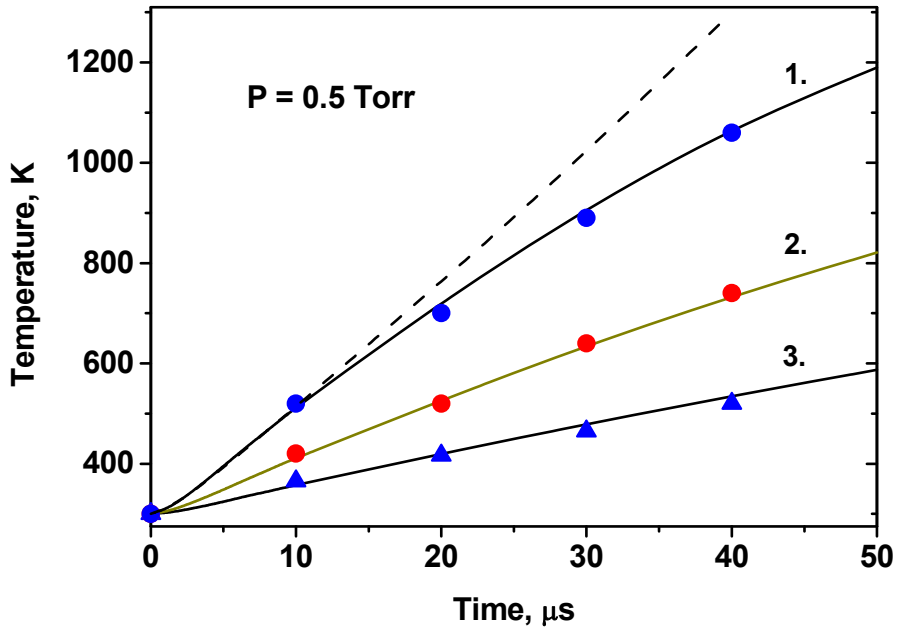

Figure 6. The dynamics of gas heating in the discharge with parameters [94]: $P = 0.5$ Torr, with current density: 1 - $j = 4$ A/cm^2, 2 - 2 A/cm^2, 3- 1 A/cm^2. The symbols represent experimental data [94], the curves represent the results of calculation [29], see text for the details.

We describe FGH as fast relaxation of energy from charged and electronically excited species in reactions with atomic and molecular particles. This is different from relatively slow process of VT-relaxation. Fast gas heating is more efficient at high E/N because more energy is stored in high energy electronic states of atoms and molecules [26], [95]. The effect of VT-relaxation acceleration by fast gas heating due to an increase in gas temperature at the initial stage of the discharge and thus an increase in VT-relaxation rate has been observed experimentally. In [67], measurements of gas heating were made in a pulsed glow discharge in air at $P = 6$ Torr, $I = 0.9$ A. The discharge tube radius was $R = 1.5$ cm. Radial profiles and time dynamics of gas temperature were studied with an optical interferometry method. Under the considered conditions, E/N varies in the range of 50-70 Td [29] and the main part of the discharge energy is spent to vibrational excitation of nitrogen molecules. The most of gas heating is caused by VT-relaxation in collisions with oxygen atoms.

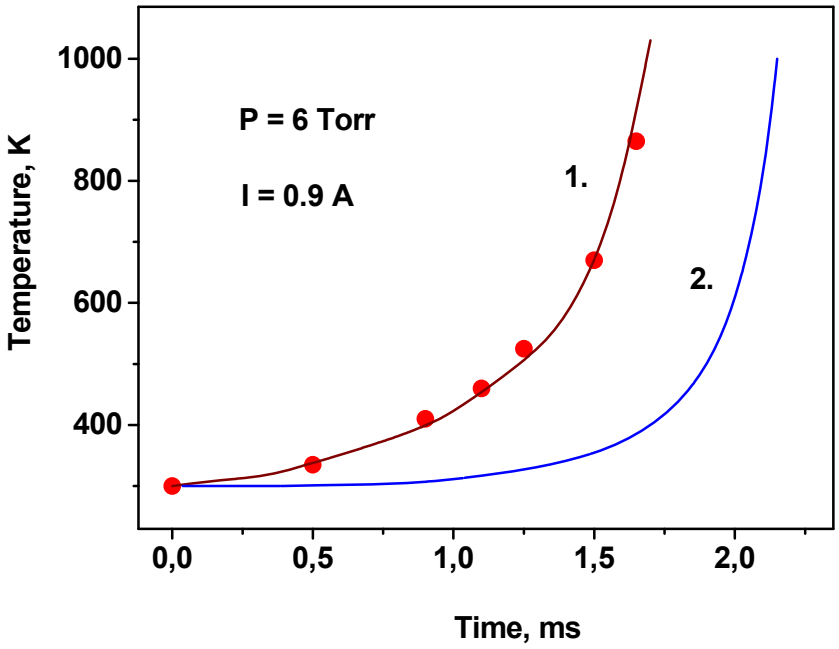

Figure 7. Gas heating dynamics at the axis of a glow discharge in air. The points represent experimental data [67], the curves represent calculations with (1) and without (2) taking into account the mechanism of fast gas heating [29].

Figure 7 shows experimental [67] and calculated [29] time dependences of gas temperature near the discharge axis. Calculations based on a model involving fast gas heating due to the relaxation of the electronic excitation of atoms and molecules (curve 1) are in good agreement with experimental data. Temperature increase caused only by VT-relaxation (curve 2) is much slower: there is a 500 - 600 μs delay in gas heating time.

In [42], [67], [94] measurements were made at relatively low gas pressures of $P \leq 6$ Torr. Modern experiments provide information about fast heating at pressures close to atmospheric. Measurements of gas temperature and vibrational distribution function (VDF) of N_2 molecules in atmospheric pressure air excited by a pulsed nanosecond discharge are provided in [69]. The discharge was ignited in the point-to-plane gap at interelectrode distance $d = 6.5$ mm and pulse repetition frequency $f = 10$ Hz. Gas temperature and VDF were measured by spontaneous Raman scattering.

Figure 8 shows the results of discharge current [69] measurements (solid black curve), as well as the results of calculated [96] dynamics of the specific energy deposition at the plasma channel axis. The waveform of electrical current derived from modelling is shown as a red dashed curve, it was used as input data. The main energy release in the discharge occurs at field values $E/N = 100 \pm 20$ Td, the maximum value of the specific energy deposition reaches $W = 0.75$ eV/mol. The value of the energy deposited in the discharge of 23 mJ resulting from calculations [96] is close to the experimentally measured value of ≈ 20 mJ [69].

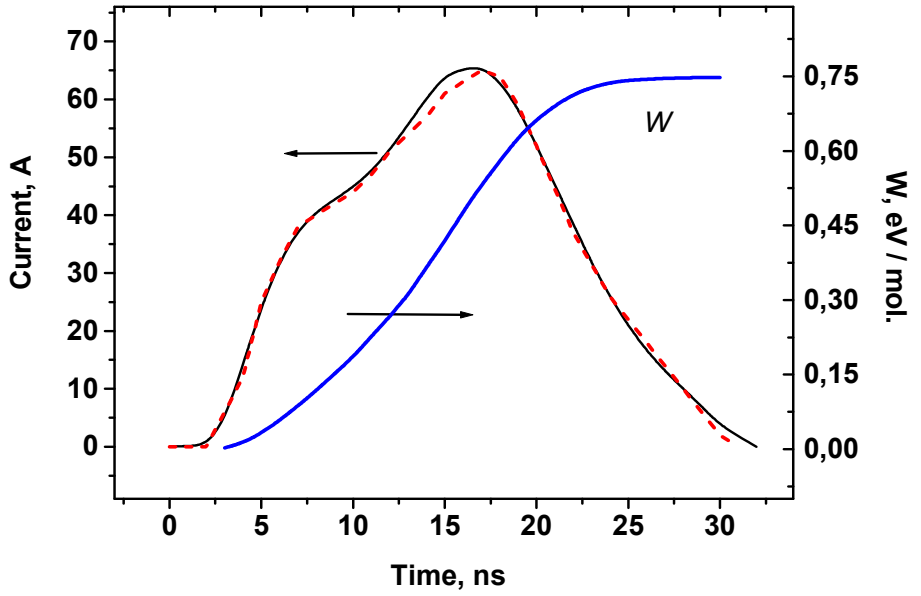

Figure 8. Temporal dynamics of conductivity current (solid curve - experimental data, dashed curve - approximation used in numerical modelling), and specific energy deposition at the discharge axis for the following conditions[69]: P = 760 Torr, T_0 = 300 K.

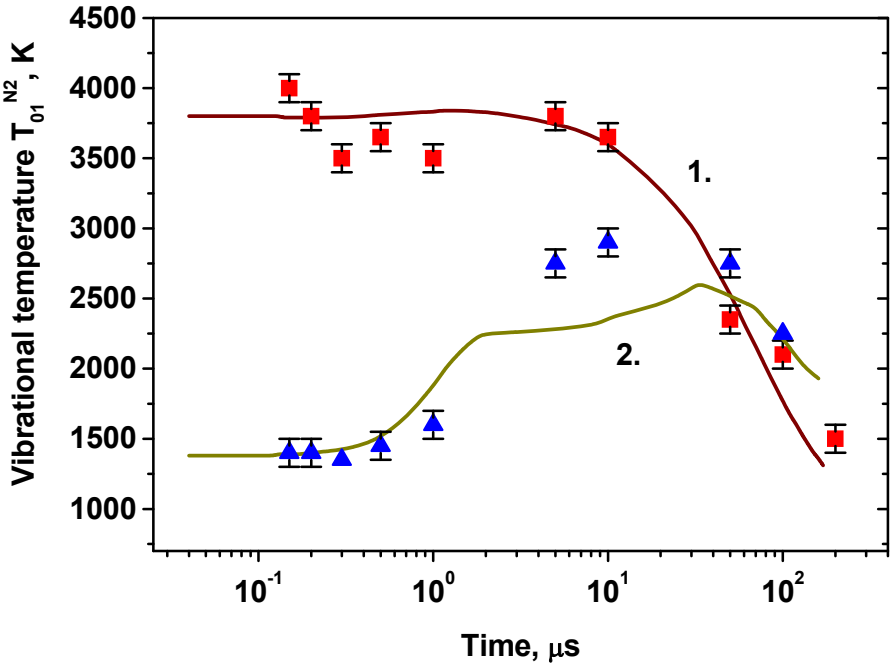

Figure 9. Temporal dynamics of vibrational temperature of nitrogen molecules: curve 1 - at the discharge channel axis (r = 0), curve 2 - at distance r = 0.7 mm from the axis. The symbols represent experimental data [69], the curves represent the calculation results [96].

Figure 9 shows the evolution of vibrational temperature T_{01}^{N2} at relative population v = 0 and 1, vibrational levels of nitrogen molecules:

$$T_{01}^{N2} = \frac{\hbar\omega}{\ln\left(N_2(v=1)/N_2(v=0)\right)}.$$

The main relaxation of vibrational excitation of $N_2(v)$ occurs in collisions with oxygen atoms $O(^3P)$. The change in vibrational temperature T_{01}^{N2} at the discharge axis at $t < 10$ μs is insignificant. The growth of T_{01}^{N2} at the periphery of the discharge channel (at $r = 0.7$ mm) at times $t = 0.5$ - 2 μs (curve 2) is associated with the motion of vibrationally excited $N_2(v)$ molecules from the near-axis region to the periphery because of gas-dynamic expansion of the channel.

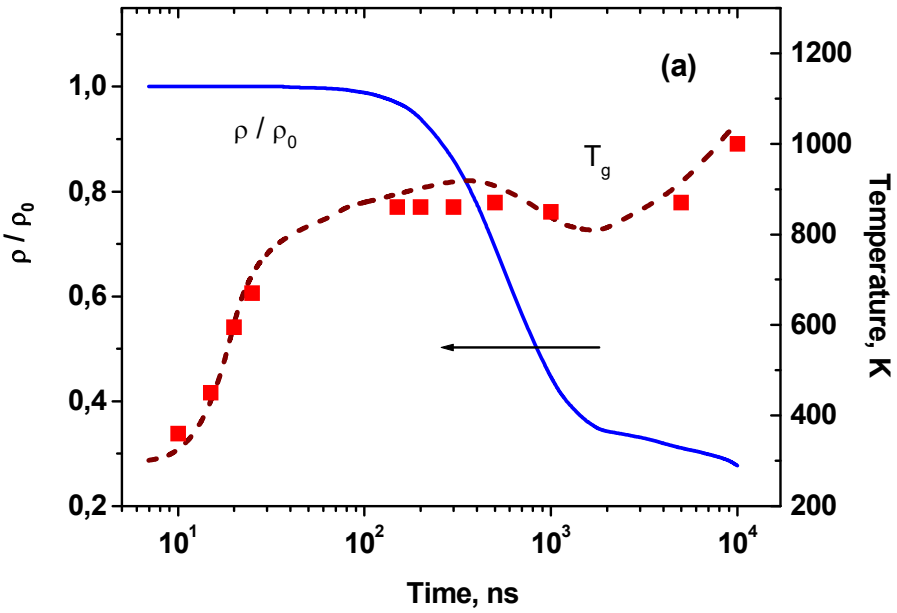

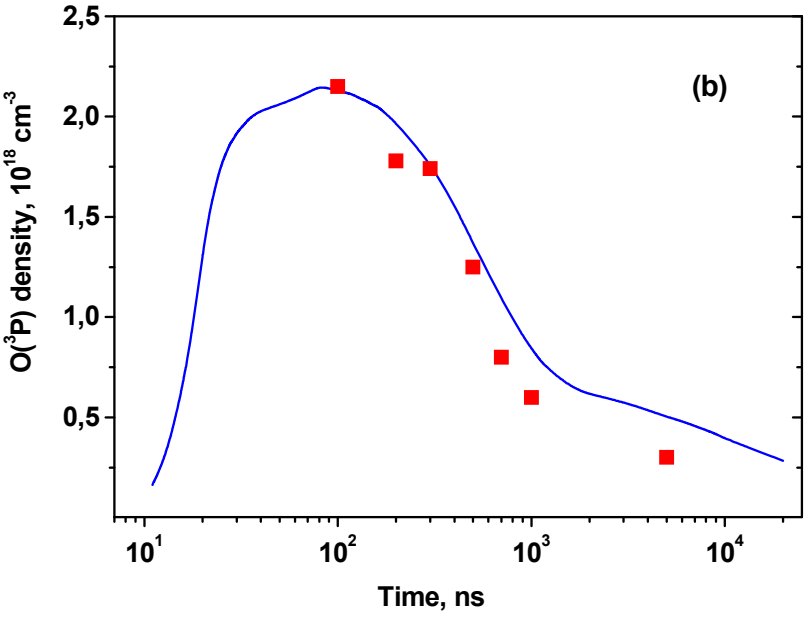

Figure 10 (*a*) Temporal dynamics of gas temperature and gas density, **(*b*)** temporal dynamics of O-atom density at the discharge axis. Air, P = 760 Torr, T_0 = 300 K. The symbols represent experimental data [69], [75], the curves represent the calculation result [96].

Figure 10(a) shows the results of measurements [69], [75] and the result calculating [96] temporal evolution of gas temperature at the discharge axis. Gas heating in the near-axis region for the first 200 ns is ΔT = 550 - 600 K, then the temperature decrease associated with the gas-dynamic expansion of the channel is observed. The further temperature increase at $t > 2$ μs is due to the VV-exchange processes and VT-relaxation of $N_2(v)$ by oxygen atoms. At $t > 6$ μs, gas pressure reaches its unperturbed value P = 760 Torr, and starting from this point, the parameters of the channel can be calculated in the isobaric approximation.

Figure 10 (*b*) shows measurement data and results of calculating atomic oxygen density temporal dynamics at the discharge axis. The density of atoms reaches $2 \cdot 10^{18}$ cm^{-3}, which corresponds to a ≈30% degree of oxygen dissociation. A decrease in O(^{3}P)-atoms density at 0.1-2 μs is explained by the drop of gas density due to gas-dynamic expansion of the hot channel. At the axis, energy fraction spent on fast heating at t ≤ 100 ns is about 17%; about 27% is spent on dissociation and about 55% on vibrational excitation of nitrogen molecules [96].

5.2. Studies of fast air heating in the range of field E/N = 150 - 400 Td

Papers [65], [97], [98] consider heating of nitrogen-oxygen mixtures at P = 3-9 mbar in a pulsed nanosecond discharge. The discharge was triggered by a sequence of 2-3 pulses, in a duration of 20 ns at FWHM and a pause between pulses was about 250 ns. Specific energy deposited in the discharge reached 0.08-0.11 eV/molecule. Calculations were based on the measured waveform of the discharge current. Figure 11 shows an example of the measurements (solid curves) and the calculation results (dashed curves) of E/N behavior for P = 9 mbar. It is clearly seen that the agreement of the calculations and measurements is rather good, and so allows adequate description of plasma-chemical processes with the model.

Table 1.

Energy deposited in the discharge (10^{-3} eV/mol) in each of three pulses W_1, W_2, and W_3 for pressures P = 3, 6, and 9 mbar.

	W_1 (exp / cal)	$W_1 + W_2$ (exp / cal)	$W_1 + W_2 + W_3$ (exp / cal)
3 mbar	3.0 / 3.5	120.4 / 121.0	129.6 / 129.0
6 mbar	53.0 / 53.6	102.8 / 103.0	107.0 / 107.0
9 mbar	40.7 / 40.7	72.0 / 72.4	76.5 / 76.6

Table 1 compares calculated and measured values of the specific deposited energy in a series of discharge pulses for different pressures [65]. The main energy input to the discharge is at E/N =

200-400 Td, which corresponds to the efficient excitation of electronic states and dissociation of molecules and, consequently, efficient fast gas heating.

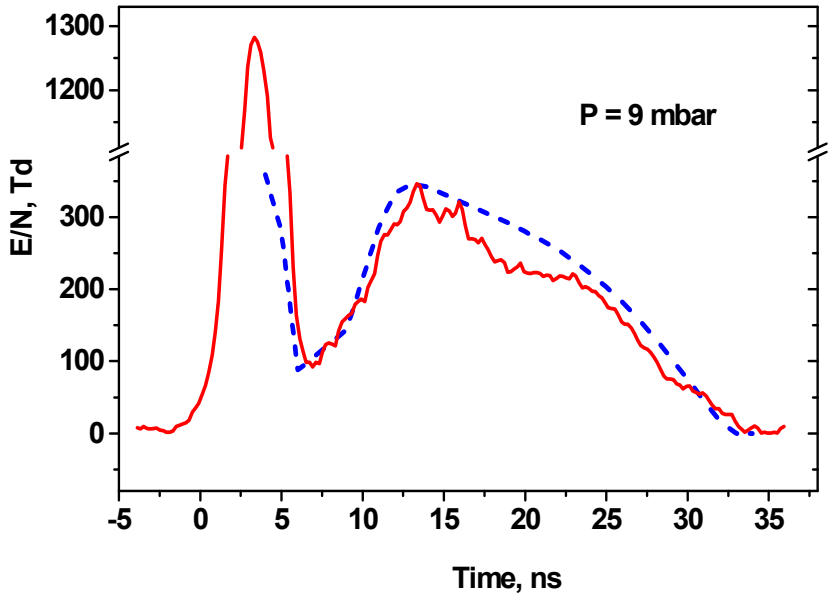

Figure 11. Reduced electric field in the first pulse in air at P = 9 mbar [65]. Solid curve represents measurement data, dashed curve represents calculation results.

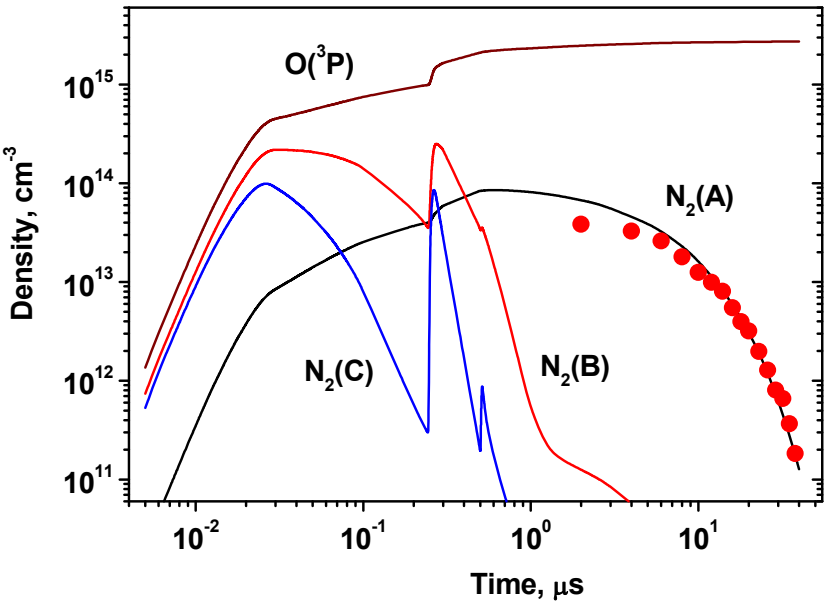

Figure 12. Kinetic curves of O(^{3}P) atoms and electronically excited molecules $N_2(A^3\Sigma_u^+)$, $N_2(B^3\Pi_g)$, $N_2(C^3\Pi_u)$ at P = 6 mbar [65]. Points represent experimental data (in arb. units) [99], curves represent calculation results [65].

Figure 12 shows the calculated kinetic curves of oxygen atoms and electronically excited $N_2(A^3\Sigma_u^+)$, $N_2(B^3\Pi_g)$, $N_2(C^3\Pi_u)$ molecules at P = 6 mbar. In addition to the calculations, the results of $N_2(A^3\Sigma_u^+, v{=}0)$ density CRDS measurements, in arbitrary units, are shown with symbols. One should note a high dissociation degree of oxygen molecules, reaching $[O(^3P)]/[O_2] \approx 10\%$.

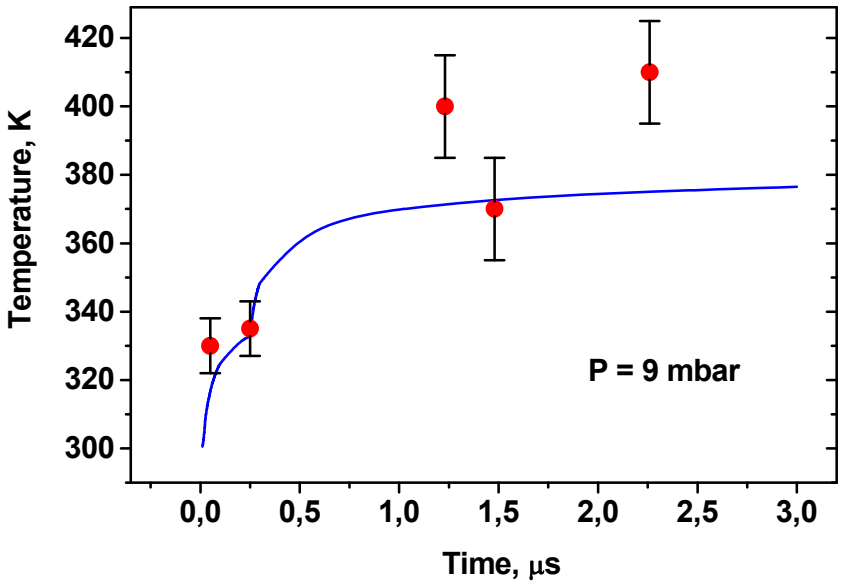

Figure 13(a). Temporal gas temperature dynamics at $P = 9$ mbar [65]. Symbols represent experimental data, the curve represents calculation data.

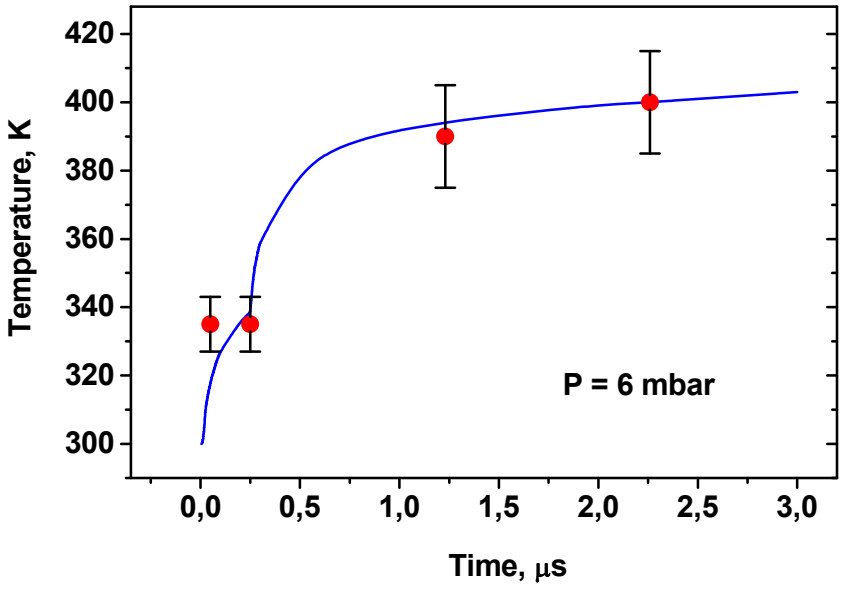

Figure 13(b). Temporal gas temperature dynamics at $P = 6$ mbar [65]. Symbols represent experimental data, the curve represents calculation data.

Calculated (curves) and experimentally measured (symbols) gas temperatures for $P = 9$ and 6 mbar, respectively, is shown in Figure 13. A step corresponding to the second discharge pulse at 250 ns is clearly seen. A significant part of the discharge energy transforms to gas heating in the near afterglow due to quenching of the electronically-excited states of nitrogen molecules by oxygen and quenching of excited $O(^1D)$ atoms by N_2.

The results of calculations [65] show that the discharge energy distribution in the early afterglow is as follows: approximately 24% of the energy is spent on gas heating, 43 to 47%, depending

on pressure, – on the dissociation of oxygen molecules, and the rest – on the excitation of vibrational levels of $N_2(v)$. Calculated energy efficiency of atomic oxygen production in a given discharge is G = 18-19 (where G is the number of oxygen atoms per 100 eV of deposited energy), which is close to the maximum achievable value for electric discharges in air [100].

Evolution of a single plasma channel of a pin-to-pin nanosecond discharge in atmospheric pressure air is provided in [70], [73], [101], [102]. Numerical modelling of the discharge parameters was considered in a one-dimensional axisymmetric formulation [96]. This approximation seems justified, since under the conditions of [70], [73], [101], [102], radial gradients of the plasma parameters are in strong comparison with axial gradients.

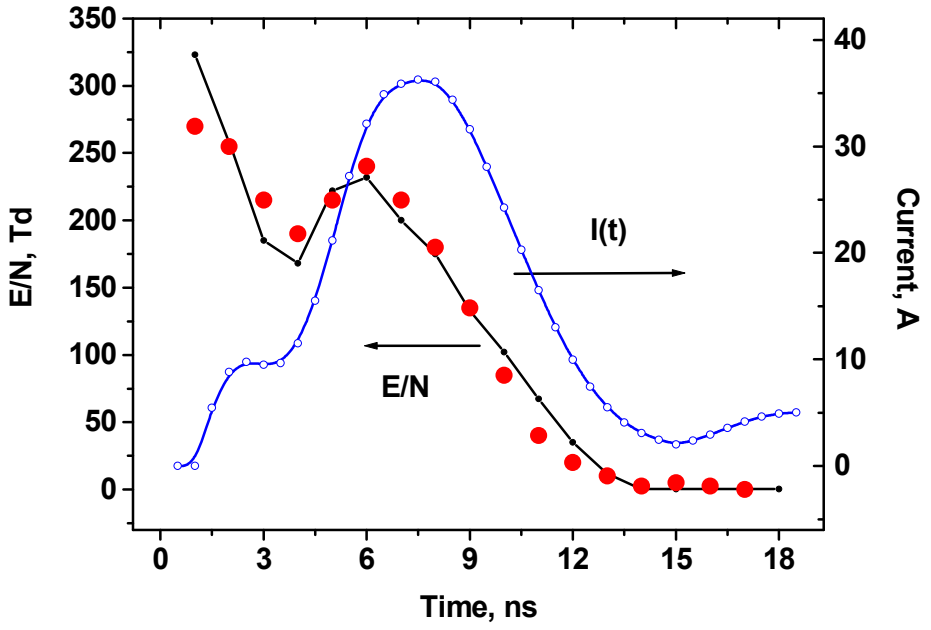

Figure 14. Temporal dynamics of the current pulse and reduced electric field E/N for the conditions [73], [102]. Red symbols represent *E/N* estimates based on the measured values *U(t)*: $E/N = (U-U_c)/d \cdot N$, curve *E(t)/N* represents calculation results [96].

Figure 14 shows temporal profiles of the discharge current [73], [102] and the results calculating reduced electric field *E/N* [96]. Symbols in the same figure represent the results of estimating the value of *E/N* using the following expression

$$E = (U-U_c)/d,$$

where *U(t)* measured in [73] is voltage value, U_c – the cathode potential drop value [27], d – the interelectrode distance. The main energy release in the discharge under study is at field values *E/N* = 100-200 Td, and the maximum energy deposit reaches W = 0.8 eV/mol. The energy input into the discharge (0.67 mJ) resulting from calculations [96] is close to the experimentally measured value of 0.65 mJ [73].

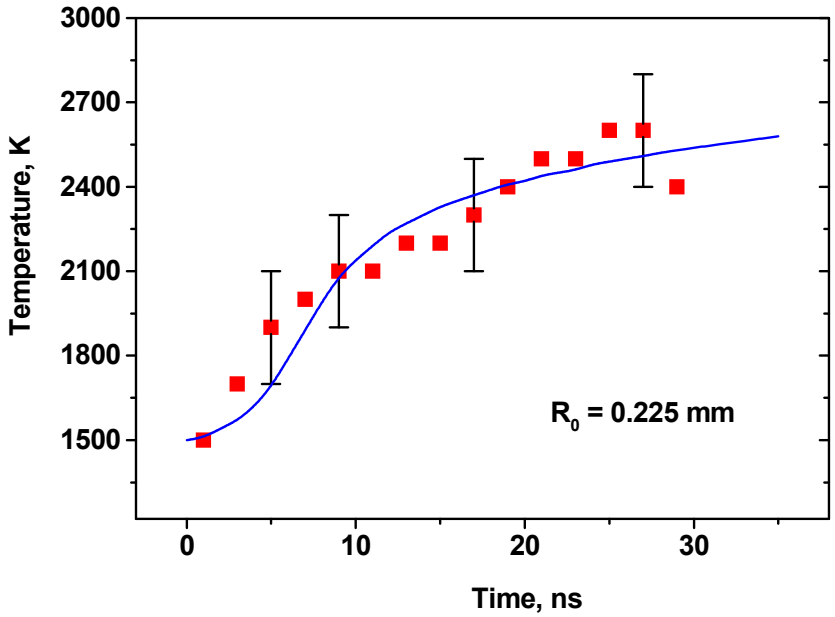

Figure 15. Time dependence of gas temperature at the discharge axis for the conditions of [73]. Symbols represent experimental data [73], the curve represents calculation results [96]. Discharge conditions correspond to Figure 14.

Figure 15 shows experimental data and calculation results of gas heating dynamics for the discharge pulse with the parameters given in Figure 14. The rate of gas heating is extremely high of $(3\text{-}5)\cdot10^{10}$ K/s. About 25% of the discharge energy transforms into gas heating under the considered conditions [96]. The discharge is characterized by a high molecular oxygen dissociation degree at high *E/N*, a parameter closely linked to high efficiency of fast gas heating.

The density of $O(^3P)$ - atoms was measured in [73], [101] using a two-photon absorption laser-induced fluorescence (TALIF). Measurement results [73] are given in Figure 16 (symbols), together with the calculated kinetic curves of atomic oxygen (lines). Two stages of $O(^3P)$ generation are clearly distinguished:

1) dissociation of oxygen by direct electron impact during the discharge pulse:

$$e + O_2 \rightarrow O(^3P) + O(^3P), \quad e + O_2 \rightarrow O(^3P) + O(^1D) \qquad (A1)$$

and formation of atoms in the quenching reactions involving electronically excited $N_2(C^3\Pi_u)$, $N_2(B^3\Pi_g)$ molecules:

$$N_2(B^3\Pi_g) + O_2 \rightarrow N_2(v) + 2\cdot O(^3P), \qquad (A2)$$

$$N_2(C^3\Pi_u) + O_2 \rightarrow N_2(v) + 2\cdot O(^3P,^1D), \qquad (A3)$$

characteristic time of these reactions does not exceed 3-4 ns, therefore, the first stage duration is mainly determined by pulse duration, 12 ns in case of [73] (Figure 16);

2) dissociation of oxygen by quenching of $N_2(a'^1\Sigma_u^-)$, $N_2(A^3\Sigma_u^+)$ molecules:

$$N_2(a'^1\Sigma_u^-) + O_2 \rightarrow N_2(v) + 2\cdot O(^3P,^1D), \quad (A4)$$

$$N_2(A^3\Sigma_u^+) + O_2 \rightarrow N_2(v) + 2\cdot O(^3P), \quad (A5)$$

with a typical time of tens of nanoseconds.

Reliable data on the quenching products of electronically excited states $N_2(B^3\Pi_g, C^3\Pi_u, a'^1\Sigma_u^-)$ by oxygen molecules are not available. In most kinetic models (see [64], [66], [95], [103] et al.), it is assumed that quenching of $N_2(B^3\Pi_g, C^3\Pi_u, a'^1\Sigma_u^-)$ molecules by oxygen leads to O_2 dissociation (reactions (A2)-(A4)). We will call this approach "model 1". Quenching of $N_2(B^3\Pi_g, C^3\Pi_u, a'^1\Sigma_u^-)$ can alternatively result in formation of $N_2(A^3\Sigma_u^+)$ molecules followed by the generation of atomic oxygen in reaction (A5). We will call this approach "model 2"; it was suggested in [104] based on measurements of $O(^3P)$ atom density in the afterglow of a pulsed nanosecond discharge. Results of calculations [96] or models 1 (curve 1) and 2 (curve 2) are shown in Figure 16. Only model 1 is in a good agreement with experimental data [73]. This allows us to conclude that quenching of electronically excited states of $N_2(B^3\Pi_g)$, $N_2(C^3\Pi_u)$, $N_2(a'^1\Sigma_u^-)$ by oxygen mainly leads to dissociation of O_2.

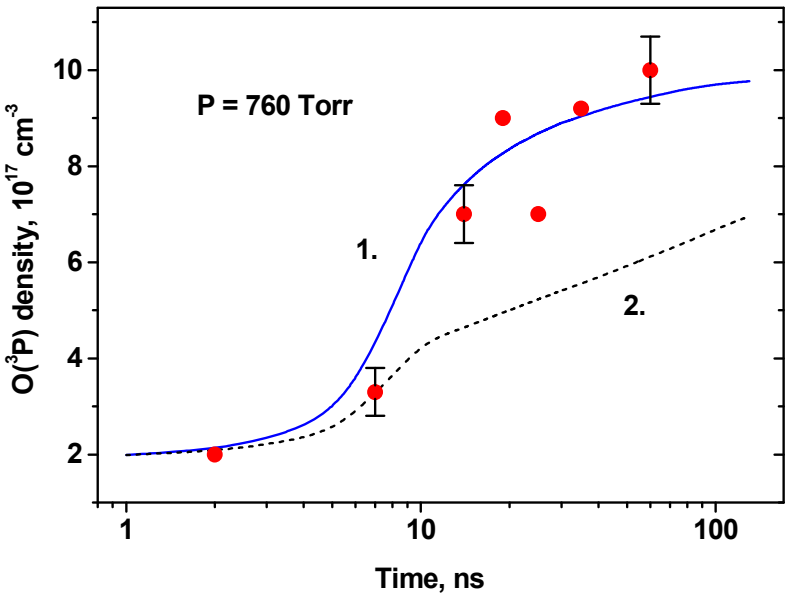

Figure 16. Density of $O(^3P)$ atoms at the discharge axis as a function of time for the conditions of [73]. Symbols represent experimental data [73], curves 1 and 2 represent calculation results [96] using kinetic models 1 and 2 respectively (see the text). Discharge conditions correspond to Fig. 14.

Significant energy release during a short time interval leads to noticeable hydrodynamic perturbation. Paper [71] provides measurement data and simulation results of the gas-dynamic phenomena initiated by a pulsed-periodic nanosecond discharge with parameters close to [73]. The studies were held in atmospheric pressure air at various initial gas temperatures in the range of

300-1000 K. The discharge was initiated by HV pulses with a duration of 10 ns at repetition frequency f = 1-10 kHz. Energy deposition in each pulse was approximately 1 mJ. Gas density at times t = 50 ns - 3 μs after the discharge was obtained using Schlieren technique. The resulting data was compared with the results of calculations made using a 1-D axisymmetric model with a given radial heat source profile. This resulted in the dependence of energy fraction spent on fast gas heating η_R on the value of E/N in the discharge: η_R varied from 25% at E/N = 164 Td to 75% at E/N = 270 Td. It should be noted, however, that in air at E/N = 250-300 Td, about 40-50% of the discharge energy is spent on dissociation of oxygen molecules [96], [100], therefore η_R value should not exceed 50% in this range of electric fields (see curve II in Figure 1). The fraction of energy that goes to O_2 dissociation is defined as $E_{diss}^{O2}/2 \cdot G$, where E_{diss}^{O2} = 5.12 eV is the dissociation energy of O_2 molecules [93], G is the energy cost of O-atom production [100]. That is, value $\eta_R \approx 75\%$ obtained in [71] at E/N = 270 Td appears to be overestimated.

One of the important parameters used in [71] for the analysis of measurement is the radius of the heat release zone R_0. Depending on initial gas temperature, value R_0 varied from R_0 = 200 μm at T_0 = 300 K to R_0 = 480 μm at T_0 = 1000 K. These data were obtained on the basis of Schlieren measurements at the 50th nanosecond after the discharge pulse.

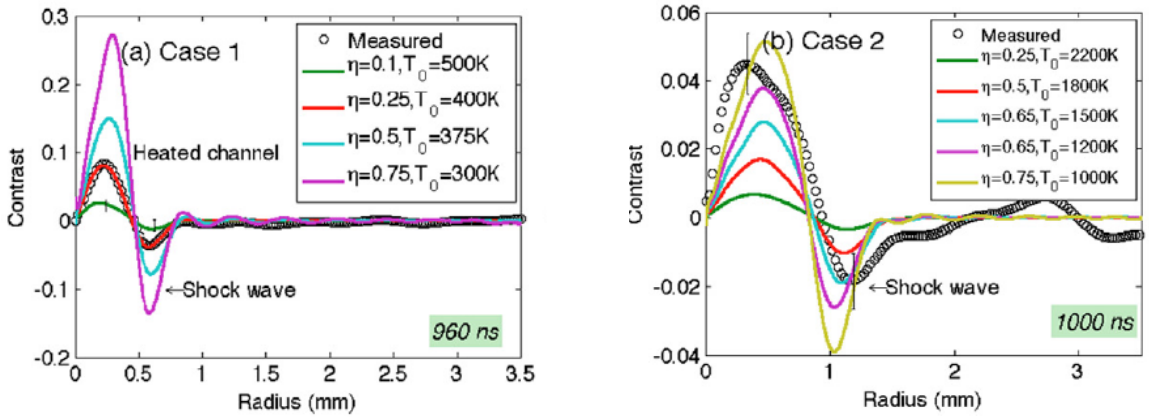

Figure 17 (*a, b*). Comparison of contrast profiles in the shock wave to determine initial gas temperature and the fraction of energy spent on fast heating, case 1 and 2 [71]. The best fit is for η_R = 0.25 ± 0.1 and T_0 = 400 ± 50 K (case 1) and for η_R = 0.65 ± 0.15 and T_0 = 1350 ± 300 K (case 2). Symbols represent experimental data, and lines are results of calculations.

Figure 17 shows the results of comparing calculated and measured contrast profiles at different times for the following conditions: case 1 - U = 7.5 kV, f = 1 kHz, d = 2 mm, T_0 = 300 K; case 2 - U = 8.1 kV, f = 1 kHz, d = 4 mm, T_0 = 1000 K [71]. The calculations were performed assuming a Gaussian initial distribution of the heat release source with characteristic radius R_0. In case 1, the experimental contrast curve and the results of modelling at R_0 = 200 μm are in a good agreement, and the efficiency of fast gas heating is η_R = 0.25 ± 0.1. In case 2, the experimental maximum

"contrast", i.e. the maximum of gas density gradient, is achieved at smaller radii than in the calculations at R_0 = 380 μm. This may indicate the use of an overestimated value of R_0 in the model in case 2. Besides, this case resulted in extremely high energy efficiency of fast gas heating η_R = 0.65 ± 0.15. For additional validation of the results provided by [*Xu* 2014], it would be interesting to measure characteristic dimensions of the energy deposition region based on the radial profiles of the luminescence intensity of 2^+ nitrogen system, similar to [70], and compare the resulting radius to R_0 value.

5.3. Studies of fast air heating in the range of field E/N > 400 Td

At $E/N \leq$ 200-300 Td, about 70% of fast gas heating is explained by quenching of $N_2(B^3\Pi_g)$, $N_2(C^3\Pi_u)$ electronically excited states by molecular oxygen and by quenching of $O(^1D)$ atoms excited by N_2 [64], [65]. With an increase in E/N value, the role of electron impact dissociation of N_2 molecules and processes involving charged particles increase, and at $E/N >$ 600-700 Td, it becomes dominant [64], [66].

Paper [66] considered the interaction of weak shock waves (M = 1.5-3) with plasma generated in air at P = 20 Torr by a pulsed high-current nanosecond discharge with the following parameters: pulse duration $\tau_{imp} \leq$ 50 ns, voltage U = 100 - 160 kV, maximum current $I_{max} \approx$ 2 kA. The results of measurements of the shock wave velocity V/V_0 increase during propagation through plasma were provided. The authors [66] concluded that the velocity increases due to heat release in plasma region and that up to 40% of discharge energy at E/N = 600 Td is spent on gas heating.

Another experiment in [66] was dedicated to measuring gas temperature in a nanosecond surface dielectric barrier discharge in air at pressures P = 200-800 Torr. These measurements were used to estimate the fraction of discharge energy spent on fast gas heating. SDBD at high pressures consists of separate streamers; therefore spatial distribution of the specific input energy is essentially non-uniform. In [66], the data on emission intensity distribution for the 2^+ molecular nitrogen system were used to analyze plasma spatial distribution. It was assumed that emission intensity is proportional to the specific delivered energy, which is identical to the assumption of the constant energy cost of generating $N_2(C^3\Pi_u)$ molecules in the range of fields under consideration. This assumption is not always correct and should be thoroughly analyzed for each particular case.

The discharge energy η_R fraction spent on fast gas heating in a pulsed nanosecond discharge in air at P = 400-800 Torr (Figure 18) was measured in [77]. It was shown that the value of η_R almost does not depend on gas pressure and is equal to η_R = 40 - 95%, depending on the applied voltage and oxygen fraction in the mixture (dashed curves in Fig. 18). The paper also provided the results of calculating η_R dependence on E/N value in the discharge. The dependence of η_R on pressure resulting from the calculations is stronger than in the experiment. This is a consequence of the fact that, at high electric fields, a significant part of the discharge energy goes to ionization.

Further relaxation of this energy to heating, according to [66], [77], depends strongly on gas pressure, as the composition of positive ions changes considerably with pressure, leading to a change in the fraction of energy spent on gas heating in electron-ion recombination reactions.

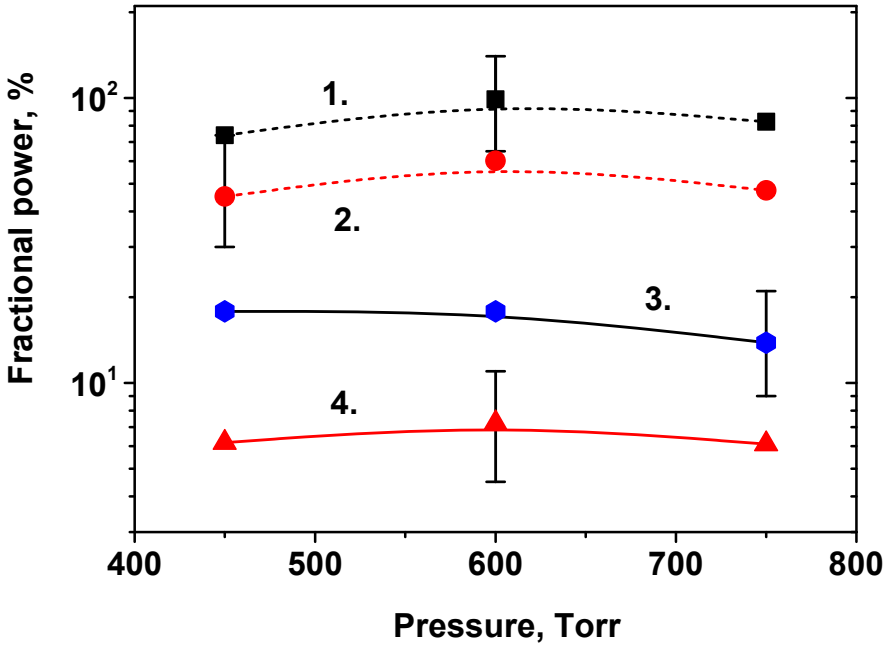

Figure 18. Experimentally obtained data on fractional electron power transferred to heat during the discharge phase and 1 μs after the discharge as a function of gas pressure for the voltage pulses of 17.5 and 20.5 kV: (1) – 1 μs, 20.5 kV, (2) – 1 μs, 17.5 kV, (3) – discharge, 20.5 kV, (4) – discharge, 17.5 kV [77].

It is seen from Figure 18 that immediately after the discharge η_R = 6 - 18%, but at time interval t = 0.1 - 1 μs, η_R increases to 60 - 90% at pressures $P \geq 600$ Torr. It is not possible to explain this effect using the existing models of fast gas heating which include quenching of electronically excited species and recombination of charged particles: the typical time of the mentioned processes is less than 100 ns. This statement is confirmed by experimental data [69], analyzed in the previous section: according to the data given in Figure 10(a), gas temperature in the discharge and near the afterglow increases at $t < 60$ ns but remains almost constant at t = 0.1-1 μs. So the explanation of a significant increase of gas temperature and efficiency of fast gas heating at t = 0.1-1 μs obtained experimentally in [66], [77], still remains open.

There are a few experimental difficulties which can influence the results of measurements [66], [77]. First, it is extremely difficult to measure the discharge region volume and specific input energy value with acceptable accuracy, since the SDBD discharge at atmospheric pressure is significantly inhomogeneous in space. Second, for SDBD measurements of the efficient reduced electric field $(E/N)_{eff}$ at which most of the discharge energy is deposited in gas is a very complex problem. According to modern considerations [54], [61], [105], [106], the distribution of E/N in the SDBD discharge at atmospheric pressure is strongly non-uniform: the fields are extremely high in the ionization front and relatively low, about 100 Td, in the discharge channel. A region of high

electric field exists between the plasma channel and the dielectric surface [54], [61], [90], but the electron density in this region, and thus the role of this layer in the energetic balance of the discharge, is small. As a result, the main energy deposition should occur after the front at the field values $E/N \approx 100$ Td, and the role of the high electric field region in the front of the discharge decreases with an increase in the channel length.

To summarize, when $E/N > 600$ Td, not related to the mentioned experimental difficulties, the processes involving charged particles play an important role in the mechanism of fast gas heating. For most reactions of electron-ion and ion-ion recombination, as well as for ion-molecular reactions, there are no data on the energy distribution in the degrees of freedom for the products of these reactions. Therefore, according to [66], [77], only preliminary estimates of energy fraction spent on fast heating of nitrogen-oxygen mixtures in gas-discharge plasma at high *E/N* are possible at this stage.

6. Theoretical research. Analysis of the model.

A kinetic model describing the dynamics of the main nitrogen-oxygen mixture components excited by a discharge with a relatively strong reduced electric field was proposed in [29], [64]. A significant fraction of the discharge energy at high *E/N* is consumed by the electronic degrees of freedom, dissociation and ionization of molecules. It was assumed that atoms and molecules in the discharge are excited from the ground electronic state mainly by electron impact. *E/N* dependences of the rates of the corresponding reactions were calculated using *BOLSIG+* free software [72]. The change of rate constants with the increasing degree of vibrational excitation of N_2 molecules was described similar to [107]. The main reactions involving neutral particles and rate constants can be found in [29], [103], [108], [26]. To describe the dynamics of gas heating in the discharge, the model [29], [64] took into account the following heat release processes:

6.1. Electron-impact dissociation of nitrogen and oxygen molecules.

$$e + O_2 \rightarrow e + O_2(A,v), \qquad O_2(A,v) \rightarrow O(^3P) + O(^3P) + \varepsilon_R,$$

$$O_2(A,v) = O_2(A^3\Sigma_u^+, C^3\Delta_u, c^1\Sigma_u^-),$$

$$e + O_2 \rightarrow e + O_2(B^3\Sigma_u^-,v), \quad O_2(B^3\Sigma_u^-,v) \rightarrow O(^3P) + O(^1D) + \varepsilon_R,$$

$$e + N_2 \rightarrow e + N_2^*, \qquad N_2^* \rightarrow N(^4S) + N(^2D) + \varepsilon_R.$$

Dissociation of N_2 and O_2 proceeds *via* pre-dissociation of electronically excited states of the molecules [26], [29], populated via electron impact from the ground state. The kinetic energy of the products of pre-dissociation reactions ε_R can be significant:

$$\varepsilon_R = \varepsilon_{th} - \varepsilon_{diss},$$

where ε_{th} is the energy threshold of electron-impact excitation of the pre-dissociating state and ε_{diss} is the energy of the relevant dissociation limit. In oxygen, the data obtained in [109], [110] were used to determine the values of ε_{th}; the data on ε_{diss} were taken from [93].

In air, at high *E/N* values, a significant part of the discharge energy can be consumed by dissociation of nitrogen molecules. As a rule, for *E/N* > 100 Td, the main source of nitrogen atoms are rapidly pre-dissociating (~10^{10} s^{-1} [111], [112]) singlet states of N_2^* = N_2($b^1\Pi_u$, $c^1\Pi_u$, $o^1\Pi_u$, $e^1\Pi_u$, $b^1\Sigma_u^+$, $c^1\Sigma_u^+$, $e^1\Sigma_u^+$) etc. with excitation energy exceeding 12.25 eV. In [112], it was shown that these electronically excited states pre-dissociate with generation of N(^{4}S) + N(^{2}D) atoms. Thus, no more than ε_{th} - ε_{diss} ≤ 1 eV can be consumed directly by gas heating in this process (ε_{th} ≈ 13 eV is the effective threshold of electron-impact excitation of these states, ε_{diss} = 12.1 eV is dissociation limit N(^{4}S) + N(^{2}D)). The generated N(^{2}D) atoms react fairly fast with O_2 molecules [103], [108] (see reaction (R14) in Table 2) with the generation of excited O(^{1}D) atoms. Their quenching (see section 6.3 below) also leads to gas heating. Taking into account rapid relaxation of NO vibrational excitation, approximately 2.99 eV can be transformed to heat release in reaction (R14), and the total energy going to gas heating during dissociation of nitrogen molecules (e + N_2 → e + N(^{4}S) + N(^{2}D)) can reach 4 eV, which is ~ 30% of the excitation energy ε_{th}.

6.2. Quenching of electronically excited states of nitrogen by oxygen

Quenching of electronically excited nitrogen molecules by O_2 leads to the population of O_2($B^3\Sigma_u^-$,*v*), O_2($A^3\Sigma_u^+$,*v*), O_2($c^1\Sigma_u^-$,*v*) excited states. Pre-dissociation of these states leads to the decomposition of O_2 molecules and the excess energy release into translational degrees of freedom of the generated oxygen atoms [113]. Thermalization of "hot" atoms takes place in a few collisions, and the energy released in this case is consumed primarily by rotational excitation of molecules and gas heating.

The main reactions of electronically excited states of N_2 in nitrogen-oxygen mixtures are summarized in Table 2.

Table 2

Main reactions determining quenching of N_2($A^3\Sigma_u^+$, $B^3\Pi_g$, $C^3\Pi_u$, $a'^1\Sigma_u^-$) molecules, N(^{2}D) and O(^{1}D) atoms in N_2 : O_2 mixtures

No	Reaction	K, cm^3/s	Ref.
R1	$N_2(A^3\Sigma_u^+) + O_2 \rightarrow N_2(v) + 2\cdot O(^3P) + \varepsilon_1$	$1.7\cdot10^{-12}$	[108]
R2	$N_2(A^3\Sigma_u^+) + O_2 \rightarrow N_2(v) + O_2(b^1\Sigma_g^+)$	$7.5\cdot10^{-13}$	[108]
R3	$2\cdot N_2(A^3\Sigma_u^+) \rightarrow N_2(v) + N_2(B^3\Pi_g) + \varepsilon_3$	$7.7\cdot10^{-11}$	[64], [103]
R4	$2\cdot N_2(A^3\Sigma_u^+) \rightarrow N_2(v) + N_2(C^3\Pi_u)$	$1.6\cdot10^{-10}$	[64], [103]
R5	$N_2(A^3\Sigma_u^+) + O(^3P) \rightarrow N_2(v) + O(^1S) + \varepsilon_5$	$3.0\cdot10^{-11}$	[108]
R6	$N_2(B^3\Pi_g) + O_2 \rightarrow N_2(v) + 2\cdot O(^3P) + \varepsilon_6$	$3.0\cdot10^{-10}$	[64], [103]
R7	$N_2(B^3\Pi_g,v=0) + N_2 \rightarrow N_2(A^3\Sigma_u^+,v) + N_2(v)$	$1.0\cdot10^{-11}$	[64], [103]
R8	$N_2(a'^1\Sigma_u^-) + O_2 \rightarrow N_2(v) + O(^3P) + O(^1D) + \varepsilon_8$	$2.8\cdot10^{-11}$	[64], [103]

R9	$N_2(a'^1\Sigma_u^-) + N_2 \rightarrow N_2(B^3\Pi_g) + N_2(v)$	$2.0\cdot10^{-13}$	[64], [103]
R10	$N_2(C^3\Pi_u) + O_2 \rightarrow N_2 + O(^3P) + O(^3P, ^1D) + \varepsilon_{10}$	$2.5\cdot10^{-10}$	[82], [114]
R11	$N_2(C^3\Pi_u) + N_2 \rightarrow N_2(B^3\Pi_g) + N_2(v)$	$1.0\cdot10^{-11}$	[82], [103]
R12	$N_2(B^3\Pi_g) + O(^3P) \rightarrow NO + N(^4S, ^2D) + \varepsilon_{12}$	$3.0\cdot10^{-10}$	[82]
R13	$N_2(C^3\Pi_u) + O(^3P) \rightarrow NO + N(^4S, ^2D) + \varepsilon_{13}$	$3.0\cdot10^{-10}$	[82]
R14	$N_2(a'^1\Sigma_u^-) + O(^3P) \rightarrow NO + N(^4S, ^2D) + \varepsilon_{14}$	$3.0\cdot10^{-10}$	[82]
R15	$N(^2D) + O_2 \rightarrow NO(v) + O(^3P, ^1D) + \varepsilon_{15}$	$7.5\cdot10^{-12}$	[64], [103]
R16	$O(^1D) + N_2 \rightarrow O(^3P) + N_2(v) + \varepsilon_{16}$	$2.57\cdot10^{-11}$	[64], [103]
R17	$O(^1D) + O_2 \rightarrow O(^3P) + O_2(b^1\Sigma_g^+, X^3\Sigma_g^-) + \varepsilon_{17}$	$4.0\cdot10^{-11}$	[64], [103]

Triplet electronic states $N_2(B^3\Pi_g, B'^3\Sigma_u^-, W^3\Delta_u)$ actively populated via electron impact from the ground state $N_2(X^1\Sigma_g^+)$, also participate in O_2 dissociation [64], [115]. The most efficient way to describe their kinetics is to introduce effective state $N_2(B)$, with a population rate determined by the total concentration of molecules in these electronic states and with a quenching rate determined *via* the corresponding data on the $N_2(B^3\Pi_g)$ state. This approach is possible because of the resonant energy exchange between $N_2(B^3\Pi_g, B'^3\Sigma_u^-, W^3\Delta_u)$ states [26], [44], [45].

Similar considerations are also valid for the group of singlet states $N_2(a^1\Pi_g, a'^1\Sigma_u^-, w^1\Delta_u)$ [116] described in the model [64] by a single state $N_2(a)$. The deactivation rate of $N_2(a)$ was assumed to be equal to quenching rate of $N_2(a'^1\Sigma_u^-)$ [117]. Analyzing the scheme of electronic terms of the singlet states in nitrogen molecule [29] makes it possible to suggest that quenching of $N_2(a'^1\Sigma_u^-)$ by oxygen leads to dissociation of O_2 molecules primarily through the $B^3\Sigma_u^-$ state (reaction (R8) from Table 2).

Consider a possibility of gas heating in the process of $N_2(C^3\Pi_u)$ quenching by molecular oxygen (R10). The rate of this reaction is $k = (2.5 \div 3)\cdot10^{-10}$ cm^3/s [82], [114], so this process should play an important role in mixtures where the fraction of oxygen is great enough, for example, in the air. In [96], it was shown that the main result of reaction (R10) is dissociation of O_2 molecules (see Table 1). To determine the fraction of $N_2(C^3\Pi_u,v)$ ($\varepsilon^*_{C,v=0}$ = 11.03 eV [93]) excitation energy consumed by gas heating, we should calculate the ratio of dissociation channels leading to generation of $O(^3P)$, $O(^1D)$, $O(^1S)$ atoms. In [64], it was assumed that the ratio of $(O(^3P) + O(^3P))$, $(O(^1D) + O(^3P))$, $(O(^1S) + O(^3P))$ dissociation channels in reaction (R10) is approximately the same as in oxygen quenching of excited argon atoms $Ar(^3P_{0,2})$ (excitation energy 11.6 eV) and is, according to measurements [118], 0.46:0.52:0.02. Then the total energy of the resulting fragments of $O(^3P,^1D,^1S) + O(^3P)$ is ε_{diss} = 6.2 eV.

At high dissociation degrees, $[O(^3P)]/[O_2]$, quenching of electronically excited nitrogen molecules by oxygen atoms becomes important. For $N_2(A^3\Sigma_u^+)$ molecules, this process was studied in detail in [119]. Recently, in the afterglow of the pulsed nanosecond discharge in air at P = 100 Torr and T = 300-350 K [120] on the basis of experimentally measured kinetic curves of $O(^3P)$, $N(^4S)$ atoms and NO molecules, the rate constant of reactions (R12)-(R14), $k = 3\cdot10^{-10}$ cm^3/s, were obtained. Taking into account subsequent reactions of $N(^2D)$ quenching by molecular oxygen (R15) and rapid VT- relaxation of NO(v), the fraction of electronic excitation energy of $N_2(A^3\Sigma_u^+$, $B^3\Pi_g$, $C^3\Pi_u$, $a'^1\Sigma_u^-$) molecules consumed by gas heating in reactions (R12)-(R15), is significant. Note that this fraction is much greater than in reactions of $N_2(A^3\Sigma_u^+$, $B^3\Pi_g$, $C^3\Pi_u$, $a'^1\Sigma_u^-$) quenching by molecular oxygen, where most of the excitation energy was consumed by O_2 dissociation.

6.3. Quenching of excited $O(^1D)$ atoms.

A significant part of reactions leading to O_2 dissociation occurs with the generation of excited $O(^1D)$ oxygen atoms. In nitrogen-oxygen mixtures, these atoms are quenched primarily in the following processes:

$$O(^1D) + N_2 \rightarrow O(^3P) + N_2(v) + \varepsilon_{16}, \qquad \text{(R16)}$$

$$O(^1D) + O_2 \rightarrow O(^3P) + O_2(b^1\Sigma_g^+, X^3\Sigma_g^-) + \varepsilon_{17}. \qquad \text{(R17)}$$

Deactivation of $O(^1D)$ by nitrogen molecules has been studied in a number of papers where it has been shown that this reaction proceeds with the formation of an intermediate complex. The reaction rate values resulting from calculations of [121] are in good agreement with experimental data, and measurements of [122] confirmed the calculated value of the energy fraction (30 ± 10%) spent on N_2 vibrational excitation. Based on the results of these studies, it was assumed [29] that ~ 70% of $O(^1D)$ excitation energy is consumed by gas heating, that is, for reaction (R16) $\varepsilon_{16} \approx 1.38$ eV.

6.4. Ion-molecular reactions, electron-ion and ion-ion recombination

In air, for E/N > 400 Td, a significant part of the discharge energy is consumed by ionization of nitrogen and oxygen molecules. Therefore, at high E/N values, reactions involving charged particles can make a significant contribution to gas heating [66]. The system of reactions given in Table 3 was used in [64] to describe the evolution of ionic composition in nitrogen-oxygen mixtures.

Table 3

Reactions involving charged particles in nitrogen-oxygen mixtures

No	Reaction	Rate constant, cm^3/s, cm^6/s	Ref.
C1	$N_2^+ + N_2 + M \rightarrow N_4^+ + M$	$5.0\cdot10^{-29}$	[103]
C2	$N_4^+ + e \rightarrow N_2(B^3\Pi_g, C^3\Pi_u) + N_2$	$2.0\cdot10^{-6}\cdot(300/T_e)^{0.5}$	[103]
C3	$N_4^+ + O_2 \rightarrow O_2^+ + N_2 + N_2$	$2.5\cdot10^{-10}$	[103]

C4	$N_2^+ + O_2 \rightarrow O_2^+ + N_2$	$6.0 \cdot 10^{-11}$	[103]
C5	$O_2^+ + N_2 + N_2 \rightarrow O_2^+ \cdot N_2 + N_2$	$9.0 \cdot 10^{-31} \cdot (300/T)^2$	[103]
C6	$O_2^+ \cdot N_2 + O_2 \rightarrow O_4^+ + N_2$	$1.0 \cdot 10^{-9}$	[103]
C7	$O_2^+ \cdot N_2 + N_2 \rightarrow O_2^+ + N_2 + N_2$	$1.1 \cdot 10^{-6} \cdot (300/T)^{5.3} \cdot \exp(-2357/T)$	[103]
C8	$O_2^+ + O_2 + N_2 \rightarrow O_4^+ + O_2 + O_2$	$2.4 \cdot 10^{-30} \cdot (300/T)^{3.2}$	[103]
C9	$O_4^+ + O_2 \rightarrow O_2^+ + O_2$	$3.3 \cdot 10^{-6} \cdot (300/T)^4 \cdot \exp(-5030/T)$	[103]
C10	$O_2^+ + e \rightarrow O(^3P) + O(^3P,^1D)$	$1.95 \cdot 10^{-7} \cdot (300/T_e)^{0.7}$	[123]
C11	$O_4^+ + e \rightarrow O(^3P) + O(^3P,^1D) + O_2$	$4.2 \cdot 10^{-6} \cdot (300/T_e)^{0.48}$	[123], [124]
C12	$e + O_2 + O_2 \rightarrow O_2^- + O_2$	$k(T, T_e)$	[103]
C13	$O_2^- + O_2 + O_2 \rightarrow O_4^- + O_2$	$2.4 \cdot 10^{-30} \cdot (300/T)^{3.2}$	[103]
C14	$O_4^- + O_2 \rightarrow O_2^- + O_2$	$10^{-10} \cdot \exp(-1044/T)$	[103]
C15	$O_2^- + O(^3P) \rightarrow O_3 + e$	$1.5 \cdot 10^{-10}$	[103]
C16	$O_2^- + O_3 \rightarrow O_3^- + O_2$	$4.0 \cdot 10^{-10}$	[103]
C17	$O_4^- + O(^3P) \rightarrow O_3^- + O_2$	$4.0 \cdot 10^{-10}$	[103]
C18	$O_3^- + O(^3P) \rightarrow O_2 + O_2 + e$	$3.0 \cdot 10^{-10}$	[103]
C19	$O_3^- + O(^3P) \rightarrow O_2^- + O_2$	$3.2 \cdot 10^{-10}$	[103]
C20	$O_2^- + O_2^+ + O_2 \rightarrow 2 \cdot O + 2 \cdot O_2$	$2.0 \cdot 10^{-25} \cdot (300/T)^{2.5}$	[103]
C21	$O_2^- + O_4^+ + O_2 \rightarrow 2 \cdot O + 3 \cdot O_2$	$2.0 \cdot 10^{-25} \cdot (300/T)^{2.5}$	[103]
C22	$O_4^- + O_2^+ + O_2 \rightarrow 2 \cdot O + 3 \cdot O_2$	$2.0 \cdot 10^{-25} \cdot (300/T)^{2.5}$	[103]
C23	$O_4^- + O_4^+ + O_2 \rightarrow 2 \cdot O + 4 \cdot O_2$	$2.0 \cdot 10^{-25} \cdot (300/T)^{2.5}$	[103]

At high pressures, N_2^+ ions generated in the discharge are rapidly transformed into to N_4^+ in reaction

$$N_2^+ + N_2 + M \rightarrow N_4^+ + M. \qquad \text{(C1)}$$

In addition, the reactions of charge exchange from N_4^+ and N_2^+ to O_2^+ ions are possible:

$$N_4^+ + O_2 \rightarrow O_2^+ + N_2 + N_2, \qquad \text{(C3)}$$

$$N_2^+ + O_2 \rightarrow O_2^+ + N_2, \qquad \text{(C4)}$$

In [66], it was assumed that in charge exchange reactions (C3)-(C4), all the released energy is spent on mixture heating, in particular due to rapid relaxation of vibrational excitation of the generated $O_2^+(v)$ ions [125].

The channel ratio of the reaction of electron-ion recombination (C10), according to [123], is as follows:

$$\begin{aligned} O_2^+ + e &\rightarrow O(^3P) + O(^3P) + 6.95\ \text{eV} \quad 32\% \\ &\rightarrow O(^1D) + O(^3P) + 4.99\ \text{eV} \quad 43\% \qquad \text{(C10)} \\ &\rightarrow O(^1D) + O(^1D) + 3.02\ \text{eV} \quad 20\% \end{aligned}$$

$$\rightarrow O(^1D) + O(^1S) + 0.80\ eV \qquad 4\%$$

Thus, the total energy spent on gas heating in reaction (C10) is 5.0 eV.

In atmospheric pressure air, O_2^+ ions are rapidly converted to O_4^+ in reactions (C5)-(C8) [103]. Thus, a significant part of electrons will recombine in the reaction $e + O_4^+ \rightarrow product$. The rate constant of this process is $k_{C11} = 4.2 \cdot 10^{-6}\ (300/T_e)^{0.48}$ cm^3/s [123], [126]. Since the dissociation energy of $O_2^+ \cdot O_2$ ion is relatively low (0.42 eV), it was assumed in [126] that the electron-ion recombination of $O_2^+ \cdot O_2$ ion is similar to that of O_2^+, that is, the following channel is most likely:

$$e + O_4^+ \rightarrow O(^3P) + O(^3P,^1D,^1S) + O_2. \qquad (C11)$$

This assumption is confirmed by the data of experiments on ozone generation in oxygen plasma of pulsed high-current electron beams [124], [127], [128] et al. The energy consumed by gas heating in reaction (C11) does not exceed $\varepsilon_{C11} \leq 4.6$ eV.

In [66], it was assumed that both in reaction (C11) and in reactions of three-body ion-ion recombination (C20)-(C23), dissociation of oxygen molecules is unlikely, and the main channels are:

$$O_4^+ + e \rightarrow 2 \cdot O_2, \quad O_2^- + O_2^+ + O_2 \rightarrow 3 \cdot O_2, \quad O_4^- + O_4^+ + O_2 \rightarrow 5 \cdot O_2,$$

moreover, all the energy released in these processes is consumed by gas heating. The analysis of this assumption, as well as the analysis of experimental data on energy efficiency of ozone production by electron beams [124], [127] can be found in [64].

Will consider possible uncertainties in the modeling of the fast gas heating linked to uncertainties in the key elementary reactions in N_2:O_2 mixtures. In the field range E/N = 60 - 300 Td, the main reactions responsible for the fast gas heating are quenching of electronically excited states $N_2(A^3\Sigma_u^+)$, $N_2(B^3\Pi_g)$, $N_2(C^3\Pi_u)$ by O_2 molecules, dissociation of O_2 and N_2 by electron impact, and quenching of excited $O(^1D)$ atoms by molecular nitrogen (see Figure 4).

Production of electronically excited $N_2(A^3\Sigma_u^+)$, $N_2(B^3\Pi_g)$, $N_2(C^3\Pi_u)$ molecules takes place mainly via direct electron impact from the ground state of molecular nitrogen. The rates of excitation are calculated by solving the Boltzmann equation in the two-term approximation using the BOLSIG+ code [72]. Self-consistent set of the cross-sections for elastic and inelastic electron collisions with N_2 molecules is taken from [129]. These cross-sections have been tested in numerous papers comparing calculated and measured swarm parameters, namely drift velocities and ionization coefficients, as well as excitation of $N_2(C^3\Pi_u)$ state and excitation of the sum of triplet electronic states $N_2(A^3\Sigma_u^+)$, $N_2(B^3\Pi_g)$, $N_2(C^3\Pi_u)$ for different E/N values (see, for example, Over the last decade, considerable progress [129], [130] etc). Using these cross-sections for calculation of the rate constants in air and combustible mixtures introduces an error in the rate constants of around 10-20% [131].

Table 2 contains the rate constants for the reactions of quenching of electronically excited states $N_2(A^3\Sigma_u^+)$, $N_2(B^3\Pi_g)$, $N_2(C^3\Pi_u)$ by molecular oxygen (reactions (R1), (R2), (R6) and (R10)). The values of the taken rate constants are in a good agreement with numerous literature sources [26], [82], [95], [103], [108]. Will note that change of these reaction rates in the limits given in the literature will not change an absolute value of temperature increase at the conditions that the considered reactions (R1), (R2), (R6), (R10) are the dominant channels of quenching of $N_2(A^3\Sigma_u^+$, $B^3\Pi_g$, $C^3\Pi_u)$.

One of the key reactions for fast gas heating are the dissociation of O_2 molecules by electron impact. A self-consistent set of electron collision cross-sections for oxygen molecules is described and analyzed in [132],[133]. In oxygen plasma using these cross-sections for calculation of the rate constants of O_2 dissociation introduces an error of about 10-15% [133]. It should be noted that electronically excited $O(^1D)$ atoms can be produced due to O_2 dissociation; their quenching is also important for the FGH. The accuracy of the rate constants of quenching of $O(^1D)$ atoms by N_2 and O_2 molecules (reactions (R16) and (R17) from the table 2) is about 20% [134]. Cross-section of N_2 dissociation by electron impact, as well as part of energy transmitted in gas heating in dissociation is discussed in [112]. There is no enough data in the literature to estimate the error of resulting rates of dissociation (see, for example, [135]), but according to the calculations provided in Figure 4, curve 4, the role of N_2 dissociation in air at low and moderate electric fields is relatively small and does not exceed 12% at $E/N < 300$ Td.

The main mechanism of production of atomic oxygen in air plasma at high electric fields is based on O_2 dissociation by electron impact and dissociative quenching of $N_2(A^3\Sigma_u^+$, $B^3\Pi_g$, $C^3\Pi_u)$ states by oxygen molecules described above. This provides a solid ground for validation of the rate constants of key elementary reactions for the fast gas heating, since all the reactions of O_2 dissociation are accompanied by fast heat release [64]. Corresponding calculations show agreement in time profile and absolute values of atomic oxygen, within 30-40%, with experimentally obtained TALIF-data [70] (see Figure 16). Another comparison provides 20-30% difference between calculated [30] and measured [136] energy efficiency of $O(^3P)$ atoms production for the reduced electric fields in the range $E/N = 150$ - 350 Td.

It should be noted that further research is needed to develop and validate the model of fast gas heating in discharge plasmas at high gas pressures ($P = 3$-30 atm) and high reduced electric fields ($E/N = 600$-1000 Td).

7. Fast gas heating in discharge plasma of hydrogen-air mixtures and its effect on the ignition of combustible mixtures

In hydrogen-containing mixtures, even at fuel-to-oxidizer ratio close to stoichiometric, the density of hydrogen exceeds the density of oxygen: $[H_2]/[O_2] \geq 1$. This is the difference between hydrogen-containing mixtures and mixtures containing hydrocarbons where ratio $[C_xH_y]/[O_2] < 1$

even at ER = 1. At ER > 0.3, due to the relatively great fraction of hydrogen in the H_2-air mixture, processes involving hydrogen molecules can play a significant role in the thermalization of non-equilibrium excitation energy.

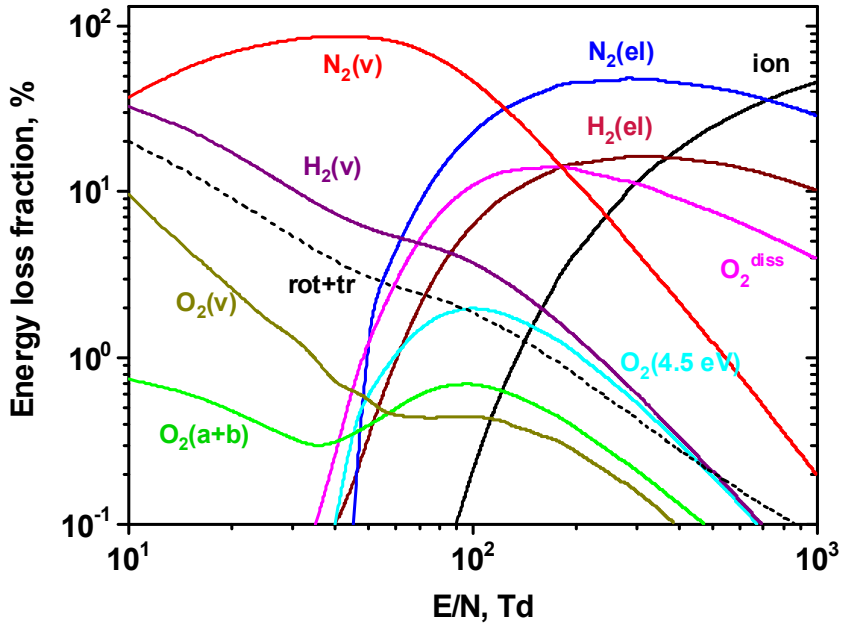

Figure 19. Calculated fractional power dissipated by electrons into the different molecular degrees of freedom as a function of *E/N* in stoichiometric H_2-air mixture [2].

Figure 19 shows the results of calculating the distribution of electron energy loss into various degrees of freedom as a function of *E/N* in stoichiometric H_2-air mixture [2]. In the range of fields *E/N* = 80-300 Td, most of the discharge energy goes to electronic excitation of nitrogen and hydrogen molecules, as well as dissociation of oxygen molecules by electron impact. To describe fast gas heating in hydrogen-air plasma, consider the possibility of gas heating in the relaxation of electron excitation energy for hydrogen, nitrogen and oxygen molecules. Dissociation of hydrogen molecules by electron impact

$$e + H_2(X^1\Sigma_g^+) \rightarrow e + H(^1S) + H(^1S) + \varepsilon_H$$

occurs through excitation of pre-dissociating electronic state of $H_2(b^3\Sigma_u^+)$, either directly or by excitation of states of $H_2(B^1\Sigma_u^+)$, $H_2(C^3\Pi_u)$, $H_2(a^3\Sigma_g^+)$, $H_2(d^3\Pi_u)$ etc., followed by a radiation-collision transition to $H_2(b^3\Sigma_u^+)$. Energy ε_H equal to the difference between the excitation energy of $H_2(b^3\Sigma_u^+)$ (ε_b = 8.9 eV) [137] and dissociation energy of H_2 molecules, ε_{diss} = 4.478 eV [93], is released to gas heating [137].

As already noted, in hydrogen-air mixtures, at *E/N* > 100 Td, a significant fraction of the discharge energy can be consumed by the electronic excitation of $N_2(A^3\Sigma_u^+)$, $N_2(B^3\Pi_g)$, $N_2(C^3\Pi_u)$ nitrogen molecules. Compare the rates of quenching these electronically excited states with hydrogen and oxygen molecules:

(Q1) $N_2(A^3\Sigma_u^+) + O_2 \rightarrow N_2(v) + O(^3P) + O(^3P)$, $k_{Q1} = 2.5\cdot10^{-12}$ cm^3/s [64], [108],

(Q2) $N_2(A^3\Sigma_u^+, v=0) + H_2 \rightarrow N_2 + H + H$, $k_{Q2} = 1.65\cdot10^{-14}\cdot(T/300)^{4.265}\cdot\exp(-416.5/T)$ cm^3/s [138].

At temperatures $T < 700$ K, the ratio of rate constants $k_{Q1}/k_{Q2} >> 1$, so the role of reaction (Q2) in the mechanism of fast gas heating is relatively small. However, as gas temperature increases, the contribution of this process will increase markedly.

(Q3) $N_2(B^3\Pi_g) + O_2 \rightarrow N_2(v) + O(^3P) + O(^3P)$, $k_{Q3} = 3\cdot10^{-10}$ cm^3/s [64], [108],

(Q4) $N_2(B^3\Pi_g) + H_2 \rightarrow N_2(A^3\Sigma_u^+, v) + H_2(v)$, $k_{Q4} = 2.5\cdot10^{-11}$ cm^3/s [95]

The ratio of rate constants for reactions (Q3) and (Q4) $k_{Q3}/k_{Q4} >> 1$, and the role of the quenching reaction of $N_2(B^3\Pi_g)$ states by H_2 will be relatively small.

(Q5) $N_2(C^3\Pi_u) + O_2 \rightarrow N_2(v) + O(^3P) + O(^1D)$, $k_{Q5} = 3\cdot10^{-10}$ cm^3/s [82]

(Q6) $N_2(C^3\Pi_u) + H_2 \rightarrow N_2(v) + H + H$, $k_{Q6} = 3\cdot10^{-10}$ cm^3/s [82]

Reaction (Q6) proceeds in two stages:

$$N_2(C^3\Pi_u) + H_2 \rightarrow N_2(X^1\Sigma_g^+) + H_2(b^3\Sigma_u^+), \quad H_2(b^3\Sigma_u^+) \rightarrow H(^1S) + H(^1S) + \varepsilon_{Q6}.$$

As a result, the difference between the excitation energy of $N_2(C^3\Pi_u)$ (11.03 eV) and the dissociation energy of H_2 (4.478 eV) goes to gas heating. The role of reaction (Q6) in fast gas heating can be significant, since the rate constant of this reaction is very great [82] and a significant fraction of the excitation energy of $N_2(C^3\Pi_u)$ can be spent on gas heating: $\varepsilon_{Q6} \approx 6.5$ eV.

Another important process that can make a significant contribution to rapid heating of H_2-air mixtures is the quenching of electronically excited $O(^1D)$ atoms:

(Q7) $O(^1D) + N_2 \rightarrow O(^3P) + N_2(v = 8,9)$, $k_{Q7} = 1.8\cdot10^{-11}\cdot\exp(107/T)$ cm^3/s [103]

(Q8) $O(^1D) + O_2 \rightarrow O(^3P) + O_2(b^1\Sigma_g^+)$, $k_{Q8} = 3.2\cdot10^{-11}\cdot\exp(67/T)$ cm^3/s [103]

(Q9) $O(^1D) + H_2 \rightarrow OH(v) + H$, $k_{Q9} = 1.1\cdot10^{-10}$ cm^3/s [30]

In reaction (Q7), $\varepsilon_{Q7} = 1.37$ eV [64] goes to gas heating, while in reaction (Q9) (taking into account fast vibrational relaxation of $OH(v)$), $\varepsilon_{Q9} = 1.89$ eV.

It should also be noted that there's a possibility of rapid quenching of electronically-excited $O_2(b^1\Sigma_g^+)$ molecules generated in reaction (Q10), with hydrogen molecules:

(Q10) $O_2(b^1\Sigma_g^+) + H_2 \rightarrow O_2(a^1\Delta_g) + H_2(v)$, $k_{Q10} = 10^{-12}$ cm^3/s [139]

In this case, the excess energy goes mainly to vibrational excitation of $H_2(v)$ molecules [139], followed by relaxation that goes to gas heating. To describe the process of VT- relaxation of $N_2(v)$

and $H_2(v)$ excitation, data on the rate constants of these reactions given in [30], [64], [95] can be used. These data are shown in Figure 20.

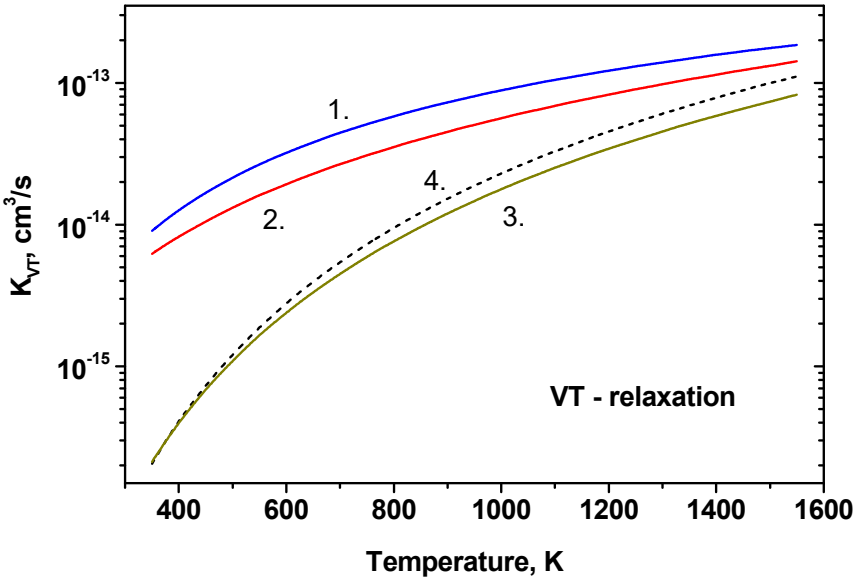

Figure 20. Calculated temperature dependences of the rates of $N_2(v=1)$ VT-relaxation in reaction with H_2O (curve 1) [30], $O(^3P)$ (curve 2) [64] and H_2 (curve 3) [30], as well as $H_2(v=1)$ relaxation in reaction with hydrogen molecules (curve 4) [95].

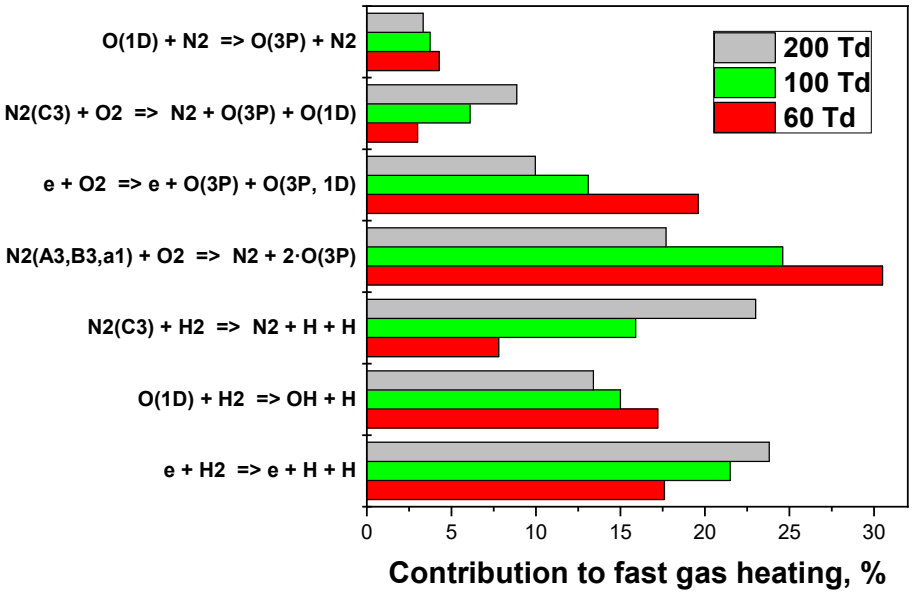

Figure 21. Comparative analysis of the distribution of energy spent to fast gas heating in the reactions with excited species and dissociation by electron impact for different *E/N* values. Calculations are done for H_2-air mixture, ER = 1.

Figure 21 shows a comparative analysis of the distribution of energy consumed by fast gas heating for the reactions with excited species and dissociation by electron impact. These data correspond to the stoichiometric H_2-air mixture. The fraction of reactions involving hydrogen molecules increases from 43% to 60% with an increase in reduced electric field *E/N* from 60 to 200 Td.

The main role belongs to the reaction of H_2 dissociation by electron impact and the quenching reaction of $N_2(C^3\Pi_u)$ with hydrogen molecules.

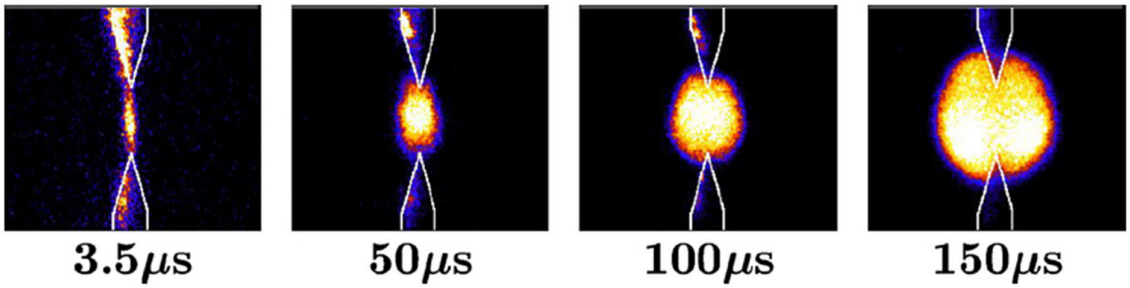

Figure 22. Two-dimensional LIF OH images at different time instants for the mixture containing 30% H_2 in air. Experiments are performed at P_0 = 1 atm and T_0 = 300 K [140].

Gas temperature and the density of OH radicals under the action a pulsed nanosecond discharge were measured in [140] in 30% H_2-air mixture at P_0 = 1 atm and T_0 = 300 K. To ignite the combustible mixture, a pin-to-pin spark nanosecond discharge located in the middle of the combustion chamber, was used. The interelectrode distance was 2 mm. Typical duration of the discharge pulse did not exceed 10 ns. The density of OH radicals in the discharge afterglow was measured using LIF technique and the temperature was determined from the ratio of two LIF OH line intensities P2(8) and Q1(11) assuming that the rotational distribution of OH radicals has reached thermal equilibrium 10 μs after the discharge. Figure 22 shows two-dimensional LIF OH images at various points in time for a mixture of 30% H_2-air at E = 0.073 mJ. The LIF signal intensity is normalized in each image and each image is for a different discharge.

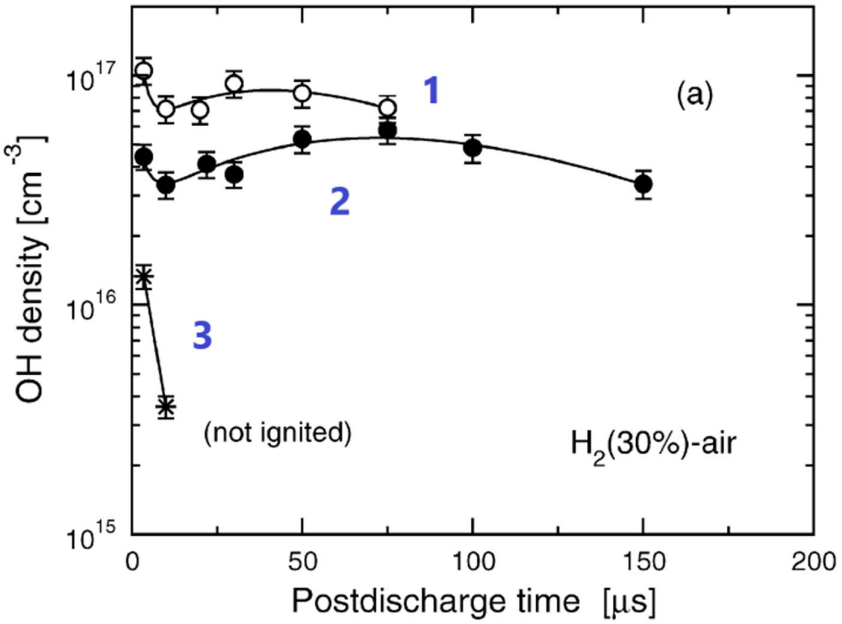

Figure 23. Experimentally measured time evolution of OH density in 30% H_2-air mixture after spark discharge [140] at P = 1 atm, T_0 = 300 K. Points (1-3) correspond to the discharge energies $\varepsilon = 1.85 \cdot \varepsilon_{min}$, $1.25 \cdot \varepsilon_{min}$ and $0.95 \cdot \varepsilon_{min}$, respectively.

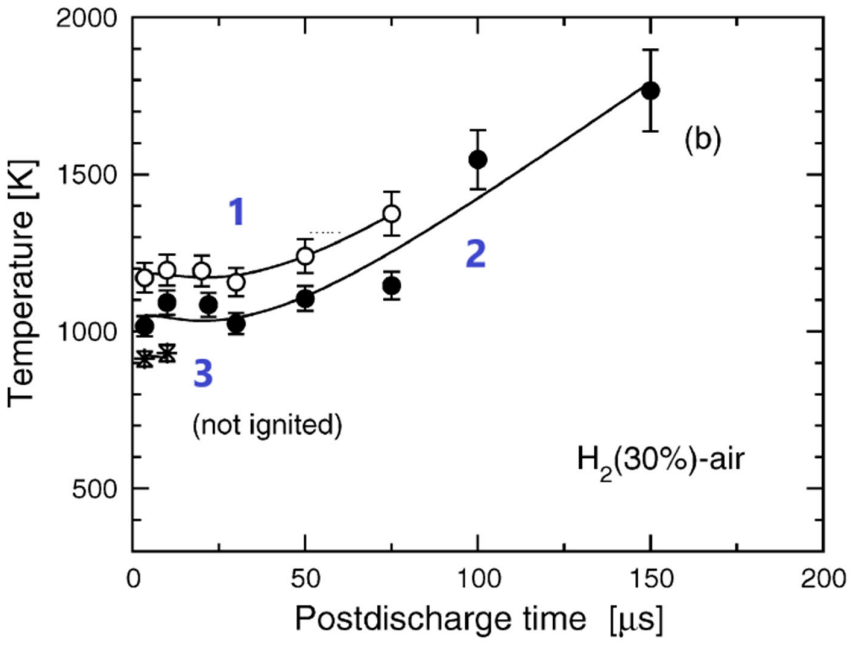

Figure 24. Experimentally measured time evolution of gas temperature in 30% H_2-air mixture after spark discharge [140] at P = 1 atm, T_0 = 300 K. Points (1-3) correspond to the discharge energies $\varepsilon = 1.85 \cdot \varepsilon_{min}$, $1.25 \cdot \varepsilon_{min}$ and $0.95 \cdot \varepsilon_{min}$, respectively.

Figures 23, 24 show the measured data on the dynamics of OH radical concentration and gas temperature after the discharge in a 30% H_2-air mixture for various values of the energy applied [140]. Here, the minimum ignition energy is ε_{min} = 0.048 mJ. According to these data, at t = 5-20 μs after the discharge, gas temperature reaches 1000-1100 K, that is, gas heating is ΔT = 700-800 K. Taking into account the gas-dynamic rarefaction of the channel, which characteristic time in this case does not exceed 500 ns, the specific energy consumed by gas heating is $W_h \approx 0.226$ eV/mol. This involves both heat release in quenching reactions of electronically excited atoms and molecules (see Figure 21) and heat release in chemical reactions proceeding in a combustible mixture.

Under conditions of [140], the main energy release is at E/N = 130-150 Td. In these fields, about half of the discharge energy is consumed by vibrational excitation of N_2 and H_2 molecules (see Figure 19). Therefore, relaxation of vibrational excitation of these molecules is important. According to Figure 20, at gas temperature T = 600 K, the rates of $N_2(v)$ and $H_2(v)$ VT-relaxation in collisions with hydrogen molecules are $k_{VT} = (2\text{-}3) \cdot 10^{-15}$ cm^3/s. Consequently, the characteristic times of vibrational relaxation exceed 100 microseconds, and these processes can be ignored at time interval of 5-10 microseconds discussed here.

Paper [141] provides the results of numerical simulation of the pulsed nanosecond discharge parameters in hydrogen-air mixtures at atmospheric pressure and initial temperature equal to T_0 = 1000 K. The studies were made using a 2D axisymmetric model for a set of equivalence ratios ER = 0, 0.3, 1 and 1.5. Nanosecond voltage of 2 ns rise time, 5.5 ns duration and 5 kV voltage amplitude was used in the calculations. The processes of fast gas heating in high-pressure hydrogen-air

mixtures were taken into account. During the streamer stage and up to the formation of a plasma channel between two pin-to-pin electrodes, a change in the mixture composition only weakly influenced the discharge dynamics and structure. Generation of main active species O(^{3}P), H, OH and an increase in gas temperature occurred as a result of quenching of electronically excited states $N_2(A^3\Sigma_u^+)$, $N_2(B^3\Pi_g)$, $N_2(C^3\Pi_u)$ with oxygen and hydrogen molecules, and quenching of electronically excited O(^{1}D) atoms with hydrogen molecules.

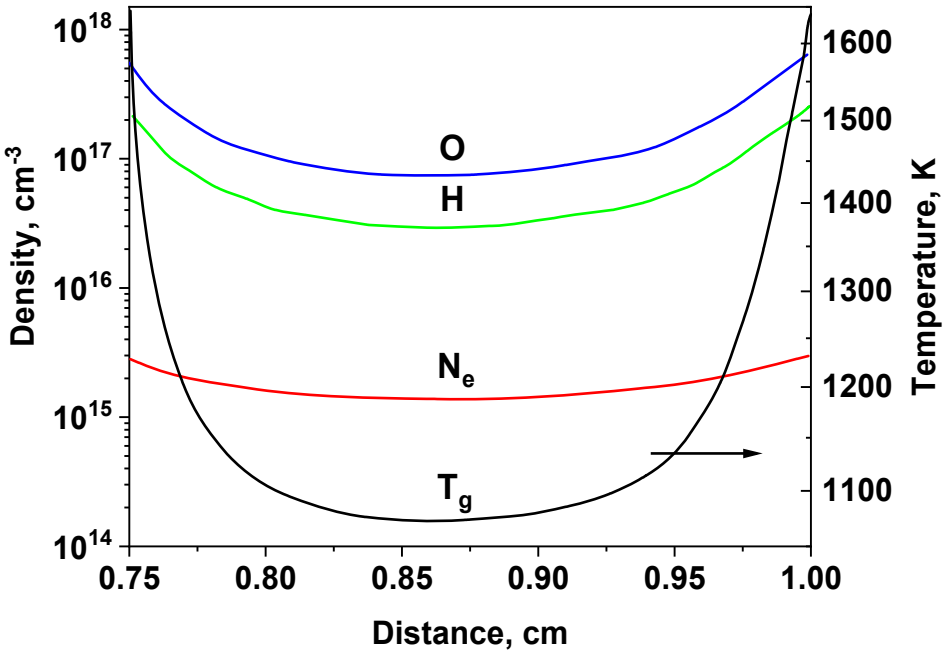

Figure 25. Calculated axial distribution of O, H atom densities, electron density and gas temperature at t = 10 ns for a lean H_2-air mixture with ER = 0.3, P_0 = 1 atm and T_0 = 1000 K [141].

Distribution of electron density, O, H atom density and gas temperature along the discharge axis for H_2-air ER = 0.3 mixture immediately after the discharge is shown in Figure 25. The densities of radicals and gas heating by the discharge show pronounced maxima near the electrodes. This effect is due to a smaller radius of the discharge channel and, accordingly, higher current density and specific energy input in these regions. Considering higher fast gas heating near the electrodes, it is essential to adequately describe the combustible mixture ignition dynamics and combustion wave formation.

8. Ignition of hydrocarbon-based mixtures and fast gas heating

Reviews on plasma-assisted combustion [2], [52] discuss the lack of cross-sections of interaction between electrons and hydrocarbon molecules. During the past 3-4 decades, the study of electron scattering cross-sections for hydrocarbon-containing gas mixtures was motivated by the development of the microelectronics. Cross-sections available for acetylene and alkanes from methane to pentane are structured and reviewed in [142]. Special attention is given to the presence/ab-

sence of the swarm parameters (ionization coefficient and drift velocity), cross-sections of ionization and attachment, and comparison of the available data with those for the other hydrocarbons. Besides these cross-sections, there are sets of cross-sections for CO_2, NO_2, N_2O, O_3, H_2O, NH_3, CH_2O_2, C_2H_4, C_2H_6, CH_3OH, C_3H_4, C_2H_4O, CH_3NH_2, C_3H_6, C_3H_8, c-C_3H_6, C_3H_6O, C_4H_6, 1,3-C_4H_6, 2-C_4H_6, C_6H_6, C_4H_8, 1-C_3H_8O, 2-C_3H_8O, C_5H_{10}, C_6H_{14}, C_6H_{12}, i-C_4H_{10}, i-C_8H_{18}, C_8H_{18}, C_4H_8O, $C_5H_{10}O_2$, C_7H_8. For complex molecules, only the selected cross-sections are typically known.

Ionization thresholds for the most of hydrocarbons are lower than for O_2 (12.1 eV) or N_2 (15.6 eV) molecules [93]. For linear alkanes C_nH_{2n+2}, ionization threshold decreases from 11.63 eV for C_2H_6 to 10.03 eV for C_7H_{16}, facilitating ionization. But in stoichiometric hydrocarbon-containing mixtures, the density of molecular oxygen dominates over the density of hydrocarbon $[C_xH_y] << [O_2]$. As a result, the frequency of hydrocarbon ionization is low comparing to ionization frequency of N_2 and O_2. Kinetic calculations does not show crucial difference in energy branching for air and fuel-air stoichiometric mixtures; the main ionization and dissociation channels typically remain unchanged. This is illustrated by Figure 26, where the rate constants of the main emitting state $N_2(C^3\Pi_u)$ excitation and total ionization

$$k_{ion}^{tot} = k_{ion}^{N_2} \cdot \frac{N_2}{M} + k_{ion}^{O_2} \cdot \frac{O_2}{M} + k_{ion}^{C_2H_6} \cdot \frac{C_2H_6}{M}$$

are compared for air and $N_2 : O_2 : C_2H_6 = 0.76 : 0.19 : 0.05$ mixture. It is clearly seen that 5% of ethane in air does not change the considered rate constants.

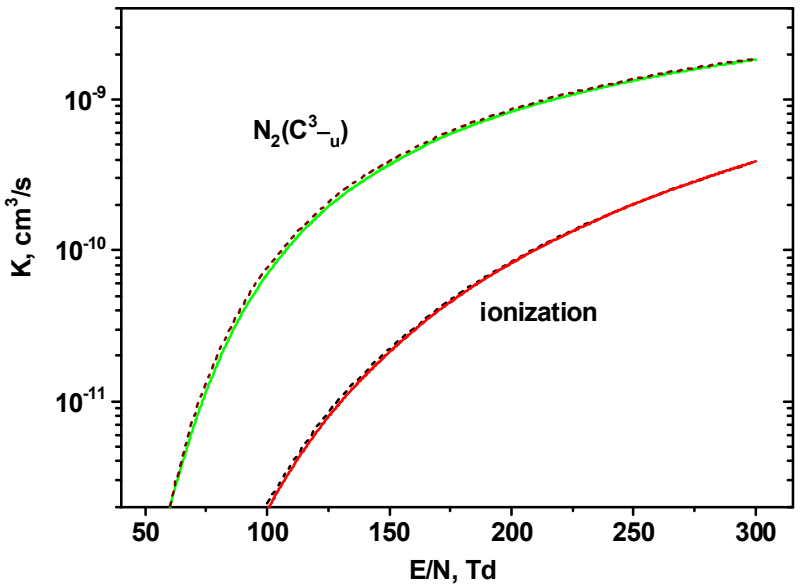

Figure 26. Rate constants of the selected processes in collisions with electrons: excitation of $N_2(C^3\Pi_u)$ and ionization in $N_2 : O_2 = 0.8 : 0.2$ (solid curves) and $N_2 : O_2 : C_2H_6 = 0.76 : 0.19 : 0.05$ (dashed curves) mixtures. Cross-sections for electron scattering on C_2H_6, O_2, and N_2 molecules were taken from [142], [132] and [129] respectively.

It should be noted that most of comprehensive kinetic studies of plasma action on hydrocarbon-containing mixtures are done for strongly diluted conditions and for low specific delivered energies (see, for example, [143], [144]). In particular, it was shown in [145] that a small amount of methane addition (1%) in He will nonlinearly affects the electron energy and number density. These studies are very important for determining the kinetic pathways and for studying energy transfer from electronically excited atoms and molecules to dissociation of oxygen and hydrocarbon but do not provide information about fast gas heating. For this reason, below we consider mainly experiments and modeling in fuel-air mixtures.

For the most of discharges, whether plasma will be uniform or not, is decided at the stage of the discharge inception. Transient discharges propagate in the form of fast ionization wave at moderate pressures [52], or streamer discharge at high pressures [146] with a well-defined zone of high electric fields in the front. Two processes are the most important in the front and in the vicinity of the discharge front: ionization by electron impact and photoionization. Ionization by electron impact is typically the strongest process providing the majority of electrons. Photoionization, although a few order of magnitude lower, ensures the density of seed electrons and the uniformity of plasma in the close vicinity of the front.

A classical model of photoionization in air is given in [147] and analyzed in details in [148]. The model is limited by low current discharges where the UV radiation comes mainly from electronically excited singlet states of nitrogen, namely $N_2(b^1\Pi$, $b'^1\Sigma^+_u$, $c^1\Pi_u$, and $c'^1\Sigma_u^+)$. Photoionization occurs upon absorption of this radiation by oxygen molecules in wavelength range λ = 98 - 102.5 nm (energies of the UV radiation of 12.65-12.09 eV). According to the model [147], at lower wavelength, the radiation is absorbed by N_2 molecules, and at $\lambda > 102.5$ nm, the photon energy is below the ionization threshold of O_2 molecules. Comparison of emission spectra, absorption and ionization yield given in [148] shows that at $\lambda < 98$ nm, the UV emission comes mainly from atoms and atomic ions of nitrogen and oxygen, and their densities are typically low in the front of the discharge.

Consider addition of hydrocarbons in air. Absorption of UV radiation by hydrocarbons is very efficient; in the series of alkanes, the photoabsorption cross-section for λ = 100 nm radiation increases from $4\cdot10^{-17}$ cm^2 for methane to $9\cdot10^{-17}$ cm^2 for n-butane, respectively [149].

As a result, different physics provide similar results for methane and higher hydrocarbons. For methane, absorption of UV radiation from singlet states of molecular nitrogen in the “classical” UV-window of 98-102.5 nm is high. Although the ionization yield of CH_4 is low and UV photons mainly cause dissociation of CH_4, absorption of UV radiation by methane provides fast decay of the photoionization coefficient or the photoionization rate (the number of photoelectrons at a unit solid angle per unit path of radiation divided by gas pressure) with distance. This is illustrated by Figure 27, where the photoionization coefficient is plotted as a function of distance [150]

in atmospheric pressure air and in mixture $N_2 : O_2 : CH_4 = 0.715 : 0.19 : 0.095$. It is clearly seen that even at 40 μm from the source of radiation (an emitting atom or molecule in the considered case), the photoionization rate in air is more than one order of magnitude higher comparing to methane-containing mixture.

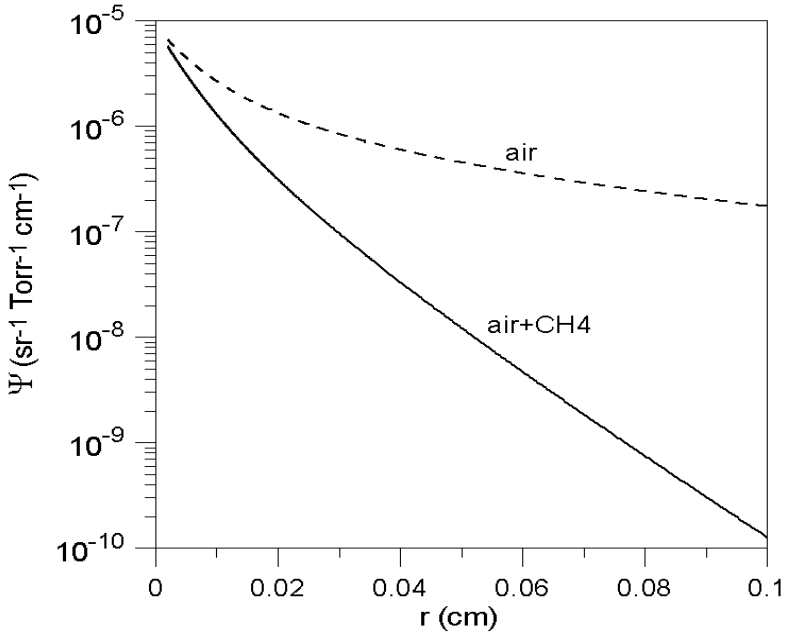

Figure 27. Photoionization coefficient Ψ(r) in air and in mixture $N_2 : O_2 : CH_4 = 0.715 : 0.19 : 0.095$, at $P = 1$ atm, $T = 300$ K [150].

For higher hydrocarbons, absorption of UV radiation provides photoionization because of lower ionization threshold and thus higher values of photoionization yield at the given wavelengths. But similar to methane-containing mixtures, the emission is absorbed at much shorter distances, and thus, it is more complicated to get uniform plasma in hydrocarbon-containing mixtures comparing to air.

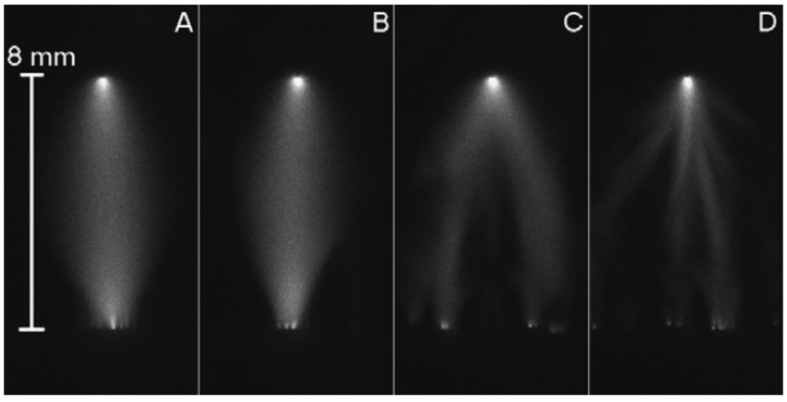

Figure 28. Experimentally obtained ICCD images of nanosecond discharge in (a) air, ER = 0; (b) C_3H_8-air, ER = 0.4; (c) C_3H_8-air, ER = 0.8; (d) C_3H_8-air, ER = 2.1 at $P = 1$ atm, $T = 300$ K. ICCD gate is 3 ns [151].

Experimental observations prove the considerations given above and show formation of a multi-channel structure and constriction of discharges with additions of hydrocarbon. The authors of [151] report on an increase in branching with the increasing fuel content in the mixture (Figure 28). These data are in good agreement with the data of other authors: constriction of moderate pressure (P = 40 Torr) nanosecond discharge in ethylene-air mixtures with ER = 0.1 and 0.01 has been reported in [104]; a significant dependence of the results upon the spatial structure of the discharge was directly confirmed by comparative study of the ignition of C_3H_8 : air and C_7H_{16} : air mixtures at atmospheric pressure and temperature [152].

The authors [151] point out that, despite noticeable macroscopic differences in different mixtures – appearing branching and the fact that the discharge pulses in richer mixtures were audibly louder – the measured electrical characteristics remained essentially identical, with no more than 5% variation in pulse width, peak current, peak voltage and energy delivered. On the contrary, the authors [3] report on significant, 6 times decrease of the energy delivered in the discharge, increasing CH_4 density in the CH_4 : O_2 : Ar mixture from ER = 0.3 to ER = 1.

The general conclusion is that noticeable branching of the discharge is observed when adding even a few percent of C_xH_y in air. A physical reason for filamentation and formation of a multi-channel structure is a decrease in a typical absorption length and thus, a significant drop in the rate of photoinization comparing to hydrocarbon-free mixture. Filamentation leads to a local increase in the specific delivered energy, and inevitably, to an increased fast gas heating.

Similar effect, namely a decrease in the density of photoelectrons, is observed when passing from air to mixtures with lower densities of molecular oxygen. The results of 3D PIC-MCC calculations in N_2 - 20% O_2 and N_2 - 0.2% O_2 mixtures at time points t = 1.5, 2.5 and 3.5 ns, are shown in Figure 29 [153]. A decrease in discharge uniformity and branching similar to the mixtures with additions of hydrocarbons, are clearly seen.

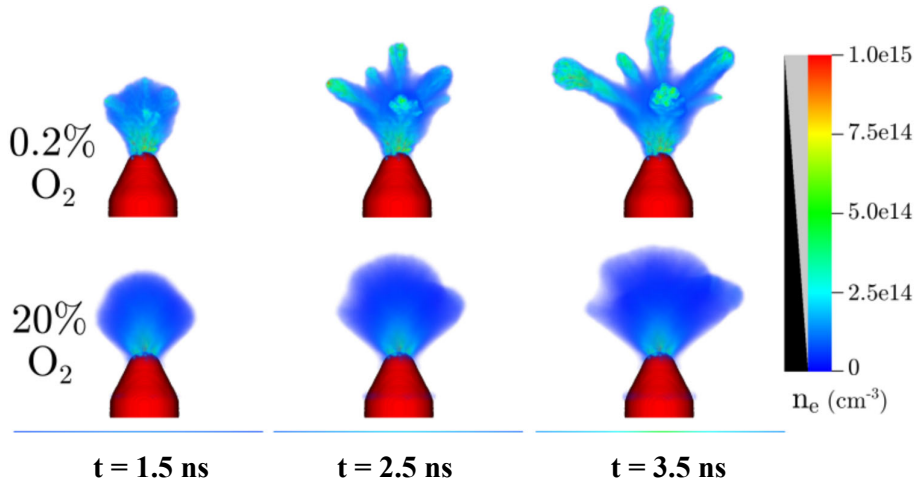

Figure 29. Development of the discharge at atmospheric pressure in N_2 - 20% O_2 and N_2 - 0.2% O_2 mixtures. Particle-in-cell simulation of the electron density [153].

Another effect important for C_xH_y : O_2 mixtures is thermal instability of the discharge and so the redistribution of the specific delivered discharge energy. This effect is clearly demonstrated in [154] for pulse-periodic discharge in CH_4 : O_2 : Ar = 6.6 : 13.4 : 80 mixture. Measurements of the electric field using 1D femtosecond E-FISH technique and gas density with laser Rayleigh scattering technique accompanied by CMOS/ICCD imaging allowed detailed analysis of transition from uniform to filamentary form of the discharge with an increase in the number of pulses. Comparing the results for CH_4 : Ar = 6.6 : 93.4 and O_2 : Ar = 13.4 : 86.6 mixtures, it was proven that heat release in plasma-assisted low temperature fuel oxidation and pyrolysis provoke plasma excited instability.

Similar to air, gas heating by the discharge in hydrocarbon-containing mixtures can be divided into the fast stage explained by relaxation of electronically excited species in collisions with molecules or atoms, and relatively slow stage due to VV'-exchange and the following VT-relaxation. It should be noted that for a peculiar case of C_xH_y : O_2 mixtures, VT-relaxation of vibrationally excited oxygen molecules in reaction with hydrocarbons is fast and provides significant heat increase within a gas-dynamic time. Indeed, typical time τ_v for vibrational relaxation of $O_2(v)$ in reaction with C_2H_4 molecules was measured in [155] for T = 430-1350 K. It was shown that $P \cdot \tau_v = 1.2 \cdot 10^{-7}$ atm·s for the considered temperature range. In this case the rate constant of VT-relaxation is equal to

$$k_{VT} = 3.4 \cdot 10^{-13} \cdot (T/300) \text{ cm}^3/\text{s},$$

and typical time of VT-relaxation of $O_2(v)$ in stoichiometric C_2H_4/O_2 mixture is equal to

$$\tau_{VT} \approx 0.5 \text{ μs} \cdot (1 \text{ atm}/P).$$

So, in stoichiometric C_xH_y/O_2 mixtures at pressures higher than 1 bar, VT-relaxation at the times shorter than gas-dynamic time can influence formation and propagation of the combustion waves.

Will also note an important role of reactions of excited atoms $O(^1D)$ with fuel molecules [Yan 2020]: it was shown in [Popov 2016] that these reactions can be the main pathway of C_xH_y dissociation in hydrocarbon-air non-equilibrium plasma. In stoichiometric C_xH_y - air mixtures, the frequencies of reactions $O(^1D)$ with C_xH_y molecules can be comparable to the frequencies of quenching $O(^1D)$ by N_2 and O_2 molecules [Popov 2016,]; therefore, these reactions should be taken into account in the mechanist of fast gas heating.

The studies of fast gas heating in hydrocarbon/air mixtures are rather complicated, since heating due to quenching of electronically excited states of atoms and molecules is accompanied by intense heat release in oxidation reactions of hydrocarbon molecules, in particular, in reactions with atomic species actively generated in non-equilibrium gas-discharge plasma. It is very difficult to experimentally separate the stage of fast gas heating and the initial stage of the combustible mixture oxidation. Several papers combining the study of discharge parameters and fast gas heating calculations and measurements in hydrocarbon-air mixtures are discussed below.

Fast gas heating in acetylene-containing mixtures was theoretically studied in [77]. The authors performed kinetic calculations for C_2H_2/air mixture based on the kinetic scheme developed earlier to describe fast gas heating in $C_2H_2/O_2/Ar$ mixtures under shock-tube conditions [131]. They compared the fractional electron power spent on gas heating in a stoichiometric C_2H_2/air mixture and in air at T_0 = 300 K and P = 1 atm versus reduced electric field E/N at which the energy was deposited.

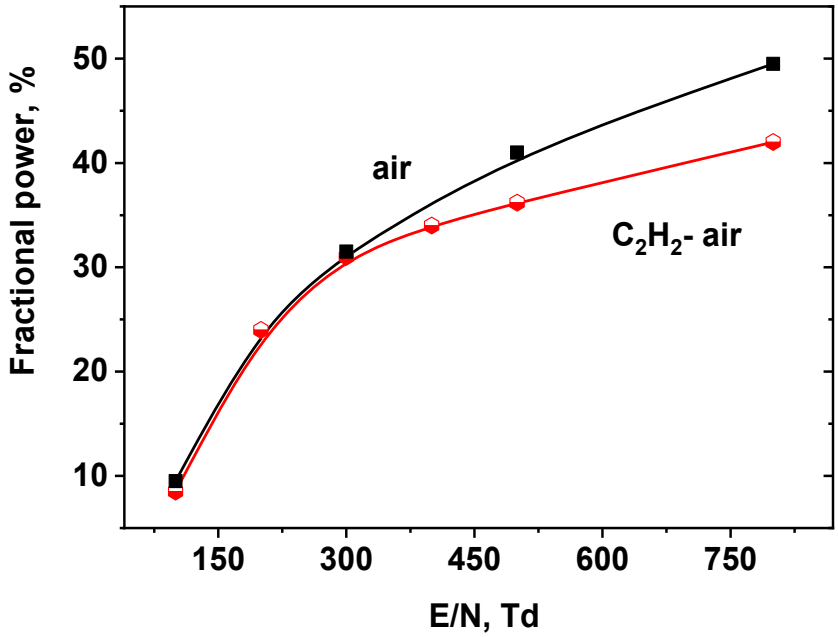

Figure 30. Calculated fractional electron power transferred to heat in a stoichiometric C_2H_2/air mixture and in air at 300 K and 1 atm as a function of E/N (according to [77]).

According to the calculations (Figure 30), at reduced electric fields in range E/N = 100-400 Td, fractional power spent on fast gas heating is practically the same for air and C_2H_2/air mixture. At higher fields, fractional power in acetylene-air mixture becomes lower than in air. This difference is due to a change in positive-ion composition in the presence of C_2H_2 molecules. In atmospheric pressure air, oxygen ions O_2^+ are rapidly transformed to O_4^+. According to the model [66], [77], the energy released in reaction of electron-ion recombination of O_4^+ is consumed by gas heating with a low probability of the dissociative channel (see discussion in section 6). Addition of C_2H_2 molecules changes the composition of positive ions due to the fast charge exchange reaction

$$O_2^+ + C_2H_2 \rightarrow O_2 + C_2H_2^+, \quad k = 10^{-9}\ \mathrm{cm^3/s}\ \ [131],$$

In the following reaction of electron-ion recombination $e + C_2H_2^+$, a noticeable part of the energy is spent to dissociation of C_2H_2 molecules [156] which reduces the fast gas heating efficiency at E/N > 400 Td (see Figure 30).

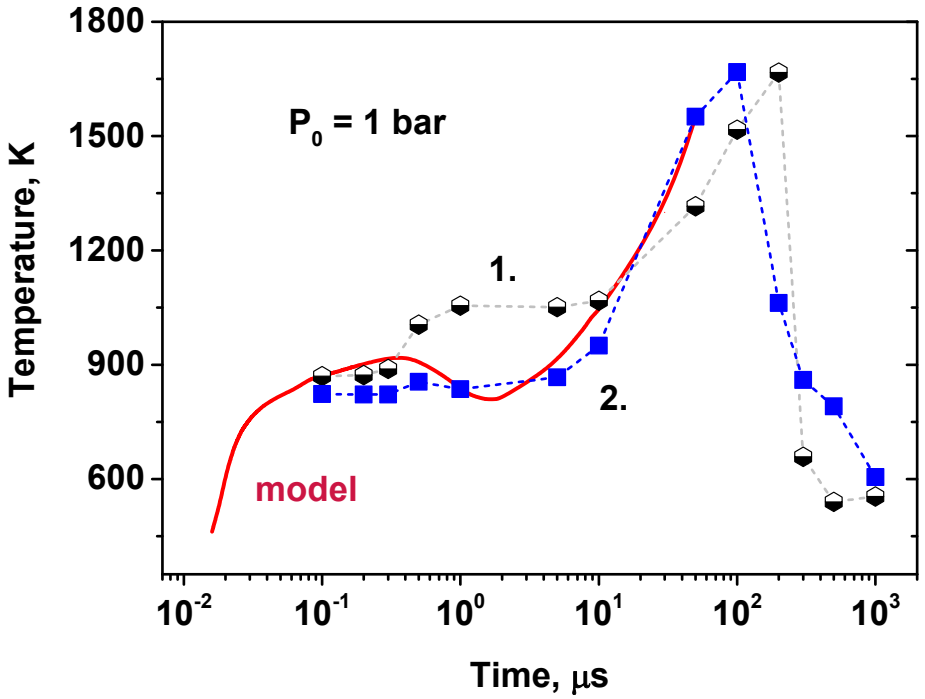

Figure 31. Measured gas temperature (symbols and dashed lines) in C_3H_8 - air mixture (ER = 0.4) (1) and in air (2) at P = 1 atm and at the ambient initial temperature under the effect of nanosecond discharges (based on [157]). Solid curve corresponds to calculations in air for the given conditions [96].

Experimental work [157] compared the temporal behavior of gas temperature and of vibrational temperature of nitrogen molecules $T_v(N_2)$ in a pulsed nanosecond discharge and in the afterglow in air and lean nonflammable C_3H_8 /air (ER = 0.4) mixtures at P_0 = 1 atm, T_0 = 300 K. Experimental data in Figure 31 are obtained in the center of the discharge gap, 3.25 mm from the high voltage electrode. Calculations is air (solid curve) are in good agreement with the experimental results. Even during the discharge, gas temperature increases to 800-900 K being just slightly (100 K) higher in propane-containing mixture than in the air. Thus, the effect of small (1.5%) additions of C_3H_8 does not noticeably influence the dynamics of fast gas heating. The only observed difference, about 200 K within t = 300-700 ns can be related to heat release in C_3H_8 oxidation reactions. Temperature rise at t > 1 μs is due to VT-relaxation of molecular nitrogen $N_2(v)$ in reaction with atomic oxygen (O-atoms density reaching $[O(^3P)] \approx 2\cdot10^{18}$ cm^{-3}, see the calculation results in Figure 10b of this review).

No agreement between gas temperatures in air and methane-containing mixture is reported in [158], [159]. Gas temperature and vibrational temperature T_v^{N2} were measured under identical conditions in atmospheric pressure pin-to-pin discharge at ambient initial temperature using N_2 CARS thermometry. High-voltage pulse of 19 kV amplitude, 70 ns FWHM and 100 Hz repetitive frequency was used in the experiments. The data were compared for air and premixed CH_4/air flows. The mixture equivalence ratio varied within the range ER = 0 - 2. Summary of the data obtained by CARS technique is shown in Figure 32. Numerical 0-D simulations were performed

using CHEMKIN-based code involving GRI Mech 3.0 mechanism with artificial addition of radicals at the initial stage. The authors of [159] claim that the energy transfer induced by collisions between N_2 and CH_4 results in significant, up to 2500 K, gas heating at the very early stage of ignition (about 100 ns). Unfortunately, no detailed information about kinetic calculations is given in the paper, so no analysis can be done.

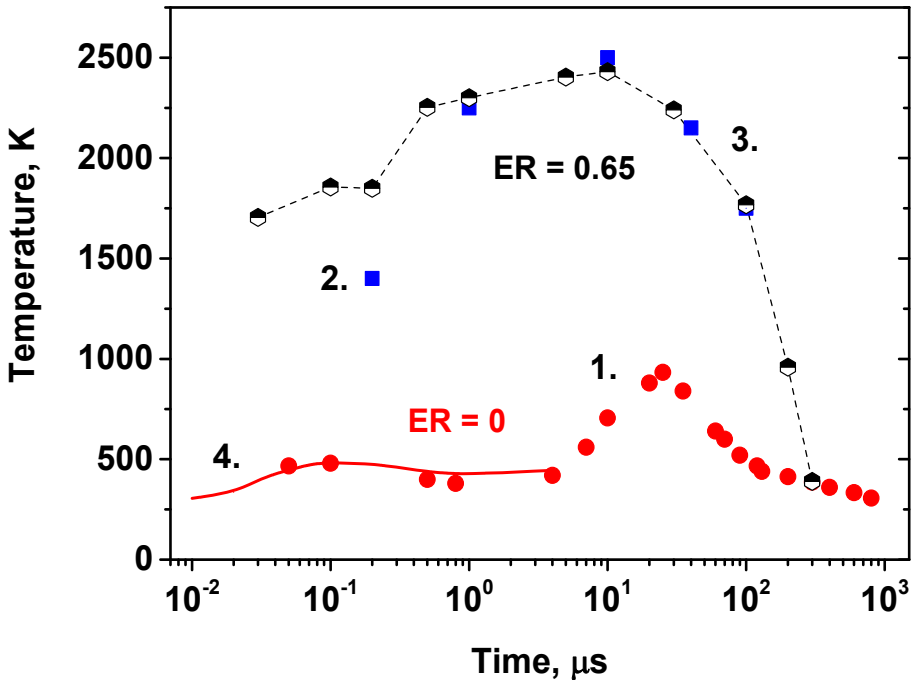

Figure 32. Temporal evolution of gas temperature in air and CH_4/air mixture (ER = 0.65) at P = 1 atm in the afterglow of pulsed nanosecond discharge. Symbols represent experimental data: 1 – air [158], 2, 3 - CH_4/air mixture [158], [159], solid line 4 represents calculation results of fast gas heating in air using the model from [96].

If the discharge energy, taking into account relaxation of vibrationally excited $N_2(v)$ is completely thermalized, then the resulting increase in gas temperature in air will be $\Delta T = 640$ K. Measurements in the CH_4/air mixture result in significantly higher heating values $\Delta T \approx 2100$ K, therefore, the main temperature rise in this mixture is associated with heat release in methane oxidation reactions. The temperature of completely burnt CH_4/air mixture at ER = 0.65 is 1790 K [160], taking into account gas heating in the discharge (640 K), the final temperature will be 2430 K, which is consistent with the measurement data (see Figure 32). Thus, the difference between gas temperature in air and ER = 0.65 methane/air mixture observed in the experiments [159] is explained by the active heat release due to the CH_4 combustion chemistry. It should be noted that the reactions of chain prolongation are intensified by additional oxygen atoms generated in the discharge and by a rise in gas temperature as a result of the described fast gas heating mechanism.

The main experimental data on fast gas heating in air, nitrogen, H_2-air and C_xH_y-air mixtures, are presented in the Table 4 added to the Appendix 2. For each experiment gas pressure, duration

of the discharge pulse, *E/N* range, gas mixture composition, specific delivered energy and part of energy spent for the fast gas heating are given.

Conclusions

The subject of this review is fast gas heating (FGH) - an abrupt increase in gas temperature in non-equilibrium transitive low-temperature plasma due to relaxation of electronically excited states of atoms and molecules. In the active flow control, fast gas heating is responsible for thermal frequency perturbations in the range of unstable frequencies of flow instabilities. These perturbations, being amplified by the flow, control a point of laminar-to-turbulent transition, a process of mixing, noise level etc. High velocity flows, up to M = 0.85, can be controlled with low power consumption. In plasma-assisted combustion, abrupt temperature increase due to FGH, together with generation of radicals in plasma, induces acceleration of combustion chemistry providing shortening of the induction delay time and intensification of combustion.

A majority of available experiments on fast gas heating is made in non-combustible mixtures, typically in air or nitrogen-oxygen mixtures. A detailed overview of FGH in these mixtures allows analysis of gas heating in lean and stoichiometric fuel-air mixtures, and scarce experiments in hydrogen-containing and hydrocarbon-containing mixtures provide experimental verification of the suggested kinetic models.

Fast gas heating was studied at different conditions and for different discharges. To generalize the results of empirical research within the frameworks of one model as much as possible, a universal parameter describing FGH has been suggested. This parameter is the fraction of energy spent on fast gas heating η_R. This paper considers the dependence of η_R on reduced electric field, gas pressure, oxygen fraction in the mixture and other parameters.

Early papers of 1980-1990 provided mainly experimentally measured dynamics of gas heating, without self-consistent study of reduced electric field and specific deposited energy, - so no parametric analysis of the part of energy spent on FGH was possible. This analysis has been made on the basis of the later papers of 2010-2020.

Depending on the value of *E/N*, the distribution of the discharge energy over the degrees of freedom changes significantly. In air, the available data were analyzed for three different intervals of the reduced electric field: (a) low fields $E/N < 100$-150 Td, (b) moderate fields $E/N = 150$-400 Td, when most of the discharge energy goes to dissociation of oxygen molecules and to electronic excitation of atoms and molecules, and (c) high fields $E/N > 400$ Td, when a significant part of the discharge energy is spent on dissociation of nitrogen molecules and ionization.

The suggested theoretical model of fast gas heating in nitrogen-oxygen gas-discharge plasma is based on quenching of electronically excited states of nitrogen molecules by O_2 and quenching of excited $O(^1D)$ atoms by N_2, and, at high specific deposited energy, quenching of electronically excited species by O atoms. At high *E/N*, heat release during dissociation of N_2 by electron impact

and reactions involving charged particles (namely, ion-molecular reactions and reactions of electron-ion and ion-ion recombination) becomes important. It should be noted that in the range of electric fields E/N = 150-300 Td, a significant part of discharge energy (50-65%) is goes to dissociation of molecular oxygen. As a result, a part of energy spent on FHG is limited for the considered interval of electric fields: $\eta_R < 50\%$.

Scarce experimental papers and dedicated modelling in fuel-containing mixtures lead to the conclusion that fast gas heating can substantially influence the earliest, sub-microsecond, stage of combustion chemistry, changing the initial conditions for combustion. In gas-discharge hydrogen-air plasmas, an important role is played by reactions of dissociation of hydrogen molecules by electron impact and reactions of quenching of electronically excited states $O(^1D)$ and $N_2(C^3\Pi_u)$ by hydrogen. In hydrocarbon-air mixtures, the role of reactions with hydrocarbons, in particular reactions of quenching of electronically excited atoms and molecules by C_xH_y, decreases with a decrease in hydrocarbons fraction in the mixture. We suggest, basing on the analysis provided in this paper, that the efficiency of fast gas heating in air can be considered as an estimate for FGH in stoichiometric air-based mixtures with heavy hydrocarbons.

With regard to prospective studies, the following should be noted. Direct experiments on fast gas heating in combustible mixtures require, at sub-microsecond scale, separation of heating caused by relaxation of discharge energy, namely FGH, and heat release in combustion chemistry. This is a challenging task complicated mainly by modification of combustion chemistry in the presence of radicals and electronically excited species generated in plasma. Direct approach demands, first of all, the experimental analysis of spatial uniformity of generated plasma and spatial-temporal distribution of the deposited energy; measurements should be made with a nanosecond time resolution. Measurements of the electric field and electron density distribution, although challenging, would provide extremely important information about the resulting discharge and post-discharge kinetics. Measurements of densities of the main active species (electronically excited atoms/molecules and radicals) throughout the discharge region and measurements of gas temperature should be made simultaneously. Measurements of the kinetic curves of main combustion intermediates and gas temperature, now on the scale of combustion chemistry, should complete the experimental picture. Finally, numerical modeling should provide validation of FGH mechanism, including combustion chemistry and fast gas heating in reactions of quenching of excited species. Special attention should be given to study of the fast gas heating at elevated pressures, where extra-high time and space resolutions will be needed.

APPENDIX 1

Fast gas heating in nitrogen and nitrogen with small additions of oxygen

The study of fast heating in pure nitrogen and nitrogen with small additions of oxygen, without referring directly to kinetics of combustion, provides better understanding of the role of electronically excited species in FGH kinetics. Collisional deactivation of the triplet $N_2(A^3\Sigma_u^+)$, $N_2(B^3\Pi_g)$, $N_2(C^3\Pi_u)$ states, excited from the ground $N_2(X^1\Sigma_g^+)$ state by an electron impact, provides significant heat release at times shorter than the time of VT-relaxation, VV- and VV'-exchange.

In [161], fast gas heating was studied in a pulsed glow discharge. The discharge was initiated in pure nitrogen at pressure P = 1.5 Torr by high voltage pulses 120-130 μs in duration. The discharge tube diameter was 12 mm. Measurements were made for currents I = 0.5, 1, and 2 A. The electric field measured with probes changes in time and is E = 18-25 V/cm at t > 40 μs for electrical currents I = 1 and 2 A [161]. Gas temperature was calculated from the measured rotational structure of 1^+ bands of the nitrogen system ($N_2(B^3\Pi_g) \rightarrow N_2(A^3\Sigma_u^+)$ transition).

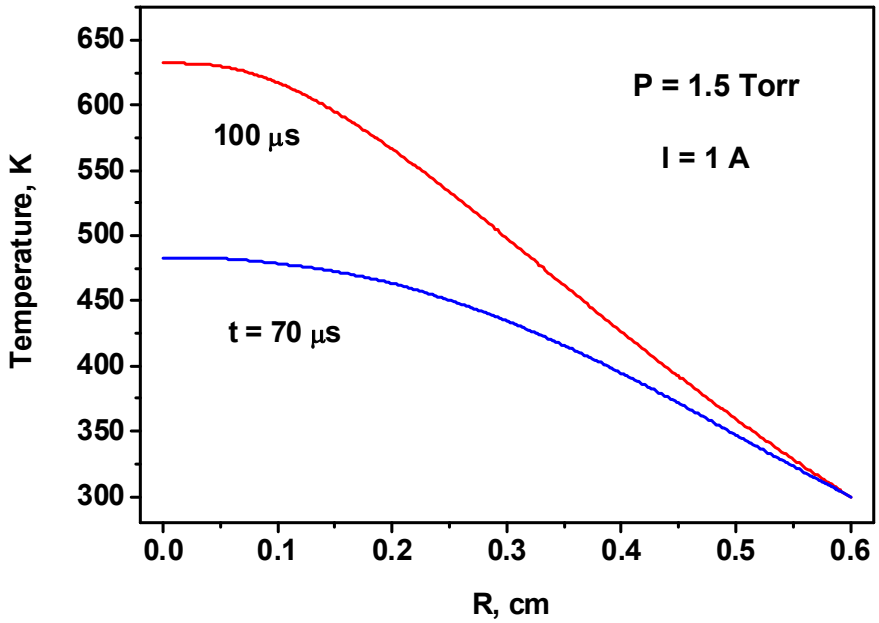

Figure 33. Radial gas temperature profiles calculated at different time points for the conditions of [161].

Calculations with one-dimensional axisymmetric model similar to [162] taking into account gas-dynamic processes have shown that the discharge parameters are highly inhomogeneous along the tube radius. Figure 33 shows the calculated profiles of gas temperature at different time points. With time, the discharge concentrates in the near-axis region, where gas is more diluted. At t > 80-90 μs, gas temperature near the axis differs significantly from the average over the volume. The

calculated electric field in the discharge is consistent with the measurements [161], the *E/N* value in the near axis region is about 60-80 Td.

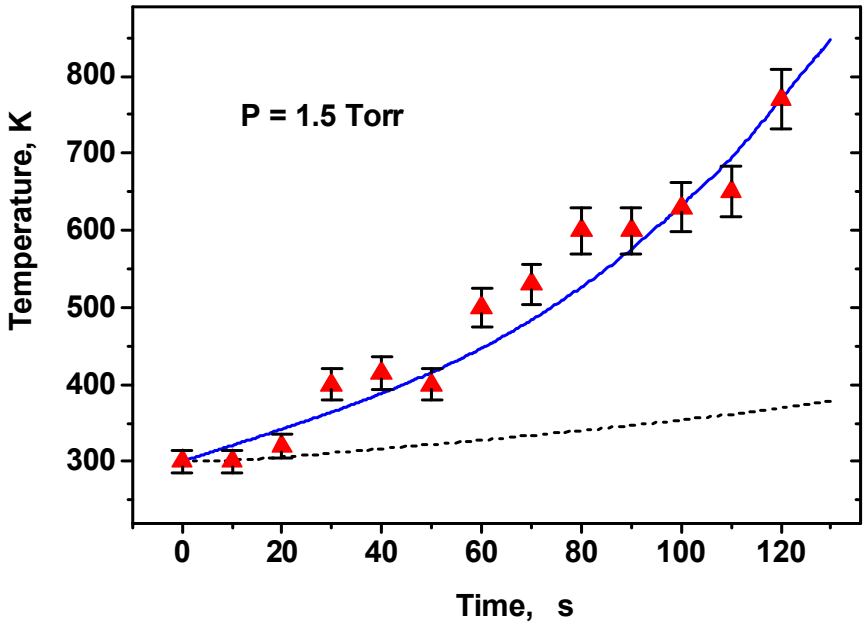

Figure 34. Temperature increase in the discharge with parameters [161] at I = 1 A. Symbols represent experimental data; blue and dashed curves represent calculation results (see text for details).

Figure 34 compares the results of measurements (symbols) and calculations at the axis of the discharge obtained using two different approaches. The dotted line shows calculations of temperature increase in the reaction:

$$N_2(A^3\Sigma_u^+) + N_2(A^3\Sigma_u^+) \rightarrow N_2(B^3\Pi_g, v) + N_2(X^1\Sigma_g^+, v') + \varepsilon_R \qquad \text{(B1)}$$

This process was proposed in [163] and used to explain experimental data of [37]. The assumption that vibrational levels $N_2(X^1\Sigma_g^+, v'=2\div3)$ and $N_2(B^3\Pi_g, v=1\div3)$ are mainly populated in reaction (B1) resulted in the energy transferring to fast gas heating equal to $\varepsilon_R \approx 4$ eV [37], [64].

It is clearly seen that heat release in reaction (B1) is not enough to explain experimental data [161]. The blue curve represents calculation results of temperature increase assuming that 10% of the discharge energy is transformed to gas heating, η_R = 10%. Under considered conditions, at *E/N* = 60-80 Td, the major part of discharge energy goes to vibrational excitation of nitrogen molecules by electron impact [26]. In order to obtain heating efficiency η_R = 10%, it should be assumed that the significant part of heat release comes from VT-exchange (for example, in the reactions between $N_2(A^3\Sigma_u^+)$ and vibrationally excited nitrogen molecules).

Similar value of the energy fraction transformed to gas heating, $\eta_R = (11 \pm 1)$%, was reported in experiments and calculations [37]. The object of the study was a gas discharge in nitrogen in the intersecting (θ = 60°) microwave beams at moderate pressure P = 10 - 40 Torr. Microwave radiation wavelength was λ = 0.8 cm, and pulse duration was $\tau \leq 50$ μs. The thickness of the plasma

sheet, $\Delta \approx 0.5$ cm, was much smaller than longitudinal and transverse dimensions of plasma. Gas temperature in the discharge was determined by two independent techniques: from relative intensity of the rotational lines of $N_2(C^3\Pi_u, v=0) \rightarrow N_2(B^3\Pi_g, v=2)$ transition, and from relative population in the rotational levels of the ground electronic state of NH_2 radicals formed during ammonia dissociation used as a diagnostic additive. These data are shown in Figure 35 by points (1) and (2), respectively. Calculations of the gas heating dynamics in [37], showed that the main energy release in the discharge occurs in the reduced electric field $E/N \approx 80$ Td, the energy deposition reaches W ≈ 0.4 eV/molecule. The best agreement with measured data in terms of the absolute value and the temporal behavior of gas temperature is achieved when the fraction of energy transferred to gas heating is $\eta_R = (11 \pm 1)\%$, see Figure 34.

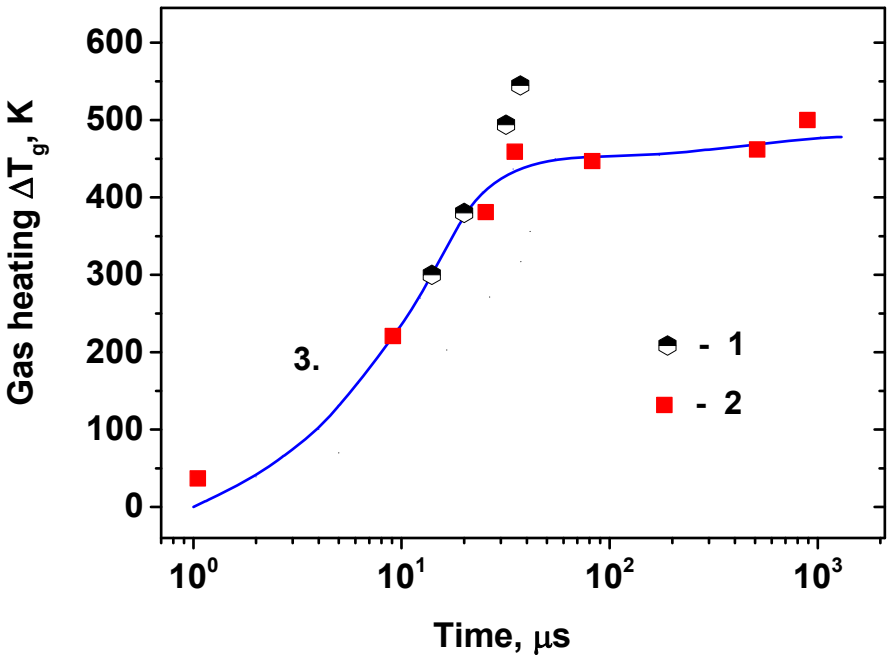

Figure 35. Measured and calculated temporal evolution of gas temperature in nitrogen at P = 30 Torr, excited by microwave discharge [37]. The symbols represent experimental data (see text), the curve represents calculation results at $\eta_R = 11\%$.

Another moderate pressure (P = 100 Torr) discharge in nitrogen with possible fraction of oxygen which did not exceed 0.01% was studied in [38]. The discharge generated spatially uniform plasma in 1.3 cm gap using capacitance C = 10 nF charged to 23 kV and then discharged through a thyratron. The current pulse duration was about 1 μs. To visualize gas-dynamic perturbations after the pulsed discharge, a Mach-Zehnder interferometer was used. The value of the thermalized energy fraction $\eta_R = 11\%$ was determined from the analysis of interferograms. It should be noted that shock waves that formed in the cathode and anode regions because of the concentrated energy release, complicate the data processing and so, the value $\eta_R = 11\%$ may turn out to be greatly overestimated.

Similar measurements in a wide range of specific deposited energies were made in pure nitrogen at P = 75 Torr [40]. The duration of the self-sustained discharge with pre-ionization was 0.5 microseconds, the specific delivered energy was in the range of 0.04-0.3 eV/mol at voltage changing from 12 to 36 kV (C = 8 nF). Holographic interferometry was used to study the dynamics of gas expansion [40]. The fraction of energy transformed to gas heating, η_R increased from 5.6% at 0.1 eV/mol to 9.8% at 0.3 eV/mol.

Figure 36 summarizes the above experimentally obtained fractions of energy η_R spent on fast gas heating as a function of the delivered energy W. It is seen that at $W \geq 0.2$ eV/mol, the fraction is almost constant: η_R = 10 - 11%. It should be noted that the majority of data in Figure 36 is taken at almost the same value of the reduced electric field: E/N = 70-80 Td. We believe that this is the main reason of the constant value of η_R, in spite of a wide range of specific delivered energies.

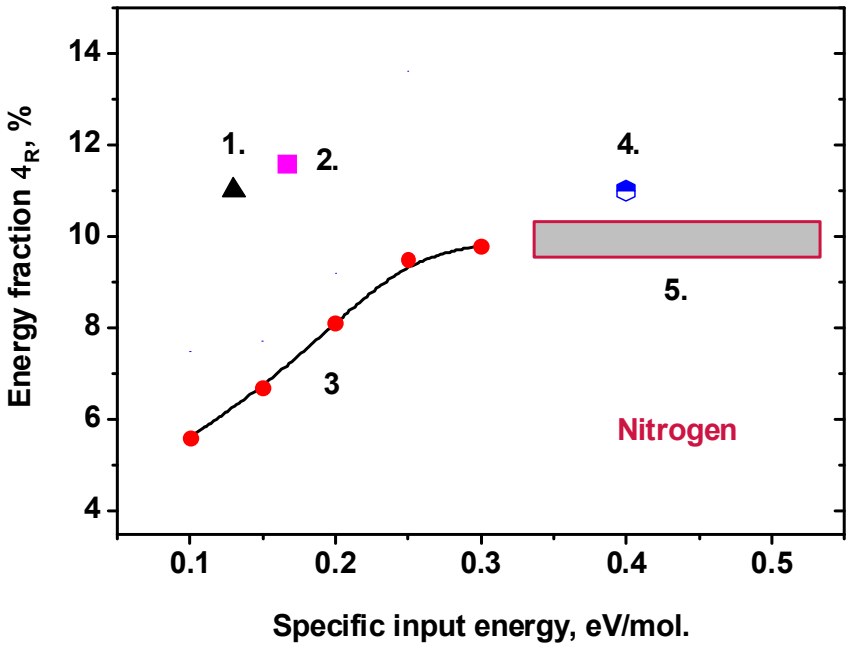

Figure 36. The fraction of energy spent on fast gas heating η_R (or energy efficiency of fast gas heating) as a function of specific delivered energy. Symbols represent experimental data: 1 - [38], 2 - [164], 3 - [40], 4 - [37], 5 - [161].

Kinetic analysis of the main processes determining fast gas heating in DC discharges in nitrogen was given in [165]. An important role of pooling reactions:

$$N_2(A^3\Sigma_u^+) + N_2(A^3\Sigma_u^+) \rightarrow N_2(B^3\Pi_g, v) + N_2(X^1\Sigma_g^+, v'), \qquad (B1)$$

$$N_2(A^3\Sigma_u^+) + N_2(A^3\Sigma_u^+) \rightarrow N_2(C^3\Pi_u, v) + N_2(X^1\Sigma_g^+, v'). \qquad (B2)$$

was emphasized. The time-dependent evolution of energy transfer to gas heating in a pure N_2 discharge at low pressures P = 1 - 10 Torr was studied for different values of the reduced electric field and discharge power. The results of the rates of gas heating at P = 10 Torr and fixed reduced electric field (E/N = 100 Td) and electron density ($N_e = 10^{11}$ cm^{-3}) are given in Figure 37. Pooling

reactions (B1) and (B2) are responsible for a smooth increase in gas temperature before the first millisecond. For longer times, gas heating is caused by vibrational energy exchange from non-resonant V-V processes between N_2 molecules and by vibration-translation (V-T) N_2–N collisions. The fraction of energy transformed to gas heating *via* excitation of electronic levels was found to be ~ 2% while the fraction of energy transformed *via* vibrational excitation was in the range of 10-35% [165].

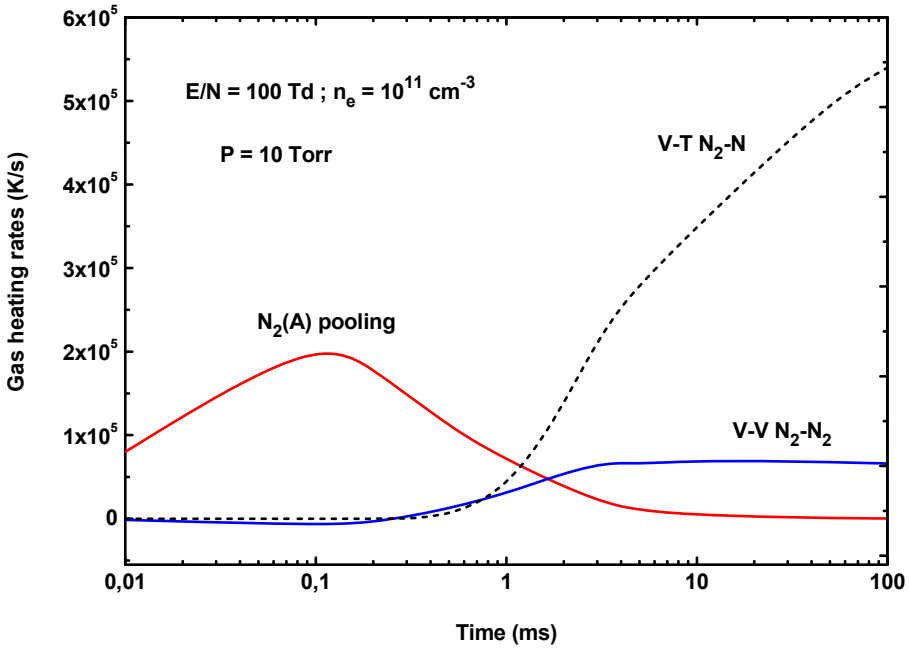

Figure 37. Calculated temporal evolution of heating rates of the most important gas heating mechanisms: pooling reactions, non-resonant V-V collisions and V-T N_2–N collisions. The discharge in pure nitrogen at P = 10 Torr, E/N = 100 Td and $N_e = 10^{11}$ cm^{-3} [165].

Important role of pooling reactions was demonstrated in [166]. In the same paper, it was shown that at high E/N, when dissociation of N_2 molecules is significant, the reaction of quenching of excited N(^{2}D) atoms provides noticeable input in fast gas heating. In [166], the discharge was initiated in nitrogen at P = 100 Torr by 10 kV high voltage pulse of 100 ns between two sphere-shape electrodes spaced 1 cm apart. Time-resolved temperature and $N_2(v)$ vibrational population was measured by picoseconds broadband coherent anti-Stokes Raman spectroscopy (CARS). Gas temperature was equal to about 500 K at 5 μs. Comparison of the experimental results with the results of 1-D numerical modeling (Figure 38) has shown that the main channels of heat release are the reaction of self-quenching of $N_2(A^3\Sigma_u^+)$ molecules ((R1, R2, R16) in Figure 38) and the reaction of quenching of excited N(^{2}D) atoms (R9). The first channel is dominant at $t < 1$ μs, while the second one prevails at $t > 2$ μs. It was assumed [166] that only 20% of nitrogen atoms generated in the discharge are in N(^{2}D) state. However, the data on molecular nitrogen dissociation by electron impact obtained in [112] show that pre-dissociation to N(^{2}D) + N(^{4}S) fragments is the primary mechanism of N_2 dissociation by electron impact. Thus, the fraction of nitrogen atoms generated

in the discharge in N(^{2}D) state obtained in [166] can be underestimated. In particular, this can be a reason of observed difference between experimental data and numerical modeling at t = 1-20 μs.

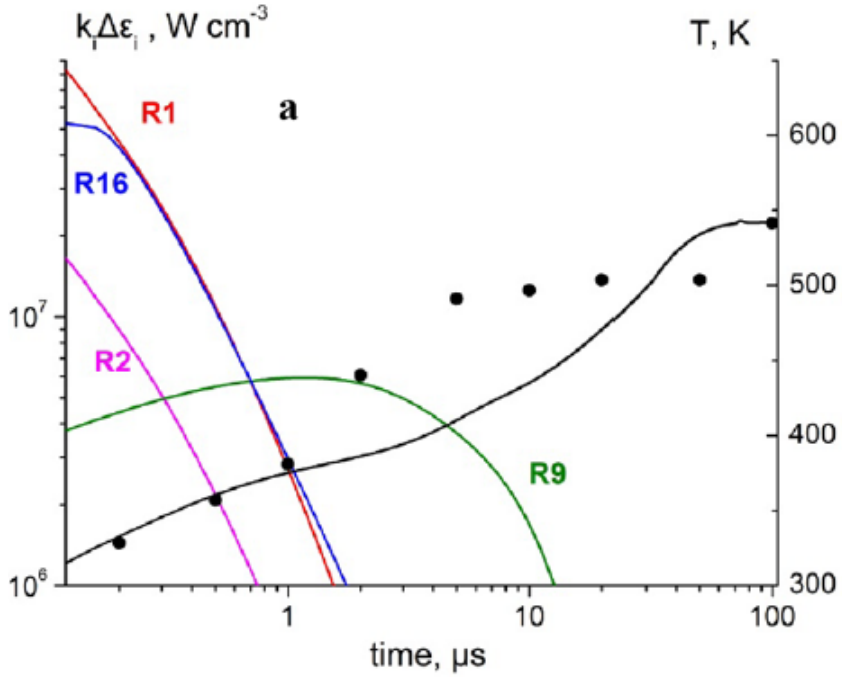

Figure 38. Time-resolved gas temperature during 100 ns and after the discharge pulse in nitrogen predicted by the model, plotted together with predicted rates of energy dissipation in dominant energy transfer processes. Symbols: experimental data, lines: model predictions [166]. (R1) and (R16) are for the reaction of $N_2(A^3\Sigma_u^+)$ self-quenching with generation and following quenching of $N_2(B^3\Pi_g)$; (R2) is for self-quenching of $N_2(A^3\Sigma_u^+)$ with generation of $N_2(C^3\Pi_u)$, and (R9) is for quenching of N(^{2}D).

Since reactions involving oxygen molecules play an important role in the mechanism of fast heating, we should expect a change in gas heating rate with a change in the δ - fraction of oxygen in the mixture. Figure 39 shows experimental data [42] and calculation results [64] for the dependence of gas heating rate on oxygen fraction in the N_2 : O_2 mixture at P = 0.4 Torr and the average current density j = 0.8 A/cm^2. At low pressures, the main channels for fast heating in air are quenching reactions of $N_2(B^3\Pi_g)$, $N_2(a'^1\Sigma_u^-)$ and other molecules by oxygen, dissociation of O_2 by electron impact and quenching of O(^{1}D) atoms by molecular nitrogen. The contributions of these processes are proportional to the O_2 concentration and, consequently, decrease with a decrease in oxygen fraction in the mixture.

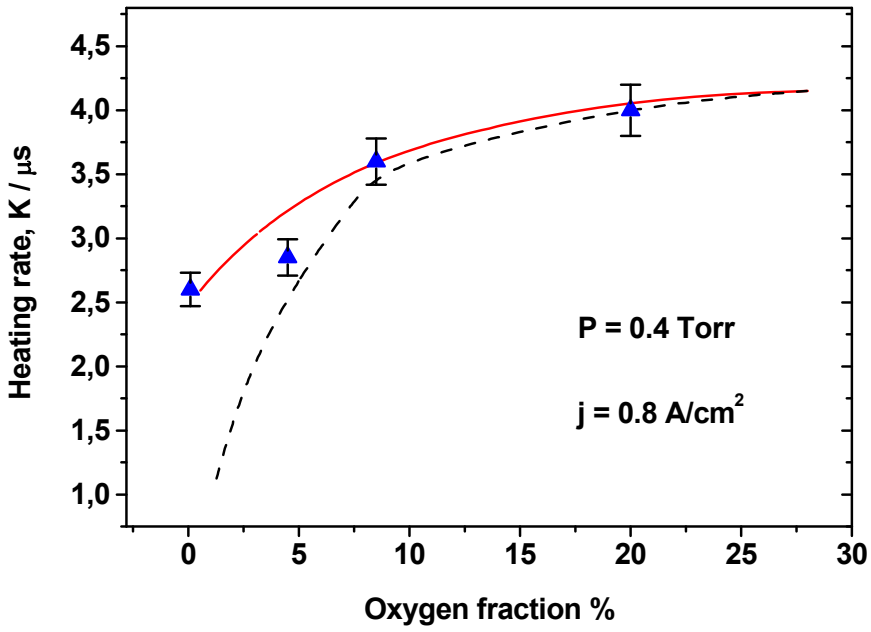

Figure 39. The dependence of gas heating rate on oxygen fraction N_2 : O_2 mixtures at P = 0.4 Torr, j = 0.8 A/cm^2. The symbols represent experimental data [42], the curves represent calculation results with (solid curve) and without (dashed curve) reaction (B1) [64].

Heating rate as a function on oxygen fraction in the mixture for the conditions [42] was calculated in [64]. Solid and dashed curves in Figure 39 correspond to taking or not into account reaction (B1). The solid curve describes experimental data on heating rate of N_2 : O_2 mixtures in the entire studied range δ = 0 - 20%. So, reaction (B1) is one of the main channels of fast gas heating in pure nitrogen and nitrogen with small oxygen additions [42], [64].

New processes responsible for fast gas heating emerge when the specific deposited energy and the reduced electric field are high, and so, the degree of electronic excitation and dissociation is high. Fast gas heating was studied experimentally and numerically under the conditions of high specific energy deposition (≈ 0.8 eV/molecule), and high reduced electric fields (E/N = 150-300 Td) in a nanosecond discharge in nitrogen at P = 20 Torr [78]. The discharge was initiated in a quartz capillary tube with an internal diameter of 1.5 mm and an inter-electrode distance of 75 mm. Three subsequent pulses about 30 ns FWHM at intervals of 250 ns were delivered to the high voltage electrode. Gas temperature was measured on the basis of distribution of emission in rotational lines of molecular nitrogen $N_2(C^3\Pi_g,v) \rightarrow N_2(B^3\Pi_g,v')$ transition. A high temperature rise over the timescale of hundreds of nanoseconds was observed experimentally: gas temperature reached 2000 K during 600 ns after the first pulse at an initial temperature equal to 300 K (see Figure 40). A similar increase in gas temperature was observed in N_2 : O_2 mixtures with 1, 10 and 20% of O_2 admixture.

Based on a comparison of experimental results with the results of numerical calculations, the mechanism of fast gas heating in pure nitrogen at high specific delivered energy was suggested. A pooling reaction between $N_2(B)$ molecules was suggested as a new process leading to heat release:

$$N_2(B) + N_2(B) \rightarrow N_2(B^3\Pi_g, C^3\Pi_u) + N_2, \quad N_2(B) = N_2(B^3, W^3, \Delta^3) \quad \text{(B3)}$$

The last process can proceed *via* production of N_4^+ ion: $N_2(B) + N_2(B) \rightarrow N_4^+ + e$, $N_4^+ + e \rightarrow N_2(B^3\Pi_g, C^3\Pi_u) + N_2$ [167] with the release of excess energy in the reaction of electron-ion recombination to gas heating.

In later paper [130] it was shown that dissociation of electronically excited $N_2(A^3\Sigma_u^+, B^3\Pi_g, C^3\Pi_u)$ molecules by electron impact

$$e + N_2(A^3\Sigma_u^+, B^3\Pi_g, C^3\Pi_u) \rightarrow e + N(^4S) + N(^2D), \quad \text{(B4)}$$

and following quenching of $N(^2D)$ atoms by ground state nitrogen molecules

$$N(^2D) + N_2(X^1\Sigma_g^+) \rightarrow N(^4S) + N_2(X^1\Sigma_g^+, v') \quad \text{(B5)}$$

are important in kinetics of nanosecond capillary discharge under the conditions of [78]. Rate constant of reaction (B5) increases with temperature, and up to 90% of the released energy goes to fast gas heating [78].

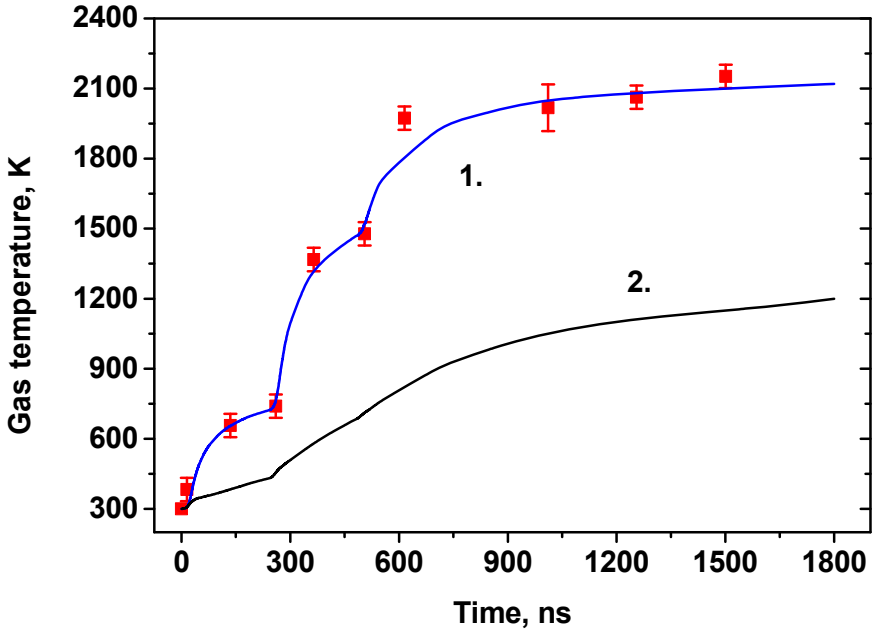

Figure 40. A temperature increase in nitrogen under the effect of pulsed nanosecond discharge (three subsequent pulses at 1, 250 and 500 ns) in nitrogen, $P = 20$ Torr [78]. Symbols represent experimental data. Solid curves represent results of numerical calculations at different assumptions about the kinetics model (see text): (1) with proposed pooling reaction (B3) and with heat release due to quenching of $N(^2D)$ atoms (B5); (2) with heat release due to quenching of $N(^2D)$ atoms (D5) but without proposed pooling reaction (B3). Pooling reactions (B1) and (B2) are included in all calculations.

Reactions (B4), (B5) change the branching ratio for fast gas heating: the role of reaction (B3) decreases and the role of (B5) increases. Nevertheless, in total, reactions (B3)-(B5) provide fast gas heating close to curve 1 in Figure 40 and are in a good correlation with measurements [78].

Thus, fast gas heating in molecular nitrogen at high reduced electric fields and high specific delivered energies is due to heat release in pooling reactions and in reactions of stepwise dissociation of nitrogen molecules by electron impact *via* electronically excited states $N_2(A^3\Sigma_u^+$, $B^3\Pi_g$, $C^3\Pi_u$, $a'^1\Sigma_u^-$) [130]. As a result, at high specific delivered energies, the fraction of discharge energy η_R spent on fast gas heating is a function of both reduced electric field *E/N* and the delivered energy [78].

APPENDIX 2

Table 4

Experimental data on fast gas heating in discharge plasma of nitrogen, air and fuel-air mixtures

No	Pressure	τ_{imp} (*)	E/N, Td	Mixture	W_d (*), eV/mol	η_R (*)	Paper
1	6 Torr	2 ms	50 - 70	air	-	3 - 6 %	[67]
2	0.5 - 1 Torr	≤ 100 μs	95 - 100	air	0.5-1.5	10 - 15%	[94]
3	760 Torr	200 ns	90 - 100	air	0.05	13 - 16 %	[68]
4	400-800 Torr	25 ns	800 - 1000	air	-	40 - 100 %	[66]
5	20 Torr	≤ 50 ns	500 - 700	air	-	36 - 40 %	[66]
6	1-10 Torr	20 ns	250 - 400	air	0.1±0.03	24 %	[65]
7	760 Torr	15 ns	100 - 200	air	0.7-0.8	25%	[70]
8	760 Torr	30 ns	100 ± 20	air	0.7-0.8	17%	[69], [75]
9a	760 Torr	15 ns	164	air	-	25 ± 10%	[71]
9b	760 Torr	15 ns	225	air	-	65 ± 15%	[71]
9c	760 Torr	15 ns	270	air	-	75 ± 25%	[71]
10	100 Torr	130 ns	100 - 150	air	0.21-0.22	17%	[166]
11	20-40 Torr	20 ns	150 - 350	$N_2 : O_2$	0.8-1.3	20 - 27%	[78]
12	100 Torr	1 μs	65-75	nitrogen	0.1-0.15	11%	[38]
13	75 Torr	0.5 μs	65 - 75	nitrogen	0.1-0.3	6 - 10%	[40]
14	40 Torr	30 μs	80	nitrogen	0.4	11 ± 1%	[37]
15	100 Torr	130 ns	100 - 150	nitrogen	0.21-0.22	15-17%	[166]
16	1.5 Torr	150 μs	60 - 80	nitrogen	0.3-0.6	10%	[161]
17	760 Torr	10 ns	100 - 160	30% H_2 : air	0.25-0.3	(**)	[140]
18	760 Torr	70 ns	70-100	CH_4 : air (ER = 0.65)	-	(**)	[159]
19	760 Torr	30 ns	100 ± 20	C_3H_8 : air (ER = 0.4)	0.7-0.8	17 - 19%	[157]

(*) τ_{imp} is a duration of the pulse, W_d is a specific deposited energy and η_R is the energy efficiency of fast gas heating;

(**) it is not possible to calculate the energy efficiency of fast gas heating, η_R: measurements of the gas temperature are performed at time scale typical for oxidation of hydrogen [140] and methane [159].

Acknowledgements

The work inspired by collaboration within the French–Russian international laboratory LIA KaPPA “Kinetics and Physics of Pulsed Plasmas and their Afterglow”. The work of S.M. Starikovskaia was partially supported by LabEx Plas@Par, the French General Directorate of Armaments (DGA) under the EP-DGA convention 2790 “Interaction of detonation with low temperature plasma” and the French National Research Agency, ANR (ASPEN Project, “Atomic Species Production via Electronically excited states in high eNergy density Plasmas”). Insightful discussions with Dr. M.N. Shneider (Princeton University) are gratefully acknowledged.

REFERENCES

[1] Starikovskaia SM. Plasma assisted ignition and combustion. J Phys D Appl Phys 2006;39. https://doi.org/10.1088/0022-3727/39/16/R01.

[2] Starikovskiy A, Aleksandrov N. Plasma-assisted ignition and combustion. Prog Energy Combust Sci 2013;39:61–110. https://doi.org/10.1016/j.pecs.2012.05.003.

[3] Boumehdi MA, Stepanyan SA, Desgroux P, Vanhove G, Starikovskaia SM. Ignition of methane- and n-butane-containing mixtures at high pressures by pulsed nanosecond discharge. Combust Flame 2015;162:1336–49. https://doi.org/10.1016/j.combustflame.2014.11.006.

[4] Adamovich I V, Lempert WR. Challenges in understanding and predictive model development of plasma-assisted combustion. Plasma Phys Control Fusion 2015;57:014001. https://doi.org/10.1088/0741-3335/57/1/014001.

[5] Ju Y, Sun W. Plasma assisted combustion: Dynamics and chemistry. Prog Energy Combust Sci 2015;48:21–83. https://doi.org/10.1016/j.pecs.2014.12.002.

[6] Alrashidi AMRN, Adam NM, Hairuddin AA, Abdullah LC. A review on plasma combustion of fuel in internal combustion engines. Int J Energy Res 2018;42:1813–33. https://doi.org/10.1002/er.3964.

[7] Moreau E. Airflow control by non-thermal plasma actuators. J Phys D Appl Phys 2007;40:605–36. https://doi.org/10.1088/0022-3727/40/3/S01.

[8] Starikovskii AY, Nikipelov AA, Nudnova MM, Roupassov D V. SDBD plasma actuator with nanosecond pulse-periodic discharge. Plasma Sources Sci Technol 2009;18:034015. https://doi.org/10.1088/0963-0252/18/3/034015.

[9] Leonov SB, Adamovich I V., Soloviev VR. Dynamics of near-surface electric discharges and mechanisms of their interaction with the airflow. Plasma Sources Sci Technol 2016;25:063001. https://doi.org/10.1088/0963-0252/25/6/063001.

[10] Samimy M, Webb N, Esfahani A. Reinventing the wheel: Excitation of flow instabilities for active flow control using plasma actuators. J Phys D Appl Phys 2019;52:354002. https://doi.org/10.1088/1361-6463/ab272d.

[11] Starikovskiy AY, Aleksandrov NL. Gasdynamic flow control by ultrafast local heating in a strongly nonequilibrium pulsed plasma. Plasma Phys Reports 2021;47:148–209.

[12] Bletzinger P, Ganguly BN, Van Wie D, Garscadden A. Plasmas in high speed aerodynamics. J Phys D Appl Phys 2005;38:R33. https://doi.org/10.1088/0022-3727/38/4/R01.

[13] Tholin F, Lacoste DA, Bourdon A. Influence of fast-heating processes and O atom production by a nanosecond spark discharge on the ignition of a lean H_2-air premixed flame. Combust Flame 2014;161:1235–46. https://doi.org/10.1016/j.combustflame.2013.11.007.

[14] Lefebvre AH. The role of fuel preparation in low-emission combustion. J Eng Gas Turbines Power 1995;117:617–54. https://doi.org/10.1115/1.2815449.

[15] Warnatz J, Maas U, Dibble RW. Combustion physical and chemical fundamentals, modeling and simulation, experiments, pollutant formation. Berlin, Heidelberg: Springer-Verlag; 2006.

[16] Liberman MA. Introduction to physics and chemistry of combustion. Explosion, flame, detonation. Springer-V. Berlin, Heidelberg: 2008.

[17] Berezhetskaya NK, Gritsinin SI, Kop'ev VA, Kossyi IA, Kuleshov PS, Popov NA, et al. Ignition of a combustible gas mixture by a high-current electric discharge in a closed volume. Plasma Phys Reports 2009;35:471–83. https://doi.org/10.1134/S1063780X09060038.

[18] Maley L, Bhattacharjee R, Lau-Chapdelaine SM, Radulescu MI. Influence of hydrodynamic instabilities on the propagation mechanism of fast flames. Proc Combust Inst 2015;35:2117–26. https://doi.org/10.1016/j.proci.2014.06.134.

[19] Shcherbanev SA, Popov NA, Starikovskaia SM. Ignition of high pressure lean H_2:air mixtures along the multiple channels of nanosecond surface discharge. Combust Flame 2017;176:272–84. https://doi.org/10.1016/j.combustflame.2016.07.035.

[20] Syred N. A review of oscillation mechanisms and the role of the precessing vortex core (PVC) in swirl combustion systems. Prog Energy Combust Sci 2006;32:93–161. https://doi.org/10.1016/j.pecs.2005.10.002.

[21] Pilla G, Galley D, Lacoste DA, Lacas F, Veynante D, Laux CO. Stabilization of a turbulent premixed flame using a nanosecond repetitively pulsed plasma. IEEE Trans Plasma Sci 2006;34:2471–7. https://doi.org/10.1109/TPS.2006.886081.

[22] Moeck J, Lacoste D, Laux C, Paschereit C. Control of combustion dynamics in a swirl-stabilized combustor with nanosecond repetitively pulsed discharges. 51st AIAA Aerosp. Sci. Meet. Incl. New Horizons Forum Aerosp. Expo., 07-10 January 2013, Dallas, Texas: 2013, p. AIAA Paper 2013-0565.

[23] Lacoste DA, Moeck JP, Durox D, Laux CO, Schuller T. Effect of nanosecond repetitively

pulsed discharges on the dynamics of a swirl-stabilized lean premixed flame. J Eng Gas Turbines Power 2013;135. https://doi.org/10.1115/1.4024961.

[24] Barbosa S, Pilla G, Lacoste DA, Scouflaire P, Ducruix S, Laux CO, et al. Influence of nanosecond repetitively pulsed discharges on the stability of a swirled propane/air burner representative of an aeronautical combustor. Philos Trans R Soc A Math Phys Eng Sci 2015;373:20140335. https://doi.org/10.1098/rsta.2014.0335.

[25] Lacoste DA, Xiong Y, Moeck JP, Chung SH, Roberts WL, Cha MS. Transfer functions of laminar premixed flames subjected to forcing by acoustic waves, AC electric fields, and non-thermal plasma discharges. Proc Combust Inst 2017;36:4183–92. https://doi.org/10.1016/j.proci.2016.05.034.

[26] Slovetskii DI. Mechanisms of chemical reactions in nonequilibrium plasmas. Moscow: Nauka; 1980.

[27] Raizer YP. Gas discharge physics. Berlin: Springer; 1991.

[28] Fridman A. Plasma Chemistry. Cambridge University Press; 2008.

[29] Popov NA. Investigation of the mechanism for rapid heating of nitrogen and air in gas discharges. Plasma Phys Reports 2001;27:886–96. https://doi.org/10.1134/1.1409722.

[30] Popov NA. Kinetics of plasma-assisted combustion: effect of non-equilibrium excitation on the ignition and oxidation of combustible mixtures. Plasma Sources Sci Technol 2016;25:043002. https://doi.org/10.1088/0963-0252/25/4/043002.

[31] Zhong H, Shneider MN, Mokrov MS, Ju Y. Thermal-chemical instability of weakly ionized plasma in a reactive flow. J Phys D Appl Phys 2019;52:484001. https://doi.org/10.1088/1361-6463/ab3d69.

[32] Zhong H, Shneider M, Mao X, Ju Y. Dynamics and chemical mode analysis of plasma thermal-chemical instability. Plasma Sources Sci Technol 2021. https://doi.org/10.1088/1361-6595/abde1c.

[33] Aleksandrov AF, Kuzovnikov AA, Shibkov VM. Freely localized shf discharge in a focused beam. J Eng Phys Thermophys 1992;62:519–25. https://doi.org/10.1007/BF00862338.

[34] Kelly S, van de Steeg A, Hughes A, Van Rooij GJ, Bogaerts A. Thermal instability and volume contraction in a pulsed microwave N_2 plasma at sub-atmospheric pressure. Plasma Sources Sci Technol 2021. https://doi.org/10.1088/1361-6595/abf1d6.

[35] Kourtzanidis K, Rogier F, Boeuf JP. Gas heating effects on the formation and propagation of a microwave streamer in air. J Appl Phys 2015;118:103301. https://doi.org/10.1063/1.4930163.

[36] Chen S, Li K, Nijdam S. Transition mechanism of negative DC corona modes in atmospheric air: From Trichel pulses to pulseless glow. Plasma Sources Sci Technol 2019;28:055017. https://doi.org/10.1088/1361-6595/aae554.

[37] Berdyshev A V., Vikharev AO, Gitlin MS, Deryugin AA, Ivanov OA, Kochetov I V., et al. Heating of a molecular gas in a pulsed microwave discharge. High Temperature. High Temp / Russ / 1988;26:661–6.

[38] Baranov VY, Vysikailo FI, Napartovich AP, Niz'ev VG, Pigul'sky SV, Starostin AN. The contraction of decaying discharge plasma in nitrogen. Plasma Phys Reports / Russ / 1978;4:358–66.

[39] Kamardin IL, Kuchinskiy AA, Rodichkin VA, Shanskiy VF. Experimental study of heating of molecular nitrogen in pulsed self-sustained discharge. High Temp / Russ / 1983;21:224–8.

[40] Kamardin IL, Kuchinskiy AA, Rodichkin VA, Smirnov VG, Shanskiy VF. Study of heating of molecular nitrogen in pulsed self-sustained discharge by holographic interferometry. High Temp / Russ / 1985;23:653–7.

[41] Baiadze KV, Vetsko VM, Zhdanok SA, et al. Abnormal heating of nitrogen in the discharge. Plasma Phys Reports / Russ / 1979;5:923–8.

[42] Kalinin AV, Shibkov VM, Shibkova LV. Influence of oxygen on kinetics of molecular gas heating in N_2 : O_2 mixture. Moscow Univ Phys Bull / Russ / 1996;51:38–43.

[43] Bezmenov IV, Rusanov VV, Silakov VP. Physics and chemistry of gas discharges in microwave beams. Proc IOFAN, Moscow Nauk Publ / Russ / 1994;47:74–107.

[44] Bachmann R, Li X, Ottinger C, Vilesov AF. Molecular-beam study of the collisional intramolecular coupling of $N_2(B^3\Pi_g)$ with the $N_2(A^3\Sigma_u^+)$ and $N_2(W^3\Delta_u)$ states. J Chem Phys 1992;96:5151–64. https://doi.org/10.1063/1.462756.

[45] Bachmann R, Li X, Ottinger C, Vilesov AF, Wulfmeyer V. Vibrational-state-to-state collision-induced intramolecular energy transfer $N_2(A^3\Sigma_u^+, v'' \rightarrow B^3\Pi_g, v')$. J Chem Phys 1993;98:8606–25. https://doi.org/10.1063/1.464469.

[46] Starikovskiy A, Aleksandrov N. Nonequilibrium plasma aerodynamics. Aeronautics and Astronautics. Rijeka: InTech; 2011.

[47] Little J, Takashima K, Nishihara M, Adamovich I, Samimy M. Separation control with nanosecond pulse driven Dielectric Barrier Discharge plasma actuators. AIAA J 2012;50:350–65.

[48] Komuro A, Takashima K, Suzuki K, Kanno S, Nonomura T, Kaneko T, et al. Gas-heating phenomenon in a nanosecond pulse discharge in atmospheric-pressure air and its application for high-speed flow control. Plasma Sources Sci Technol 2018;27:104005. https://doi.org/10.1088/1361-6595/aae23c.

[49] Pancheshnyi S V., Lacoste DA, Bourdon A, Laux CO. Ignition of propane-air mixtures by a repetitively pulsed nanosecond discharge. IEEE Trans Plasma Sci 2006;34:2478–87. https://doi.org/10.1109/TPS.2006.876421.

[50] Popov NA. Effect of a pulsed high-current discharge on hydrogen-air mixtures. Plasma

Phys Reports 2008;34:376–91. https://doi.org/10.1134/S1063780X08050048.

[51] Bak MS, Do H, Mungal MG, Cappelli MA. Plasma-assisted stabilization of laminar premixed methane/air flames around the lean flammability limit. Combust Flame 2012;159:3128–37. https://doi.org/10.1016/j.combustflame.2012.03.023.

[52] Starikovskaia SM. Plasma-assisted ignition and combustion: Nanosecond discharges and development of kinetic mechanisms. J Phys D Appl Phys 2014;47:353001. https://doi.org/10.1088/0022-3727/47/35/353001.

[53] Starikovskaia SM, Anikin NB, Pancheshnyi S V., Zatzepin D V., Starikovskii AY. Pulsed breakdown at high overvoltage: Development, propagation and energy branching. Plasma Sources Sci Technol 2001;10:344–55. https://doi.org/10.1088/0963-0252/10/2/324.

[54] Stepanyan SA, Soloviev VR, Starikovskaia SM. An electric field in nanosecond surface dielectric barrier discharge at different polarities of the high voltage pulse: Spectroscopy measurements and numerical modeling. J Phys D Appl Phys 2014;47:485201. https://doi.org/10.1088/0022-3727/47/48/485201.

[55] Simeni MS, Goldberg B, Gulko I, Frederickson K, Adamovich I V. Sub-nanosecond resolution electric field measurements during ns pulse breakdown in ambient air. J Phys D Appl Phys 2018;51:01LT01. https://doi.org/10.1088/1361-6463/aa9a80.

[56] Chng TL, Brisset A, Jeanney P, Starikovskaia SM, Adamovich I V., Tardiveau P. Electric field evolution in a diffuse ionization wave nanosecond pulse discharge in atmospheric pressure air. Plasma Sources Sci Technol 2019;28:09LT02. https://doi.org/10.1088/1361-6595/ab3cfc.

[57] Goldberg BM, Reuter S, Dogariu A, Miles RB. 1D time evolving electric field profile measurements with sub-ns resolution using the E-FISH method. Opt Lett 2019;44:3853. https://doi.org/10.1364/ol.44.003853.

[58] Roupassov D V., Nikipelov AA, Nudnova MM, Starikovskii AY. Flow separation control by plasma actuator with nanosecond pulsed-periodic discharge. AIAA J 2009;47:168–85. https://doi.org/10.2514/1.38113.

[59] Takashima K, Zuzeek Y, Lempert WR, Adamovich I V. Characterization of a surface dielectric barrier discharge plasma sustained by repetitive nanosecond pulses. Plasma Sources Sci Technol 2011;20:055009. https://doi.org/10.1088/0963-0252/20/5/055009.

[60] Zhu Y, Wu Y, Cui W, Li Y, Jia M. Modelling of plasma aerodynamic actuation driven by nanosecond SDBD discharge. J Phys D Appl Phys 2013;46:355205. https://doi.org/10.1088/0022-3727/46/35/355205.

[61] Zhu Y, Shcherbanev S, Baron B, Starikovskaia S. Nanosecond surface dielectric barrier discharge in atmospheric pressure air: I. measurements and 2D modeling of morphology, propagation and hydrodynamic perturbations. Plasma Sources Sci Technol 2017;26:125004. https://doi.org/10.1088/1361-6595/aa9304.

[62] Little J, Takashima K, Nishihara M, Adamovich I, Samimy M. High lift airfoil leading edge separation control with nanosecond pulse driven DBD plasma actuators. 41st AIAA Plasmadynamics Lasers Conf., 28 June-1 July 2010, Chicago: 2010, p. AIAA Paper 2010-4256.

[63] Stepanyan S, Hayashi J, Salmon A, Stancu GD, Laux CO. Large-volume excitation of air, argon, nitrogen and combustible mixtures by thermal jets produced by nanosecond spark discharges. Plasma Sources Sci Technol 2017;26:04LT01. https://doi.org/10.1088/1361-6595/aa5a2b.

[64] Popov NA. Fast gas heating in a nitrogen-oxygen discharge plasma: I. Kinetic mechanism. J Phys D Appl Phys 2011;44:285201. https://doi.org/10.1088/0022-3727/44/28/285201.

[65] Mintoussov EI, Pendleton SJ, Gerbault FG, Popov NA, Starikovskaia SM. Fast gas heating in nitrogen-oxygen discharge plasma: II. Energy exchange in the afterglow of a volume nanosecond discharge at moderate pressures. J Phys D Appl Phys 2011;44:285202. https://doi.org/10.1088/0022-3727/44/28/285202.

[66] Aleksandrov NL, Kindysheva S V., Nudnova MM, Starikovskiy AY. Mechanism of ultra-fast heating in a non-equilibrium weakly ionized air discharge plasma in high electric fields. J Phys D Appl Phys 2010;43:255201. https://doi.org/10.1088/0022-3727/43/25/255201.

[67] Klimov AI, Mishin GI, Fedotov AB, Shakhovatov VA. Propagation of shock waves in DC discharge. Tech Phys Lett / Russ / 1989;15:31–6.

[68] Ono R, Teramoto Y, Oda T. Gas density in a pulsed positive streamer measured using laser shadowgraph. J Phys D Appl Phys 2010;43:345203. https://doi.org/10.1088/0022-3727/43/34/345203.

[69] Lo A, Cessou A, Boubert P, Vervisch P. Space and time analysis of the nanosecond scale discharges in atmospheric pressure air: I. Gas temperature and vibrational distribution function of N_2 and O_2. J Phys D Appl Phys 2014;47:115201. https://doi.org/10.1088/0022-3727/47/11/115201.

[70] Rusterholtz DL, Lacoste DA, Stancu GD, Pai DZ, Laux CO. Ultrafast heating and oxygen dissociation in atmospheric pressure air by nanosecond repetitively pulsed discharges. J Phys D Appl Phys 2013;46:464010. https://doi.org/10.1088/0022-3727/46/46/464010.

[71] Xu DA, Shneider MN, Lacoste DA, Laux CO. Thermal and hydrodynamic effects of nanosecond discharges in atmospheric pressure air. J Phys D Appl Phys 2014;47:235202. https://doi.org/10.1088/0022-3727/47/23/235202.

[72] Hagelaar GJM, Pitchford LC. Solving the Boltzmann equation to obtain electron transport coefficients and rate coefficients for fluid models. Plasma Sources Sci Technol 2005;14:722–33. https://doi.org/10.1088/0963-0252/14/4/011.

[73] Rusterholtz DL, Pai DZ, Stancu GD, Lacoste DA, Laux CO. Ultrafast heating in

nanosecond discharges in atmospheric pressure air. 50th AIAA Aerosp. Sci. Meet. Incl. New Horizons Forum Aerosp. Ex-position, 09-12 January, Nashville, USA: 2012, p. AIAA Paper 2012-0509.

[74] Montello A, Burnette D, Nishihara M, Lempert WR, Adamovich I V. Dynamics of Rapid Localized Heating in Nanosecond Pulse Discharges for High Speed Flow Control. J Fluid Sci Technol 2013;8:147–59. https://doi.org/10.1299/jfst.8.147.

[75] Lo A, Cessou A, Vervisch P. Space and time analysis of the nanosecond scale discharges in atmospheric pressure air: II. Energy transfers during the post-discharge. J Phys D Appl Phys 2014;47:115202. https://doi.org/10.1088/0022-3727/47/11/115202.

[76] Klochko A V., Lemainque J, Booth JP, Starikovskaia SM. TALIF measurements of oxygen atom density in the afterglow of a capillary nanosecond discharge. Plasma Sources Sci Technol 2015;24:025010. https://doi.org/10.1088/0963-0252/24/2/025010.

[77] Nudnova MM, Kindysheva S V, Aleksandrov NL, Starikovskii AY. Fast gas heating in N_2/O_2 mixtures under nanosecond surface dielectric barrier discharge: the effects of gas pressure and composition. Philos Trans R Soc A Math Phys Eng Sci 2015;373:20140330. https://doi.org/10.1098/rsta.2014.0330.

[78] Lepikhin ND, Popov NA, Starikovskaia SM. Fast gas heating and radial distribution of active species in nanosecond capillary discharge in pure nitrogen and N_2:O_2 mixtures. Plasma Sources Sci Technol 2018;27:055005. https://doi.org/10.1088/1361-6595/aab74e.

[79] Parkevich E V. The installation to study the prebreakdown stage of a gas discharge by laser probing. Instruments Exp Tech 2017;60:383–9. https://doi.org/10.1134/S0020441217030137.

[80] Parkevich E V., Medvedev MA, Khirianova AI, Ivanenkov G V., Selyukov AS, Agafonov A V., et al. Extremely fast formation of anode spots in an atmospheric discharge points to a fundamental ultrafast breakdown mechanism. Plasma Sources Sci Technol 2019;28:125007. https://doi.org/10.1088/1361-6595/ab518e.

[81] Lo A, Cléon G, Vervisch P, Cessou A. Spontaneous Raman scattering: A useful tool for investigating the afterglow of nanosecond scale discharges in air. Appl Phys B Lasers Opt 2012;107:229–42. https://doi.org/10.1007/s00340-012-4874-3.

[82] Pancheshnyi S V., Starikovskaia SM, Starikovskii AY. Collisional deactivation of $N_2(C^3\Pi_u, v = 0, 1, 2, 3)$ states by N_2, O_2, H_2 and H_2O molecules. Chem Phys 2000;262:349–57. https://doi.org/10.1016/S0301-0104(00)00338-4.

[83] Babaeva NY, Naidis G V. Two-dimensional modelling of positive streamer dynamics in non-uniform electric fields in air. J Phys D Appl Phys 1996;29:2423–31. https://doi.org/10.1088/0022-3727/29/9/029.

[84] Paris P, Aints M, Laan M, Valk F. Measurement of intensity ratio of nitrogen bands as a function of field strength. J Phys D Appl Phys 2004;37:1179–84.

https://doi.org/10.1088/0022-3727/37/8/005.

[85] Paris P, Aints M, Valk F, Plank T, Haljaste A, Kozlov K V., et al. Intensity ratio of spectral bands of nitrogen as a measure of electric field strength in plasmas. J Phys D Appl Phys 2005;38:3894–9. https://doi.org/10.1088/0022-3727/38/21/010.

[86] Paris P, Aints M, Valk F. Collisional Quenching Rates of N2 +(B2Σg+,v=0). 17th Symp. Appl. Plasma Process. Visegr. Work. Res. Plasma Phys., Liptovský Ján, Slovakia January, 17-22: 2009, p. 227–8.

[87] Bilek P, Obrusnik A, Hoder T, Šimek M, Bonaventura Z. Electric field determination in air plasmas from intensity ratio of nitrogen spectral bands: II. Reduction of the uncertainty and state-of-the-art model. Plasma Sources Sci Technol 2018;27:085012. https://doi.org/10.1088/1361-6595/aad666.

[88] Obrusnik A, Bilek P, Hoder T, Šimek M, Bonaventura Z. Electric field determination in air plasmas from intensity ratio of nitrogen spectral bands: I. Sensitivity analysis and uncertainty quantification of dominant processes. Plasma Sources Sci Technol 2018;27:085013. https://doi.org/10.1088/1361-6595/aad663.

[89] Brisset A, Gazeli K, Magne L, Pasquiers S, Jeanney P, Marode E, et al. Modification of the electric field distribution in a diffuse streamer-induced discharge under extreme overvoltage. Plasma Sources Sci Technol 2019;28:055016. https://doi.org/10.1088/1361-6595/ab1989.

[90] Kosarev IN, Khorunzhenko VI, Mintoussov EI, Sagulenko PN, Popov NA, Starikovskaia SM. A nanosecond surface dielectric barrier discharge at elevated pressures: Time-resolved electric field and efficiency of initiation of combustion. Plasma Sources Sci Technol 2012;21:045012. https://doi.org/10.1088/0963-0252/21/4/045012.

[91] Chng TL, Starikovskaia SM, Schanne-Klein MC. Electric field measurements in plasmas: How focusing strongly distorts the E-FISH signal. Plasma Sources Sci Technol 2020;29:125002. https://doi.org/10.1088/1361-6595/abbf93.

[92] Bruggeman PJ, Sadeghi N, Schram DC, Linss V. Gas temperature determination from rotational lines in non-equilibrium plasmas: A review. Plasma Sources Sci Technol 2014;23:023001. https://doi.org/10.1088/0963-0252/23/2/023001.

[93] Radzig AA, Smirnov BM. Reference data on atoms, molecules and ions. Berlin: Springer; 1980.

[94] Ershov AP, Kalinin AV, Lodinev VV, Shibkov VM. Kinetics of gas heating in pulse discharge in air. Proc. XX Int. Conf. Phenom. Ioniz. Gases., Pisa. Italy.: 1991, p. 2:379-380.

[95] Capitelli M, Ferreira CM, Gordiets BF, Osipov A. Plasma kinetics in atmospheric gases. Springer; 2000.

[96] Popov NA. Pulsed nanosecond discharge in air at high specific deposited energy: fast gas

heating and active particle production. Plasma Sources Sci Technol 2016;25:044003. https://doi.org/10.1088/0963-0252/25/4/044003.

[97] Klochko AV, Lemainque J, Popov NA, Booth J-P, Starikovskaia SM. Study of fast gas heating in a capillary nanosecond discharge in air: TALIF O atoms measure-ments and kinetic modeling. 51st AIAA Aerosp. Sci. Meet. Incl. New Horizons Forum Aerosp. Expo., 07-10 January, Dallas, Texas: 2013, p. AIAA Paper 2013-0574.

[98] Klochko A V., Starikovskaia SM, Xiong Z, Kushner MJ. Investigation of capillary nanosecond discharges in air at moderate pressure: Comparison of experiments and 2D numerical modelling. J Phys D Appl Phys 2014;47:365202. https://doi.org/10.1088/0022-3727/47/36/365202.

[99] Mintusov E, Lacoste DA, Pendleton SJ, Popov NA, Stancu GD, Laux, C.O., Starikovskaia SM. Fast ionization wave experiments on fast gas heating. X Congr. Plasma Div. French Phys. Soc., 10-12 May, Bordeaux, France: 2010.

[100] Plank T, Jalakas A, Aints M, Paris P, Valk F, Viidebaum M, et al. Ozone generation efficiency as a function of electric field strength in air. J Phys D Appl Phys 2014;47:335205. https://doi.org/10.1088/0022-3727/47/33/335205.

[101] Stancu GD, Kaddouri F, Lacoste DA, Laux CO. Atmospheric pressure plasma diagnostics by OES, CRDS and TALIF. J Phys D Appl Phys 2010;43:124002. https://doi.org/10.1088/0022-3727/43/12/124002.

[102] Pai DZ, Lacoste DA, Laux CO. Nanosecond repetitively pulsed discharges in air at atmospheric pressure-the spark regime. Plasma Sources Sci Technol 2010;19:065015. https://doi.org/10.1088/0963-0252/19/6/065015.

[103] Kossyi IA, Kostinsky AY, Matveyev AA, Silakov VP. Kinetic scheme of the non-equilibrium discharge in nitrogen-oxygen mixtures. Plasma Sources Sci Technol 1992;1:207–20. https://doi.org/10.1088/0963-0252/1/3/011.

[104] Adamovich I V., Nishihara M, Choi I, Uddi M, Lempert WR. Energy coupling to the plasma in repetitive nanosecond pulse discharges. Phys Plasmas 2009;16:113505. https://doi.org/10.1063/1.3264740.

[105] Stepanyan SA, Starikovskiy AY, Popov NA, Starikovskaia SM. A nanosecond surface dielectric barrier discharge in air at high pressures and different polarities of applied pulses: Transition to filamentary mode. Plasma Sources Sci Technol 2014;23:045003. https://doi.org/10.1088/0963-0252/23/4/045003.

[106] Babaeva NY, Tereshonok D V., Naidis G V. Fluid and hybrid modeling of nanosecond surface discharges: Effect of polarity and secondary electrons emission. Plasma Sources Sci Technol 2016;25:044008. https://doi.org/10.1088/0963-0252/25/4/044008.

[107] Aleksandrov NL, Kochetov IV. Influence of vibrational excitation on rates of electronic processes in weakly ionized plasma of molecular gases and gas mixtures. Plasma Phys

Reports / Russ / 1987;25:1062.

[108] Herron JT. Evaluated chemical kinetics data for reactions of $N(^2D)$, $N(^2P)$, and $N_2(A^3\Sigma_u^+)$ in the gas phase. J Phys Chem Ref Data 1999;28:1453–83. https://doi.org/10.1063/1.556043.

[109] Shyn TW, Sweeney CJ, Grafe A, Sharp WE. Absolute differential cross sections for the excitation of molecular oxygen by electron impact: Decomposition of the Schumann-Runge continuum. Phys Rev A 1994;50:4794–801. https://doi.org/10.1103/PhysRevA.50.4794.

[110] Shyn TW, Sweeney CJ. Measurement of absolute differential excitation cross sections of molecular oxygen by electron impact: Decomposition of the Herzberg pseudocontinuum. Phys Rev A - At Mol Opt Phys 2000;62:6. https://doi.org/10.1103/PhysRevA.62.022711.

[111] Polak LS, Slovetskii DI, Sokolov AS. Dissociation of molecular nitrogen from electronically excited states. High Energy Chem / Russ / 1972;6:396–402.

[112] Cosby PC. Electron-impact dissociation of nitrogen. J Chem Phys 1993;98:9544–59. https://doi.org/10.1063/1.464385.

[113] Aleksandrov NL, Ponomarev AA, Starikovskiy AY. Monte Carlo simulation of the effect of “hot” atoms on active species kinetics in combustible mixtures excited by high-voltage pulsed discharges. Combust Flame 2017;176:181–90. https://doi.org/10.1016/j.combustflame.2016.10.006.

[114] Albugues F, Birot A, Blanc D, Brunet H, Galy J, Millet P, et al. Destruction of the levels $C^3\Pi_u$ ($v' = 0$, $v' = 1$) of nitrogen by O_2,CO_2, CH_4, and H_2O. J Chem Phys 1974;61:2695–9. https://doi.org/10.1063/1.1682401.

[115] Guerra V, Sá PA, Loureiro J. Role played by the $N_2(A^3\Sigma_u^+)$ metastable in stationary N_2 and N_2-O_2 discharges. J Phys D Appl Phys 2001;34:1745–55. https://doi.org/10.1088/0022-3727/34/12/301.

[116] Marinelli WJ, Green BD, De Faccio MA, Blumberg W. Vibrational relaxation and intersystem crossing in $N_2(a^1\Pi_g)$. J Phys Chem 1988;92:3429–37.

[117] Piper LG. Quenching rate coefficients for $N_2(a'^1\Sigma_u^-)$. J Chem Phys 1987;87:1625–9. https://doi.org/10.1063/1.453223.

[118] Balamuta J, Golde MF. Formation of electronically excited oxygen atoms in the reactions of $Ar(^3P_{0,2})$ and $Xe(^3P_2)$ atoms with O_2. J Phys Chem 1982;86:2765–9.

[119] Thomas JM, Kaufman F. An upper limit on the formation of $NO(X^2\Pi_r)$ in the reactions $N_2(A^3\Sigma_u^+) + O(^3P)$ and $N_2(A^3\Sigma_u^+) + O_2(X^3\Sigma g-)$ at 298. J Phys Chem 1996;100:8901–6. https://doi.org/10.1021/jp960164v.

[120] Shkurenkov I, Burnette D, Lempert WR, Adamovich I V. Kinetics of excited states and radicals in a nanosecond pulse discharge and afterglow in nitrogen and air. Plasma Sources Sci Technol 2014;23:065003. https://doi.org/10.1088/0963-0252/23/6/065003.

[121] Tully JC. Reactions of O(^{1}D) with atmospheric molecules. J Chem Phys 1975;62:1893–8. https://doi.org/10.1063/1.430675.

[122] Slanger TG, Black G. Electronic-to-vibrationaI energy transfer efficiency in the O(^{1}D)-N_2 and O(^{1}D)-CO systems. J Chem Phys 1974;60:468–77. https://doi.org/10.1063/1.1681064.

[123] Florescu AI, Mitchell JBA. Dissociative recombination. Phys Rep 2006;430:277–374.

[124] Willis C, Boyd AW, Young MJ, Armstrong DA. Radiation chemistry of gaseous oxygen: experimental and calculated yields. Can J Chem 1970;48:1505–14. https://doi.org/10.1139/v70-246.

[125] Ferguson EE. Vibrational quenching of small molecular ions in neutral collisions. J Phys Chem 1986;90:731–8.

[126] Dulaney JL, Biondi MA, Johnsen R. Electron-temperature dependence of the recombination of electrons with O_4^+ ions. Phys Rev 1998;37:2539–42.

[127] Ghormley JA, Hochanadel CJ, Boyle JW. Yield of ozone in the pulse radiolysis of gaseous oxygen at very high dose radiation. Use of this system as a dosimeter. J Chem Phys 1969;50:419–23.

[128] Kabanov SN, Korolyov AA, Tarhova TI. Ozone formation dynamics in oxygen including gas mixtures by electron beam injection. In: Nadezhdinskii AI, Ponomarev Y V., Sinitsa LN, editors. 11th Symp. Sch. High-Resolution Mol. Spectrosc., vol. 2205, SPIE; 1994, p. 291. https://doi.org/10.1117/12.166225.

[129] Phelps A V., Pitchford LC. Anisotropic scattering of electrons by N_2 and its effect on electron transport. Phys Rev A 1985;31:2932–49. https://doi.org/10.1103/PhysRevA.31.2932.

[130] Chng TL, Lepikhin ND, Orel IS, Popov NA, Starikovskaia SM. TALIF measurements of atomic nitrogen in the afterglow of a nanosecond capillary discharge. Plasma Sources Sci Technol 2020;29:035017. https://doi.org/10.1088/1361-6595/ab6f9c.

[131] Aleksandrov NL, Kindysheva S V., Kochetov I V. Kinetics of low-temperature plasmas for plasma-assisted combustion and aerodynamics. Plasma Sources Sci Technol 2014;23:015017. https://doi.org/10.1088/0963-0252/23/1/015017.

[132] Braginskiy O V., Vasilieva AN, Klopovskiy KS, Kovalev AS, Lopaev D V., Proshina O V., et al. Singlet oxygen generation in O_2 flow excited by RF discharge: I. Homogeneous discharge mode: α-mode. J Phys D Appl Phys 2005;38:3609–25. https://doi.org/10.1088/0022-3727/38/19/010.

[133] Kovalev AS, Lopaev D V., Mankelevich YA, Popov NA, Rakhimova T V., Poroykov AY, et al. Kinetics of $O_2(b^1\sum_g^+)$ in oxygen RF discharges. J Phys D Appl Phys 2005;38:2360–70. https://doi.org/10.1088/0022-3727/38/14/010.

[134] Atkinson R, Baulch DL, Cox RA, Hampson RF, Kerr JA, Troe J. Evaluated Kinetic and Photochemical Data for Atmospheric Chemistry: Supplement IV. IUPAC Subcommittee

on Gas Kinetic Data Evaluation for Atmospheric Chemistry. J Phys Chem Ref Data 1992;21:1125–568. https://doi.org/10.1063/1.555918.

[135] Popov NA. Dissociation of nitrogen in a pulse-periodic dielectric barrier discharge at atmospheric pressure. Plasma Phys Reports 2013;39:420–4. https://doi.org/10.1134/S1063780X13050085.

[136] Plank T, Jalakas A, Aints M, Paris P, Valk F, Viidebaum M, et al. Ozone generation efficiency as a function of electric field strength in air. J Phys D Appl Phys 2014;47:335205. https://doi.org/10.1088/0022-3727/47/33/335205.

[137] Loureiro J, Amorim J. Non-Maxwellian velocity distributions and non-Gaussian profiles of H atoms in low-pressure hydrogen discharges. Plasma Sources Sci Technol 2013;22:015016. https://doi.org/10.1088/0963-0252/22/1/015016.

[138] Pelevkin A V., Sharipov AS. Reactions of electronically excited molecular nitrogen with H_2 and H_2O molecules: Theoretical study. J Phys D Appl Phys 2018;51:184003. https://doi.org/10.1088/1361-6463/aab97f.

[139] Braithwaite M, Davidson JA, Ogryzlo EA. $O_2(^1\sum_g^+)$ relaxation in collisions. I. The influence of long range forces in the quenching by diatomic molecules. J Chem Phys 1976;65:771–8. https://doi.org/10.1063/1.433093.

[140] Ono R, Oda T. Measurement of OH density and gas temperature in incipient spark-ignited hydrogen-air flame. Combust Flame 2008;152:69–79. https://doi.org/10.1016/j.combustflame.2007.07.022.

[141] Kobayashi S, Bonaventura Z, Tholin F, Popov NA, Bourdon A. Study of nanosecond discharges in H_2-air mixtures at atmospheric pressure for plasma assisted combustion applications. Plasma Sources Sci Technol 2017;26:075004. https://doi.org/10.1088/1361-6595/aa729a.

[142] Raju GG. Gaseous Electronics. Tables, Atoms and Molecules. Boca Raton. 2012.

[143] Tsolas N, Yetter RA. Kinetics of plasma assisted pyrolysis and oxidation of ethylene. Part 1: Plasma flow reactor experiments. Combust Flame 2017;176:534–46. https://doi.org/10.1016/j.combustflame.2016.10.022.

[144] Tsolas N, Yetter RA, Adamovich I V. Kinetics of plasma assisted pyrolysis and oxidation of ethylene. Part 2: Kinetic modeling studies. Combust Flame 2017;176:462–78. https://doi.org/10.1016/j.combustflame.2016.10.023.

[145] Chen TY, Taneja TS, Rousso AC, Yang S, Kolemen E, Ju Y. Time-resolved in situ measurements and predictions of plasma-assisted methane reforming in a nanosecond-pulsed discharge. Proc Combust Inst 2020. https://doi.org/10.1016/j.proci.2020.06.100.

[146] Nijdam S, Teunissen J, Ebert U. The physics of streamer discharge phenomena. Plasma Sources Sci Technol 2020:doi.org/10.1088/1361-6595/abaa05.

[147] Zheleznyak MB, Mnatsakanyan AK, Sizykh SV. Photoionization of nitrogen and oxygen

mixtures by radiation from a gas discharge. High Temp / Russ / 1982;20:357–62.

[148] Pancheshnyi S. Photoionization produced by low-current discharges in O_2, air, N_2 and CO_2. Plasma Sources Sci Technol 2015;24:015023. https://doi.org/10.1088/0963-0252/24/1/015023.

[149] Kameta K, Kouchi N, Ukai M, Hatano Y. Photoabsorption, photoionization, and neutral-dissociation cross sections of simple hydrocar-bons in the vacuum ultraviolet range. J Electron Spectrosc Relat Phenom 2002;35:3479–86.

[150] Naidis G V. Modelling of transient plasma discharges in atmospheric-pressure methane-air mixtures. J Phys D Appl Phys 2007;40:4525–31. https://doi.org/10.1088/0022-3727/40/15/024.

[151] Pendleton SJ, Montello A, Carter C, Lempert W, Gundersen MA. Vibrational and rotational CARS measurements of nitrogen in afterglow of streamer discharge in atmospheric pressure fuel/air mixtures. J Phys D Appl Phys 2012;45:495401. https://doi.org/10.1088/0022-3727/45/49/495401.

[152] Tardiveau P, Bentaleb S, Jeanney P, Jorand F, Pasquiers S. Comparative study of air-propane and air-heptane mixtures ignition by nanosecond pulsed dis-charges. Int J Plasma Environ Sci Technol 2012;6:130–4.

[153] Teunissen J, Ebert U. 3D PIC-MCC simulations of discharge inception around a sharp anode in nitrogen/oxygen mixtures. Plasma Sources Sci Technol 2016;25:044005. https://doi.org/10.1088/0963-0252/25/4/044005.

[154] Rousso AC, Goldberg BM, Chen TY, Wu S, Dogariu A, Miles RB, et al. Time and space resolved diagnostics for plasma thermal-chemical instability of fuel oxidation in nanosecond plasma discharges. Plasma Sources Sci Technol 2020. https://doi.org/10.1088/1361-6595/abb7be.

[155] White DR. Vibrational relaxation of oxygen by methane, acetylene, and ethylene. J Chem Phys 1965;42:2028–32. https://doi.org/10.1063/1.1696241.

[156] Mitchell JBA. The dissociative recombination of molecular ions. Phys Rep 1990;186:215–48. https://doi.org/10.1016/0370-1573(90)90159-Y.

[157] Lo A, Frat F, Domingues E, Lacour A, Lecordier B, Vervisch P, et al. Nanosecond pulsed discharge in a propane-air mixture: Ignition and energy deposition. Proc Combust Inst 2017;36:4087–94. https://doi.org/10.1016/j.proci.2016.07.071.

[158] Messina D, Attal-Trétout B, Grisch F. Study of a non-equilibrium pulsed nanosecond discharge at atmospheric pressure using coherent anti-Stokes Raman scattering. Proc Combust Inst 2007;31 I:825–32. https://doi.org/10.1016/j.proci.2006.07.169.

[159] Grisch F, Grandin GA, Messina D, Attal-Tretout B. Non-equilibrium kinetic studies of plasma-assisted combustion using laser-based diagnostics. Z Phys Chem 2011:1193–1205.

[160] Lou HH, Chen D, Martin CB, Li X, Li K, Vaid H, et al. Optimal reduction of the C1-C3 combustion mechanism for the simulation of flaring. Ind Eng Chem Res 2012;51:12697–705. https://doi.org/10.1021/ie2027684.

[161] Gitlin MS, Bogatov NA, Golubev S V., Razin S V. Experimental study of the dynamics of fast gas heating in a low-pressure DC discharge in nitrogen. Plasma Sources Sci Technol 2019;28:045011. https://doi.org/10.1088/1361-6595/ab1242.

[162] Lepikhin ND, Klochko A V., Popov NA, Starikovskaia SM. Long-lived plasma and fast quenching of $N_2(C^3\Pi_u)$ by electrons in the afterglow of a nanosecond capillary discharge in nitrogen. Plasma Sources Sci Technol 2016;25:045003. https://doi.org/10.1088/0963-0252/25/4/045003.

[163] Boeuf JP, Kunhardt EE. Energy balance in a nonequilibrium weakly ionized nitrogen discharge. J Appl Phys 1986;60:915–23. https://doi.org/10.1063/1.337332.

[164] Bogatov NA, Gitlin MS, Golubev SV, Razin SV. Deactivation of $N_2(A^3\sum^+_u)$ after a discharge in nitrogen at large energy input into the gas. XIX Int. Conf. Phenom. Ioniz. Gases, 10th-14th July, Belgrade, Yugoslavia: 1989, p. 3, 604–5.

[165] Pintassilgo CD, Guerra V. Modelling of the temporal evolution of the gas temperature in N_2 discharges. Plasma Sources Sci Technol 2017;26:055001. https://doi.org/10.1088/1361-6595/aa5db2.

[166] Shkurenkov I, Adamovich I V. Energy balance in nanosecond pulse discharges in nitrogen and air. Plasma Sources Sci Technol 2016;25:015021. https://doi.org/10.1088/0963-0252/25/1/015021.

[167] Peters CJ, Shneider MN, Miles RB. Kinetics model of femtosecond laser ionization in nitrogen and comparison to experiment. J Appl Phys 2019;125:243301.